SESSION XIV

FILTRATION

Thursday, August 10, 1978
CHAIRMEN: R. Dorman, H. Gilbert

LOADING CAPACITY OF VARIOUS FILTERS FOR* SODIUM OXIDE/HYDROXIDE AEROSOLS

J. D. McCormack, R. K. Hilliard
J. R. Barreca

Hanford Engineering Development Laboratory
Operated by Westinghouse Hanford Company
Richland, Washington 99352

Abstract

The loading capacity of commercially available prefilters and HEPA filters is reported for sodium oxide and sodium hydroxide fumes in moist and normal air. The test aerosol is characterized and is considered to be typical of that which would exist during accidents involving sodium fires in breeder reactors, plants, and laboratory facilities.

Sodium pool fires of 0.6 m^2 area in a closed 330 m^3 room serve as an aerosol source to supply the recirculating filter test loop. The room and filter inlet stream is sampled to determine airborne particle size, mass concentrations, and dew point. Inlet mass concentrations of the test aerosol ranged up to 16 g/m^3. The chemical forms were mixtures of Na_2O_2, NaOH, Na_2CO_3, and their hydrates.

Seven types of HEPA filters and seven types of prefilters were examined in six test series. The holding capacity of the filters ranged from 0.6 to 3.9 kg at 5 kPa pressure drop for aerosols generated in moist and normal air. The early time and moist aerosols showed the lowest loading capacities. Up to 5.1 kg of sodium carbonate aerosols were held. Flow and media efficiency had only a minor effect on the loadings achieved. No combination of prefilters tested was effective in providing increased holding capacity for the associated HEPA filter.

Introduction

Emergency air cleaning is an accepted means of accident mitigation for light water reactors[1]. Similar air cleaning techniques for liquid metal cooled breeder reactors are still being developed and tested. A report to this conference two years ago reviewed the benefits of an Emergency Air Cleaning System (EACS) for breeder reactors and surveyed the probable usefulness of twenty-four air cleaning systems[2]. Such an air cleaning system would, of necessity, have to handle large quantities of sodium compounds, primarily the oxide and hydroxides, at high airborne concentrations and possibly under moist atmosphere conditions. Filter systems using commercial HEPA filters were well rated in the referenced evaluations because of the high degree of development, use, and reliability. These filters are known to be very efficient. However, information about loading capacity for the expected sodium compound aerosols is limited and in some cases conflicting results were reported[3-5]. Many of the early tests were

*Work performed under USDOE Contract EY-76-C-14-2170.

made with very small sodium sources in dry atmospheres or at reduced oxygen contents. Today's understanding of the hypothetical core meltdown accident give airborne concentrations of sodium oxide within containment up to 50 g/m^3. Further, water release from heated structural concrete is possible, allowing for the formation of NaOH and its hydrates. Also, if limestone aggregate concretes are used, the release of CO_2 gas with subsequent formation of sodium carbonate is possible. The objective of this work was to measure the loading capacity of several types of commercial HEPA filters and prefilters using sodium aerosols typical of those expected from breeder reactor core melt-through types of accidents.

Experimental Arrangements

Test Aerosol Generation and Sampling

The basic test facility consisted of a large closed concrete room (330 m^3 volume) containing a 0.6 m^2 heated pan for burning sodium.

The test aerosol generated in this smoke room was drawn to the filter through 13 meters of 25-cm diameter duct. The filtered air was returned to the smoke room by a blower capable of maintaining filter flow of 0.47 m^3/s (1000 ft^3/min) at 6 kPa (24 inches H_2O) pressure drop. The room atmosphere could be maintained at a slightly negative pressure to the outside by a 0.1 m^3/s room exhaust to a ventilation system. Natural in-leakage of air maintained a satisfactory oxygen concentration for combustion. Steam and CO_2 gas could be fed to the room at controlled rates. Figure 1 is a schematic of the test arrangement. Figure 2 shows the test filter housing. The housing can accommodate 60 x 60 x 60 cm HEPA filters and 60 x 60 prefilters up to 45 cm deep.

Samples of the test aerosol and atmosphere were taken in the smoke room through an airlock arrangement which allowed the sampling filter or cascade impactors to be inserted directly into the room, obviating the need for any inlet corrections. The mass concentration was determined using weighed filters. Sodium concentration was determined by titration of the filters with hydrochloric acide. Lower levels of sodium were determined on cascade impactors and a downstream sampler by flame emission spectrometry. Oxygen, CO_2 and water were measured by on-line instruments supplemented with grab samples analyzed by mass spectrometry and gravimetric means.

Cascade impactors were used for particle size measurement and electron microscope grids were exposed for particle shape information. Air flow, temperature, and pressure drop at the test filter were recorded by a 100-channel data logger on paper tape and magnetic tape for subsequent plotting and calculation.

Test Procedure

The general test procedure was to establish the initial room conditions and preheat the burn pan to 315°C. A preweighed test filter was installed in the housing, and sodium preheated to 200°C was delivered into the burn pan. Normally 50 kg of sodium was used. The room aerosol concentration was sampled and, when it was judged adequate for the test (about 3 g/m^3), loop flow was started. Flow was kept constant until the desired terminal pressure drop at the test

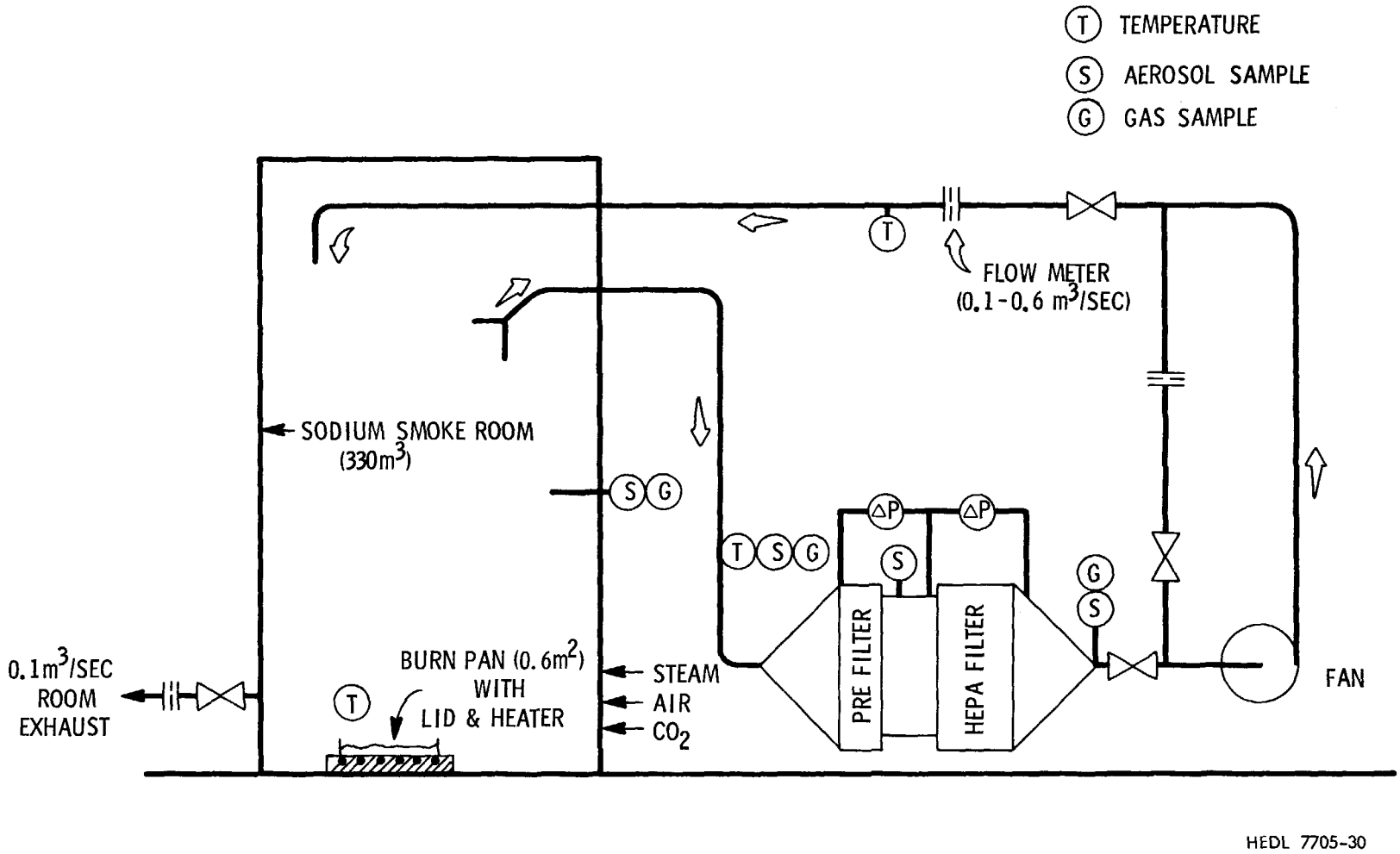

Figure 1. Filter loading loop schematic.

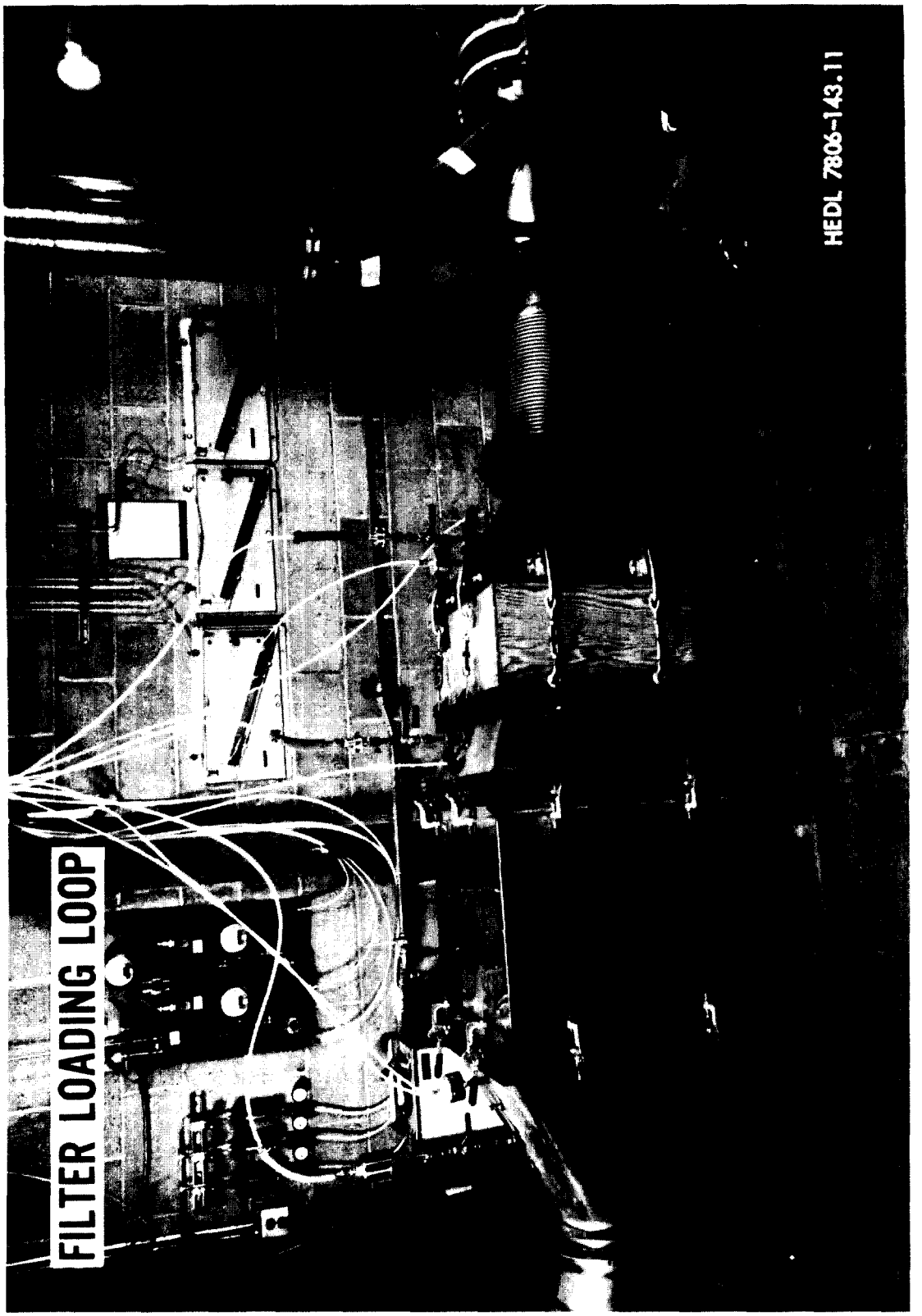

Figure 2. Filter loading loop.

filter was reached. The flow was stopped; the filter rapidly removed, weighed, and a new filter inserted. Up to seven filters could be tested during one test series. For some test series, additional sodium was added to the burn pan to maintain a high aerosol concentration.

In two test series, the loop flow was started before the sodium fire to measure loading of fresh, lower concentration aerosols. This sequence duplicated the conditions expected from filters used in a ventilation system in service at the time the sodium fire starts.

Test Filters

A variety of test filters were obtained from commercial sources. These filters were selected to be typical of various manufacturing variables thought to be of interest, such as the media efficiency, media area, size of separators or absence of separators. All the test filters had a glass media suitable for high humidity use and all the filters were 60 x 60 x 30 cm size. The relevant details are summarized in Table I, where each filter type is identified with a key number which will be used in subsequent discussions for filter identification.

Test Prefilters

Several types of prefilters were also used. These prefilters had a 60 x 60 cm face area with various thicknesses. For the thinner 5-cm thick filters, two were used in a series. The filter characteristics and the key numbers are given in Table II. The metallic media filters were washed, dried, and reused. The others were discarded after use.

Filter Loading Test Variables and Sequence

Six filter loading test series were completed. Each test series consisted of a single sodium fire in a selected atmosphere condition. The sodium oxide/hydroxide aerosols generated were used to load up to seven test filters in sequence.

Primary variables examined in these runs were:

- Filter flow rate; 20%, 50%, and 100% of nominal,
- Generation of aerosol in normal and moist atmospheres,
- Filter construction, absence of separators,
- Filter media efficiency; 60, 90, and 99.97%,
- Prefilter construction, 7 types,
- CO_2 addition to the test atmosphere.

The initial test conditions, atmosphere, and primary test variables are given in Table III.

Experimental Results

The test results of most interest are the mass loading of the filters and final pressure drop. These results are summarized in Table IV for all the runs where 37 filter combinations were measured.

Table I. Description of test filters.

Test filter key number	Vendor	Media efficiency, %	Estimated media area, m^2	Characteristics
1	F	99.97	23	Waterproof glass media, Al separator.
2	F	99.97	23	Same as 1, w/o separators.
3	Various	99.97	Various	HPS type C; water resistant glass media, non-metallic separator, 90% RH, 49°C.
4	M	99.97	30	Glass media, mini Al separator, 1500 CFM.
5	F	90(a)	17	Glass media, no separator, 100% RH, 121°C.
6	C	99.97	23	Waterproof glass media, Al separator.
7	C	60(a)	5.1	Glass media, Al separator.

(a) Per ASHRAE 53-68.

Table II. Description of test prefilters.

Test filter designator	Source	Thickness(a) cm	Eff. %	Characteristics
20	M	13	-	Knitted ss/fiber glass demister.
21	R	10	-	Crimped 14 and 18 mesh metal screen.
22	A	5	-	Progressive density; expanded metal and mesh layers.
23	A	5	-	Crimped metal screen, pyramid pocket design.
24	R	10	30(b)	Cotton fabric, nonwoven.
25	R	30	50(b)	Glass fiber mat, folded.
26	A	5	-	Crimped, expanded Al mesh, 3 layers.

(a) All were 60 x 60 cm face.

(b) Atmosphere dust spot.

Table III. Filter loading test conditions

Test No.	Initial Room Conditions				Steam Addition	Final Room Conditions			Primary Test Variable
	Temp °C	Dew Pt °C	R.H. %	CO_2 %	kg/hr	Temp °C	Dew Pt °C	R.H. %	
FL 1	14.4	-2.2	30	Normal	None	38.0	-12.6	∿3	Flow Rate, filter type(1)
FL 2	10.6	3.3	∿60	"	4.6	33.0	-12.0	4	Same as FL 1 with steam
FL 3	16.6	-1.7	26	"	None	38.0	-13.0	3	Filter construction
FL 4	21.1	6.7	39	"	9.1	43.0	8.0	12	Prefilter types, with steam
FL 5	20.0	0.6	28	"	None	46.0	-13.0	2	Prefilter, dry
FL 6	25.0	8.9	36	∿3	9.1	46.0	21.0	25	CO_2 addition with steam

(1) with and without separators.

Table IV. Summary of filter loading and pressure drop.

Test No.		Filter P.F.	Type HEPA	Flow m^3/sec	Mass on filter, kg P.F.	HEPA	Total	P, kPa P.F.	Total	Aerosol Conc., g/m^3
FL1	A	None	1	0.45	None	2.8		None	4.8	9.0
	B	None	1	0.23	None	2.6		None	4.6	7.2
	C	None	2	0.23	None	3.7		None	4.8	9.2
	D	None	2	0.45	None	3.0		None	4.8	9.4
	E	None	2	0.09	None	2.5		None	4.6	7.7
	F	None	1	0.09	None	2.7		None	4.7	6.5
FL2	A	None	1	0.47	None	0.63		None	5.0	10.7
	B	None	1	0.24	None	0.79		None	5.0	12.4
	C	None	2	0.24	None	2.5		None	4.5	16.5
	D	None	2	0.46	None	3.9		None	4.5	8.4
	E	None	2	0.09	None	1.8		None	4.5(1)	10.4
	F	None	1	0.09	None	1.8		None	4.5(1)	4.6
FL3	A*	None	3	0.45	None	0.62		None	4.5	1.8
	B	None	3	0.46	None	1.1		None	4.5	5.9
	C	None	4	0.46	None	2.0		None	4.6	5.0
	D	None	5	0.46	None	2.2		None	4.6	6.4
	E	None	6	0.46	None	1.7		None	4.5	4.9
	F	None	7	0.46	None	1.7		None	3.7	2.8
	G	None	3	0.46	None	2.0		None	4.6	6.7
FL4	A*	20	3	0.46	0.89	1.2	2.1	0.2	4.9	3.5
	B	21	3	0.47	1.1	2.2	3.3	0.05	4.7	6.9
	C	22(2)	3	0.48	0.58	2.0	2.5	0.02	5.0	6.1
	D	23(2)	3	0.48	0.51	1.5	2.0	0.02	4.8(3)	7.0
	F	24(2)	3	0.48	0.79	1.9	1.9	1.6	5.0(3)	8.2
	G	25	3	0.48	1.6	0.52	2.2	3.5	3.9	4.4
FL5	A	20	3	0.47	0.51	0.44	0.95	NM	%	5.7
	B	21	3	0.47	0.31	0.36	0.68	0.02	6.0	4.0
	C	22(2)	3	0.47	0.15	0.53	0.68	0.02	6.5	4.3
	D	23(2)	3	0.47	0.89	0.81	1.7	5.0	6.2	4.2
	E	26(2)	3	0.47	1.5	0.73	2.3	5.1	6.1(4)	6.4
	F	24	3	0.47	2.0	0.64	2.6	3.5	4.4(4)	4.4
	G	25	3	0.47	3.6	0.21	3.8	5.3	5.8	6.1
FL6	A	-	3	0.47	-	4.7	-	-	5.0	6.3
	B	-	2	0.47	-	5.1	-	-	4.9	4.9
	C	21	3	0.47	3.3	1.5	4.8	0.8	5.8	5.4
	D	25	3	0.47	1.4	0.17	1.5	5.1	5.6	7.6
	E	-	3	0.47	-	4.0	-	-	5.0	4.8

* Flow started before sodium fire
(1) Ruptured at 2.5 kPa P flow continued
(2) Two filters used in series
(3) Ruptured at 2.2 kPa
(4) Ruptured at 4.5 kPa

Table IV also lists the average aerosol mass concentration at the filter inlet, as calculated from the mass on the filter and the actual volume of air passing the filter.

Pressure Drop and Loading Capacity

For a pressure drop of about 5 kPa (20 inches H_2O), the HEPA mass loading ranged from a low of 0.6 kg to 3.9 kg for sodium aerosols generated in air. A maximum loading capacity of 5.1 kg was found for aerosols generated in a moist atmosphere containing CO_2 (test FL-6). In filter test series FL-4 and FL-5, prefilters were added to the system. The maximum combined loading was 3.8 kg. None of the prefilters tested were particularly effective in increasing the loading capacity of the following HEPA filter. In all cases the loadings and pressure drops were not evenly shared. The space used by the prefilter and HEPA filter in series would have been more effective for mass loading if two filters, with no prefilter, were arranged in parallel.

Pressure drop typically started low and then increased at an increasing rate until the filter ruptured or the test was terminated. This behavior is shown in Figures 3-7 where the pressure drops for all runs are given. Notice that filter 2-F ruptured at about 3 kPa. Figures 8 and 9 show typical filters after loading. Run FL-1 was in normal air. Steam was added during FL-2. The effect of moisture on the appearance of the filtered aerosol is especially noticeable in test series 2 where filter 2A and 2B show no visible deposit but were plugged by only 0.6 and 0.8 kg of material. As the test progressed, more deposit was visible and the later filters held from 1.8 to 3.9 kg. Although steam was added to the smoke room during test FL-2 at 4.6 kg/hr, the dew point, relative humidity, and mass/sodium ratio decreased with time. As the water content of the aerosol decreased, the filterability generally improved. Figure 10 is a plot of the mass to sodium ratio measured near the burn pan. This decreasing mass ratio behavior is typical of all the runs. The lower water content of the later aerosol samples is in accord with the reduced relative humidity of the smoke room atmosphere due to reduced dew point and increased temperatures.

Effect of Flow Rate and Filter Construction

The effect of flow rate on filter loading is shown by comparison of tests FL-1 and FL-2 for both dry and "wet" conditions. The effect of using HEPA filters without separators is also shown. These loadings are summarized in Table V.

From Table V it is apparent that flow has only a small effect on loading capacity and that except at 0.09 m^3/sec (200 cfm), filters without separators had higher loading capacities. Moisture effects are also seen in Table V where FL-2, the wet run, results in generally lower filter loadings.

The effect of variations of filter construction and media efficiency are shown by the mass loadings of FL-3. This run also shows variations in mass loading caused by aerosol changes. This is seen by comparing the results of FL-3A, B, and G in Table IV. Identical

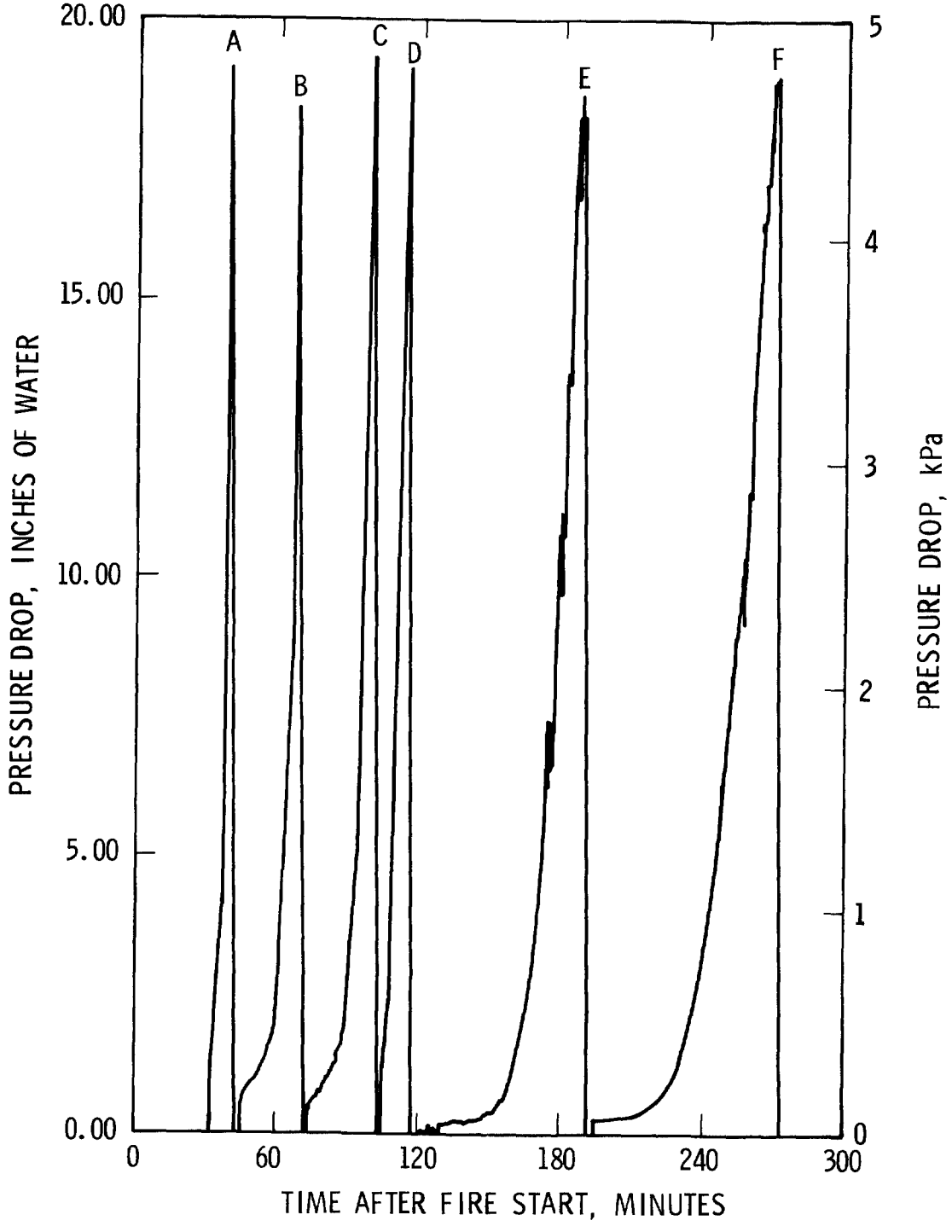

Figure 3. Pressure drop across filters, run FL-1.

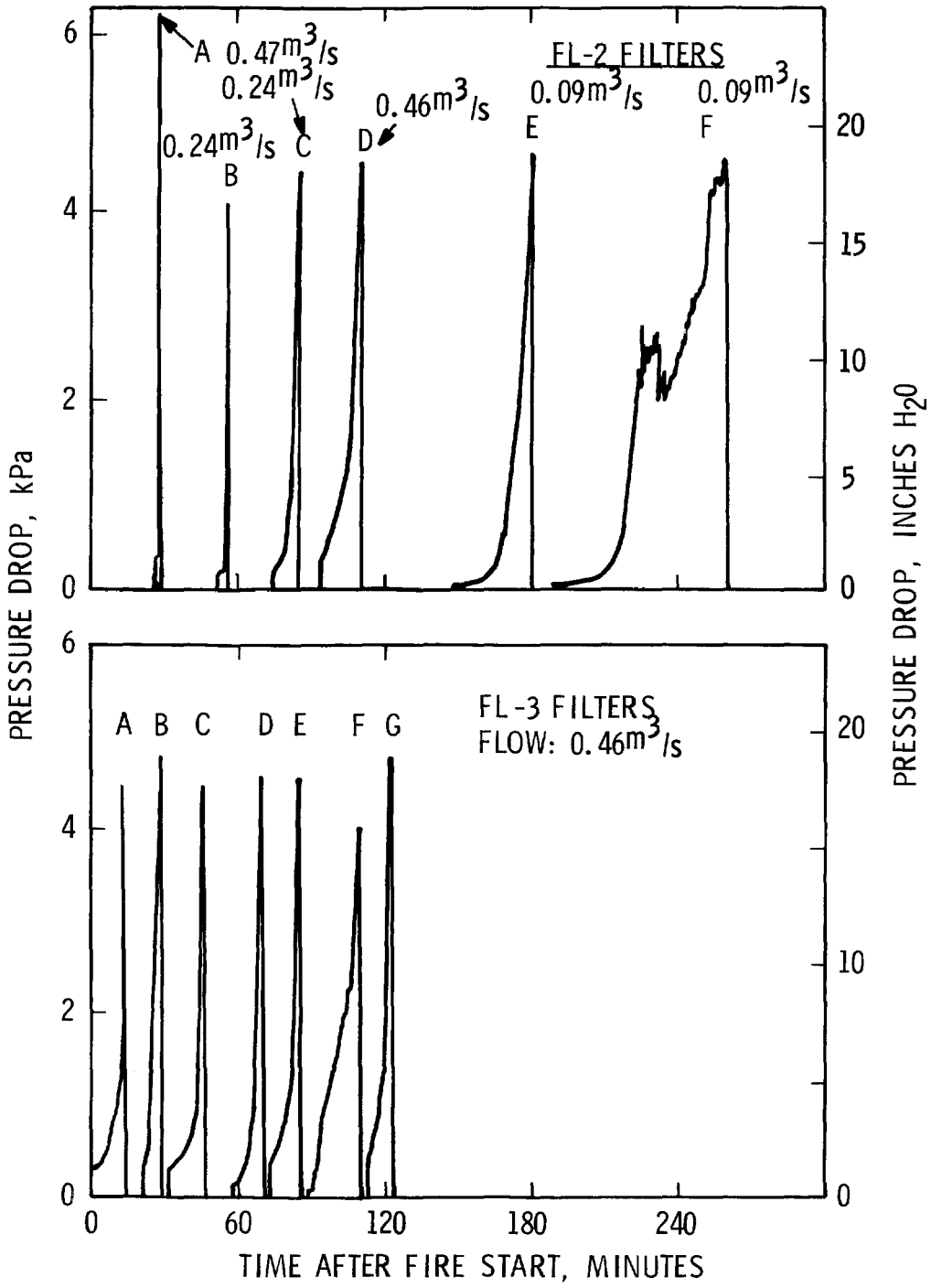

Figure 4. Pressure drop, runs FL-2 and FL-3.

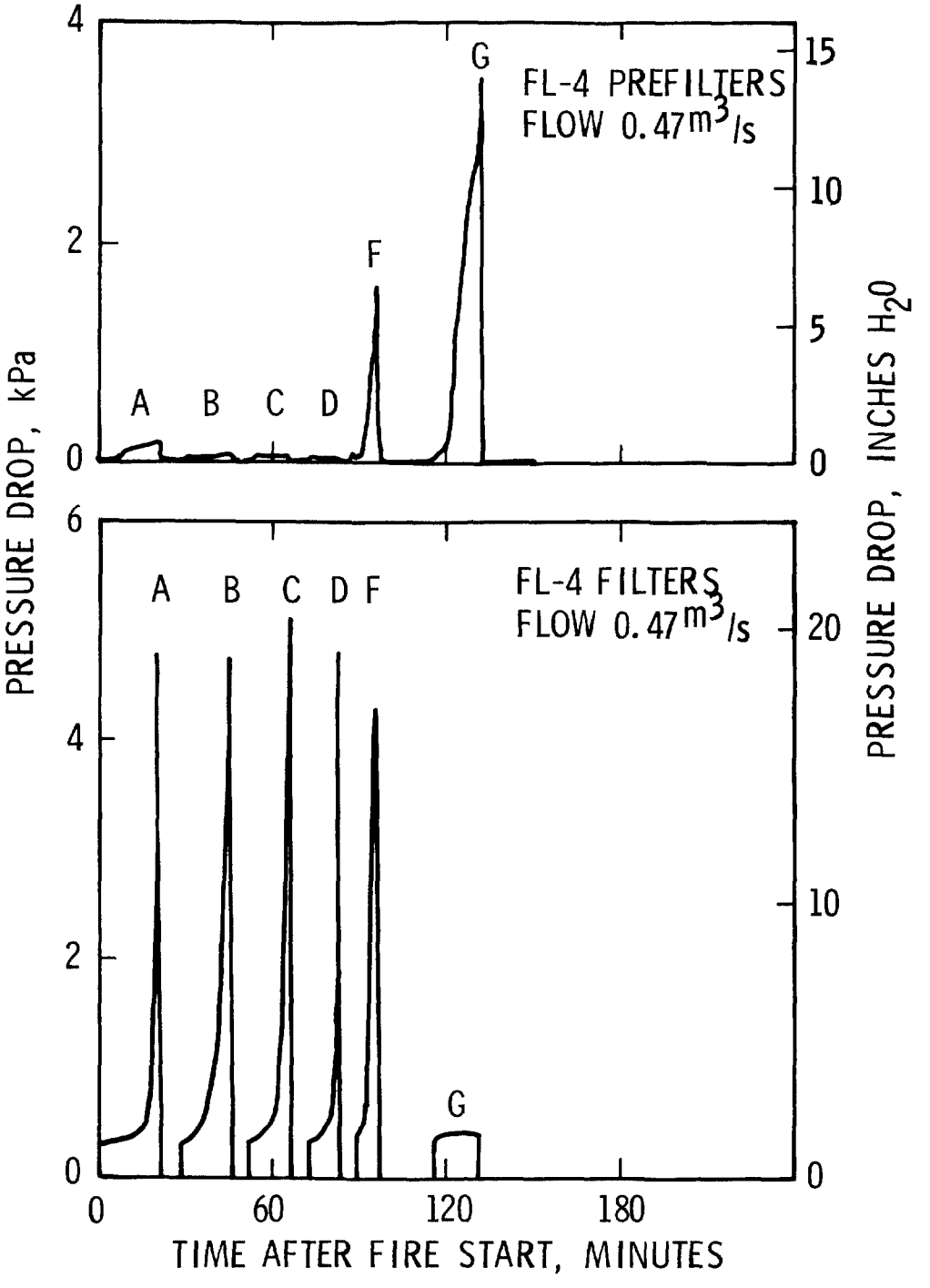

HEDL 7806-143.2

Figure 5. Pressure drop, run FL-4.

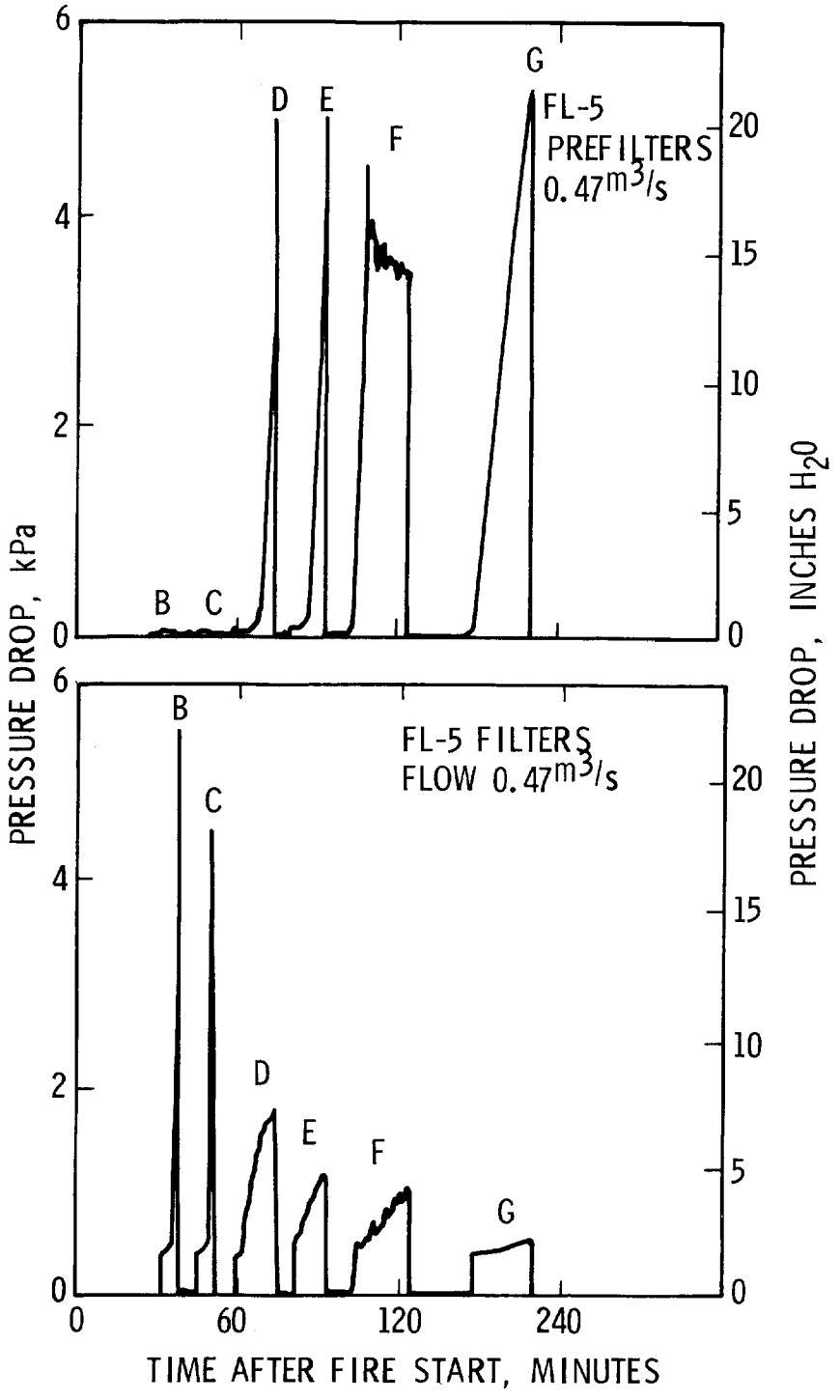

Figure 6. Pressure drop, run FL-5.

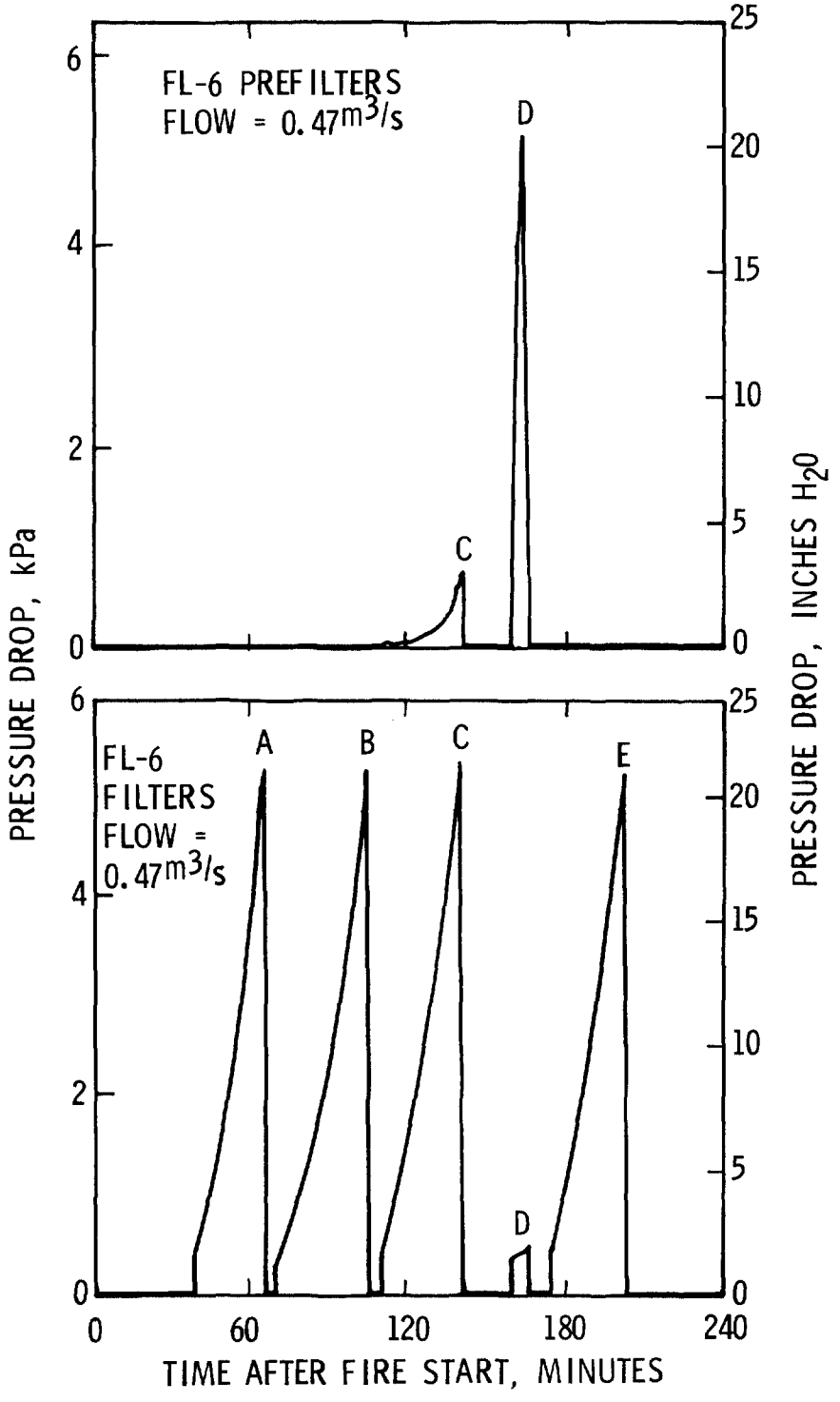

Figure 7. Pressure drop, run FL-6.

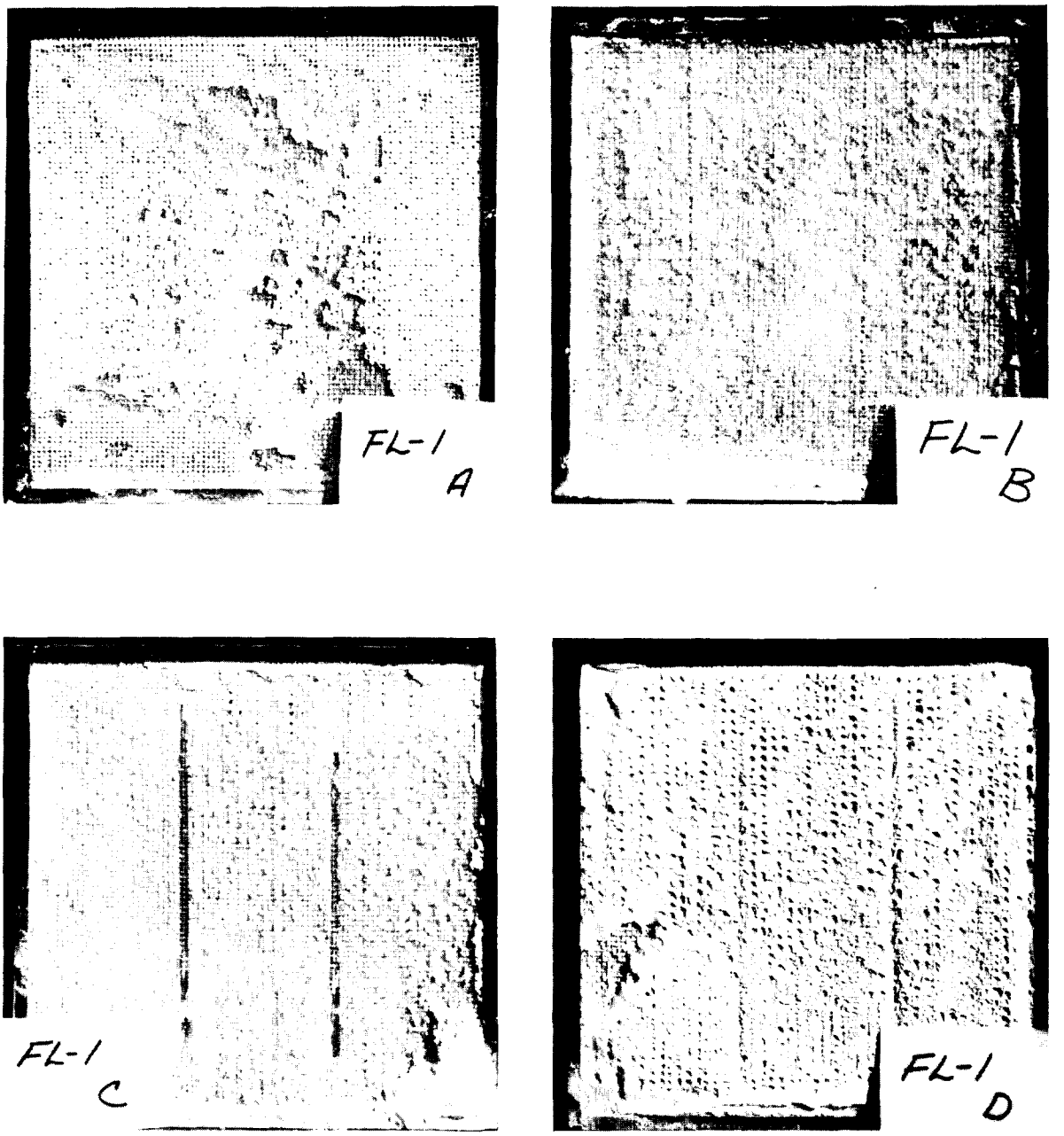

HEDL 7806-143.13

Figure 8. Filters after loading with dry aerosol.

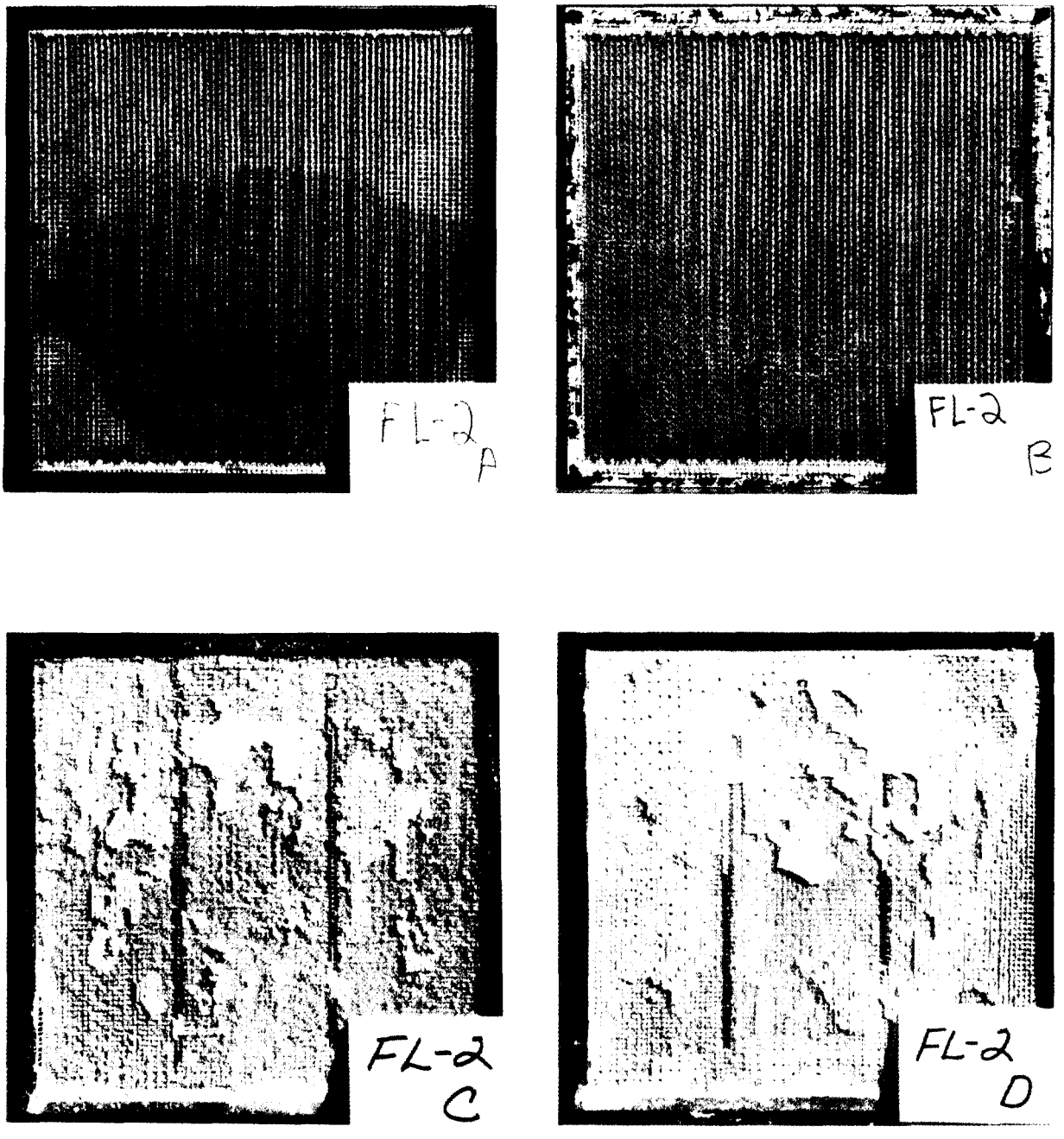

Figure 9. Filters after loading with moist aerosols.

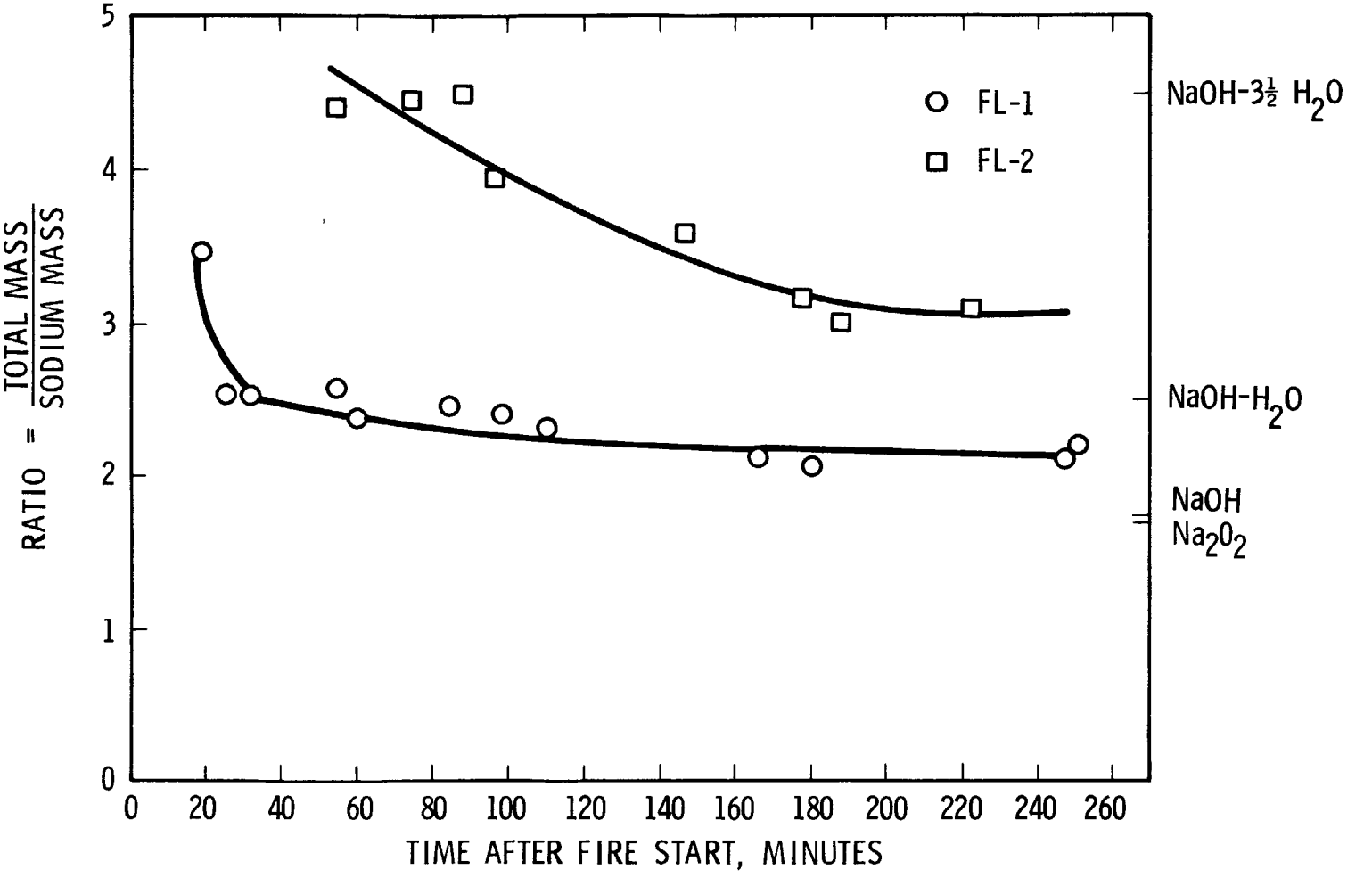

Figure 10. Smoke room aerosol mass ratios for runs FL-1 and FL-2.

Table V. Effect of flow and separators on filter loading.

		Mass loadings on filters, kg					
		w/separator flow, m^3/s			w/o separator flow, m^3/s		
Run	Atmosphere	0.09	0.24	0.47	0.09	0.24	0.47
Filter Sequence		F	B	A	E	C	D
FL 1	Normal	2.7	2.5	2.3	2.5	3.7	3.0
FL 2	Steam Added	1.8	0.79	0.63	1.8	2.5	3.9

filters were used and loadings of 0.62, 1.1, and 2.0 kg were found. In test 3, the flow through the filter was started before the fire for A, and at 22 minutes and 113 minutes for B and G, respectively. The lowest loading was found for filtering at early stages of the fires. This is thought to be due to the high moisture content of the aerosol relative to the sodium.

Variations in loading for the other filters, where 60 and 90% efficiency filters and also 99.97% filters with "mini" aluminum separators were used are small, ranging from 1.7 kg to 2.2 kg. The highest loading was observed for the 90% (Key 5) filter. Again absence of separators appeared to help increase the loading capacity. Filter 3F ruptured at 2.2 kPa.

Prefilters

The use of prefilters was examined in runs FL4 and FL5 for aerosols generated in moist and normal humidity atmospheres. The best combination for the moist atmosphere conditions (test FL4-B) was the prefilter made of two sizes of screen mesh crimped into a herring-bone pattern (Key 21). The best combination observed for the normal humidity air was FL5-G (Key 25), a folded glass mat filter. These filters are shown in Figure 11. No combination tested was high in loading for both wet and dry test aerosols. The prefilter either removed most of the test aerosol or allowed a major fraction to penetrate, leading to loading of the backup HEPA filter. The folded glass mat prefilter (Key 25) had appreciable holding ability in both tests but is no more compact than the HEPA filters used. Prefilter FL5-F (Key 24) ruptured at 4.5 kPa.

CO_2 Addition

Addition of CO_2 gas to the smoke room atmosphere and the filtering of the subsequent sodium carbonate aerosols was examined in run FL6 for several selected filter combinations. For these conditions, enhanced loading was found with over 5 kg being held at 4.9 kPa.

The smoke room air was kept at 3% CO_2 during the fire and steam at 9.1 kg/hr was added. Chemical and x-ray diffraction analysis of the aerosols deposited on all the filters showed nearly pure

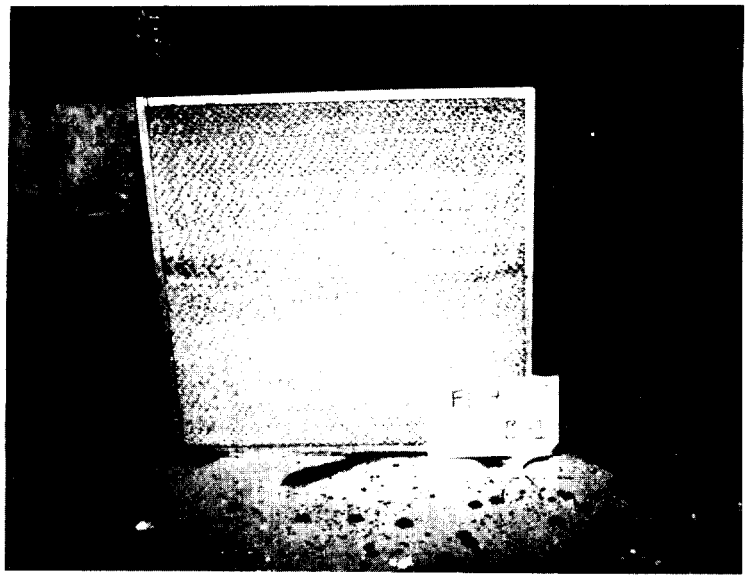

RUN FL-4, PRE FILTER B-1

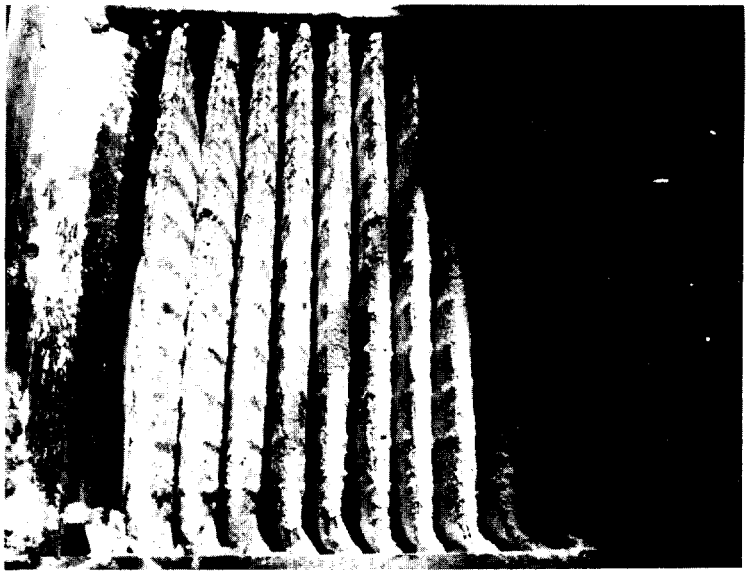

RUN FL-5, PRE FILTER G

HEDL 7806-143.14

Figure 11. Two types of prefilters after loading.

anhydrous Na_2CO_3 (see Table VI). Particle size was in the 1.4-3.6 μm aerodynamic mass median diameter (AMMD) range, about the same as measured in the other runs. Particle shape changed during this run to needle-like clusters not previously observed in the tests using air. Figure 12 shows the particle shapes as seen by transmission electron micrographs.

Chemical Form of Deposits

The chemical form of the material removed from the filters, where adequate deposits were collected, was determined by chemical analysis, and in some tests by x-ray diffraction. The amounts of Na_2O_2, Na_2CO_3, NaH and total Na were found directly by analysis. The sodium not accounted for was assumed to be NaOH and the mass not accounted for was taken to be water. Sodium hydride was always less than 0.1% and sodium monoxide was not found. Table VI summarizes the analysis of these samples. The effect of adding moisture to the fire atmosphere is seen in runs FL2 and FL4 where the Na_2O_2 content is reduced and the NaOH content increases. Run FL5 is somewhat of an anomaly; no steam was added, but high NaOH was found. This may have resulted from some unknown moisture sources in the room or duct. This run, using nominally dry air, also had many of the characteristics of a "wet" atmosphere run in the appearance of the early filters and in the relatively low mass loadings on early filters.

In run FL6, of course, CO_2 and moisture were added to the atmosphere and nearly complete conversion to anhydrous Na_2CO_3 was noted for all samples.

Aerosol Particle Size

Particle size was measured using cascade impactors in the smoke room and in the duct upstream of the filters. Two impactor types were used, one an 8-stage multijet type and the other a 6-stage radial slot type. Both impactors gave reasonably consistent data for the size being measured. Table VII presents the sizes found in the smoke room. These sizes are, however, smaller than reported by Hilliard et al.[7] at this conference for measurements made in an 850-m^3 vessel, probably because of the weaker aerosol source and the lower aerosol concentrations achieved in the present work. The sizes reported for the runs are not thought to vary by an amount which is significant to the filter loading tests.

Aerosol Release and Duct Losses

After each run the fire burned to completion and the ducts were washed to determine the sodium deposition in the duct and filter housing. For some runs the sodium aerosol on the smoke room floor was sampled and fallout determined. Table VIII presents the duct losses for each run, and also the fraction of the sodium aerosolized. The 25-cm diameter inlet duct has a 10-m horizontal length, a 3.4-m vertical length, two 90° ells and one 45° ell. The inlet was a 30° tapered section. No separate analysis of the deposition in the vertical and horizontal section was made. Duct losses are highest for the moist aerosols.

Table VI. Typical chemical analysis of deposits on filters.

Run and filter no.	Time from fire start, min	Wt %				Total Na
		Na_2CO_3	Na_2O_2	NaOH	H_2O	
FL1-CS2	125	3.2	31.8	44.0	21.0	44.5
FL2-C	76	0.6	8.6	61.4	29.4	43.0
FL3-B	22	1.2	19.5	33.7	30.6	40.0
D	58	1.0	26.6	26.9	26.0	43.0
G	113	0.9	27.7	33.5	17.4	47.0
FL4-F	89	1.8	12.2	45.9	40.1	34.4
G	108	3.6	2.3	56.1	38.0	35.2
FL5-E1	82	1.3	10.0	74.6	14.0	49.7
F1	104	3.0	12.0	69.2	15.7	48.5
FL6 (All)	39-174	100	0	0	0	44.4

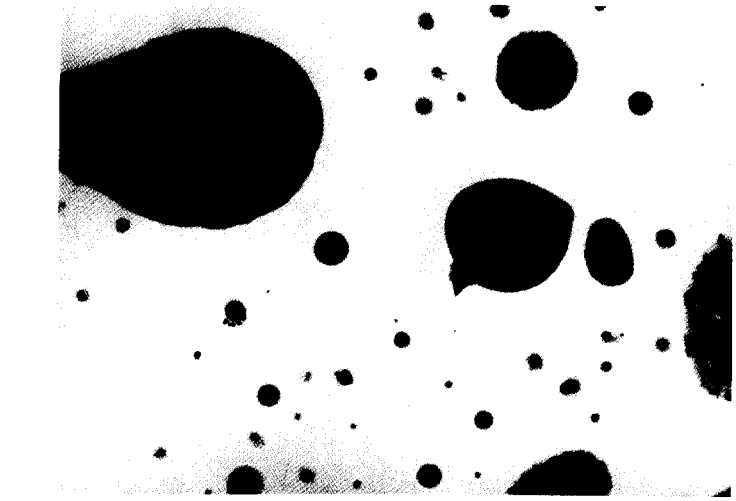

10 μm

RUN FL-1 AT 117 MINUTES - DRY ATMOSPHERE

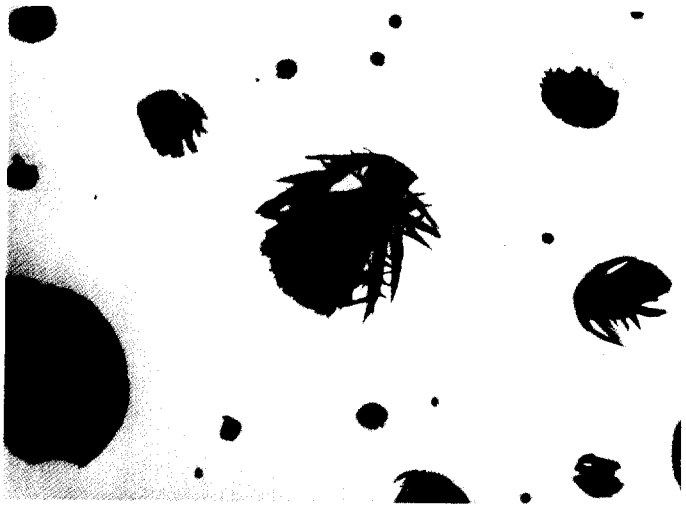

10 μm

RUN FL-6 AT 238 MINUTES - MOIST CO_2 ATMOSPHERE

HEDL 7806-143.7

Figure 12. Aerosol particles, electron photomicrographs.

Table VII. Aerosol particle sizes.

Run	Aerosol particle sizes[a]			
	Sample time, min	Impactor[b] type	AMMD[c] μm	σ_g
FL1	19	A	1.9	2.8
FL2	21	A	2.5	2.1
	197	S	6.8	2.4
FL3	10	S	2.9	4.9
	30	S	4.4	3.0
FL5	20	S	1.6	2.9
	88	A	3.0	2.7
	105	A	3.4	2.7
FL6	39	A	2.9	2.6
	71	A	1.4	3.7
	165	A	2.7	2.4
	183	A	2.6	2.4

(a) Sampled in smoke room
(b) A is multicircular jet, S is 4-radial slot
(c) Aerodynamic Mass Median Diameter

Table VIII. Sodium aerosol release and duct losses.

Run	Sodium in pan, kg	Sodium, Aerosolized %	Duct deposition % of intake
FL1	85	-	15
2	85	-	22
3	65	14	10
4	47	18	35
5	61	14	35
6	59	26	9

The fraction aerosolized is based on the amount charged to the burn pan and the amount recovered from filters, duct work, and the estimated quantity deposited on the smoke room floor.

Filter Loading at Other Pressure Drops

These filter loading tests were run to rather high pressure drops. Emergency air cleaning systems are not expected to be used often, if at all. Hence, installation costs, not operating costs, are more important. The filter bank mass loading and therefore the size can obviously be reduced by running to the highest allowable pressure drop.

If the filter loading ability is required at lower pressure drops, the amounts reported can be prorated on a time basis. For most of the runs reported, the smoke room concentrations were nearly constant during the loading of a filter and the flow rate was held constant. Hence, the mass collected on a filter increased nearly linearly with running time. If a pressure drop at a shorter time is selected, the mass will be reduced by the same fraction as the time was reduced.

During loading of filters FL5-G and 6-F, the aerosol concentration decreased a significant amount and this accounts for the apparently linear increase of pressure drop with time.

Discussion and Conclusions

These tests show that the loading capacity of filters for sodium oxide, hydroxide and carbonate aerosols is quite variable, even when loaded under similar flow conditions. The amount held on nominal 0.47 m^3/s (1000 cfm) HEPA filters ranged from 0.62 to 3.9 kg at 5 kPa for mixed Na_2O_2-NaOH aerosols. For dry sodium carbonate aerosols, up to 5.1 kg were held at 5 kPa. These values are in the same range of loadings as obtained in recent studies by other investigators. Gunn and Eaton in the 14th Air Cleaning Conference[6] reported sodium oxide loading of 0.36 to 1.3 kg at 1.5 kPa (6" H_2O) for several filter types at 0.7 m^3/s in normal humidity air. Our data for similar filters FL1-A, FL1-D, and FL3-C indicate 1.4 to 1.5 kg at 0.47 m^3/s and 1.5 kPa which is quite comparable. Jordan[5] reports 160 g/m^2 at 5 kPa for 2.6 m^2 fiberglass filters, or 1.6 kg for a HEPA containing 25 m^2 of media. Viles[4] developed 20-cm thick graded media filter packs which held about 2.8 kg/m^2 of face area at 5.2 kPa pressure drop. The face velocities were 2 to 8 m/min which is lower than used during these tests. On a filter volume basis, this loading is equivalent to 1.6 kg on a standard-sized 60 x 60 x 30 cm HEPA filter. Again, this loading is comparable to that obtained on HEPA filters in this work.

Some general conclusions about the loading of HEPA filters with sodium oxide and sodium hydroxide aerosols can be made from the work reported here.

- Holding capacity at 5 kPa pressure drop ranged from 0.6 to 3.9 for a nominal 0.47 m^3/s HEPA.
- Holding capacity is not strongly increased by using filters at lower than nominal flow.
- HEPA filters without separators have a high holding capacity.

- Holding capacity is not strongly dependent on media efficiency.
- None of the prefilters tested were effective in increasing the combined filter holding capacity.
- The prefilter/HEPA filter combination which was best for dry aerosols was not the best for moist aerosols.
- The first fumes from a sodium fire give a higher pressure drop. This is thought to be due to a higher water/sodium content of the first aerosol produced.
- Sodium carbonate generated in a moist CO_2-containing atmosphere had higher loading capacities (up to 5.1 kg).
- The variation in the aerosol is more important than the HEPA filter construction or filter media in determining the loading obtained.
- Moisture and relative humidity in the fire atmosphere decreases the filter loading capacity. Further study will be required to determine the cause of this change.

References

1. D.W. Moeller, "Current Challenges in Air Cleaning at Nuclear Facilities," Nuclear Safety, 18, pg 633 (1977).

2. J.D. McCormack, R.K. Hilliard, A.K. Postma, and L.D. Muhlestein, "An Evaluation of Alternative Air Cleaning Systems for Emergency Use in LMFBR Plants," Proceedings of the 14th ERDA Air Cleaning Conference, CONF-760822, pg 989, February 1977.

3. R. Dennis, E. Kristal, and L. Silverman, "Fibrous Filters for NaK Fume Removal," NYO-4811, Harvard Air Cleaning Laboratory, May 1, 1960.

4. R.J. Viles, Jr., P. Himot, and M.W. First, "High Capacity-High Efficiency Filters for Sodium Aerosols," NYO-841-10, Harvard Air Cleaning Laboratory, August 1967.

5. S. Jordan, A. Alexas, W. Lindner, "Filtration of Sodium Fire Aerosols," Trans Am Nuc Soc, Vol. 24, pg 526 (1977).

6. C.A. Gunn and D.M. Eaton, "HEPA Filter Performance Comparative Study," Proceedings of the 14th ERDA Air Cleaning Conference, CONF-760822, pg 630, February 1977.

7. R.K. Hilliard, J.D. McCormack, A.K. Postma, and J.A. Hassberger, "Sodium Oxide/Hydroxide Aerosol Properties and Behavior in a Large Vessel," HEDA-SA-1466, June 1978.

DISCUSSION

BURCHSTED: Did I hear you say that the pressure loading across the HEPA filter itself went to 20 to 25 in.w.g.?

McCORMACK: Yes.

BURCHSTED: That's very interesting because we have been talking about 10 in. w.g. maximum. Did you notice any damage to the filters?

McCORMACK: Yes, at least one HEPA filter ruptured, one of the non-woven cotton fabric filters ruptured, and one of the low efficiency pleated filters ruptured in the range of 10-13 in.w.g.

BURCHSTED: Did you do any follow-up DOP tests to see if non-visible degradation had occurred?

McCORMACK: We did not, but we now have a 30 day test in progress. We have been loading the filter more gradually and DOP-testing it each seven days. So far, it has maintained its original efficiency.

BURCHSTED: What is the maximum ΔP you have reached so far?

McCORMACK: Around 12 in.w.g.

MURROW: Have you considered using prefilters or systems similar to those used at the Lawrence Livermore Laboratory for smoke removal? Do you think you might?

McCORMACK: We have not tried them. I have thought of using moving prefilters and they look appealing but we wanted to start with a more passive device.

MURROW: Perhaps some of the information from the LLL fire tests might cross pollinate with your studies.

McCORMACK: Yes, I am very interested in those tests.

DYMENT: In your conclusions, you find that HEPA filters without separators have a higher holding capacity. Is the increased capacity produced by a difference in the surface area of the paper in the two types of filter?

McCORMACK: I don't know for certain but I'm sure that increased area contributes to the increased holding capacity.

SCHIKARSKI: Concerning the behavior of fiber glass filters loaded with sodium fire aerosols, we have made a number of experiments at Karlsruhe which were reported an an earlier Air Cleaning Conference. We found loading capacities similar to those reported by Mr. McCormack. However, we also found, after the test, that loaded filters showed small "puffs" (little explosions) that destroyed the filter media. We believe that these explosions are due to the fact that not all sodium fire aerosols are completely oxidized before entering the filter. Therefore, small sodium droplets covered by sodium oxide will exist in the filter media which give rise to later reactions (or small explosions) with atmospheric moisture. This effect has led to the decision that, in German LMFBRs, fiber glass HEPA filters will not be used where sodium fires may occur.

PERFORMANCE OF A WET CELL WASHER FOR SODIUM FIRE AEROSOLS

W. Hinds, J. Price, and M.W. First
Harvard Air Cleaning Laboratory
Boston, Massachusetts

Abstract

The suitability of 6 packing materials for removal of sodium fire aerosols in a wet cell scrubber was evaluated experimentally by measuring the efficiency and flow resistance of two 10.2 cm deep cells in series at air face velocities of 185 and 289 cm/sec, water flow rates of 0.210 and 0.387 $cm^3/sec/cm^2$, with and without aerosol prehumidification. The most satisfactory material was found to be 50 μm diameter stainless steel fibers at a packing density of 30 kg/m^3 (porosity = 0.99). Two 10.2 cm deep cells in series gave a removal efficiency of 85% for typical sodium fire aerosols at a face velocity of 289 cm/sec. Measurement of efficiency as a function of particle size indicated a reduction in efficiency in the 0.4 to 1.1 μm size range for all packing materials.

Introduction

One of the proposed safety systems for the LMFBR is an aerosol filtration system through which the reactor containment building atmosphere would be vented in the event of an accidental release of burning sodium. A proposed filter system consists of two stages: the first, a scrubbing system, containing a humidifying section, a wet cell washer, a water separator or demister, and a heater/dryer, and the second, consisting of a prefilter, a high efficiency particulate filter (HEPA), a zeolite bed, and another HEPA filter. Burning sodium metal in a normal oxygen atmosphere produces a dense aerosol composed of a mixture of sodium oxides, hydroxide, and carbonates. When combustion occurs at a relative humidity greater than 35%, the resulting agglomerated aerosol particles absorb water vapor and form sticky droplets that create difficult clogging and crusting problems for high efficiency air cleaning equipment.[1] Therefore, the scrubbing section would have to maintain greater than 90% removal efficiency without clogging for a period of many hours. The present study was conducted to develop performance data for the first stage scrubbing system.

Wet cell washers utilize beds of coarse fibers and are characterized by low pressure drop, high efficiency for particles above 5 μm, and the ability to recirculate the scrubbing water for long periods. A principal advantage of this device for the application described above is its ability to resist clogging by sticky water soluble sodium aerosol particles.

Experimental Apparatus and Procedures

Figure 1 is a diagram of our experimental wet cell washer. It consisted of a humidification section followed by three cells, the first two wetted and the last, a non-wetted mist eliminator. A downstream centrifugal blower drew the aerosol from the chamber through

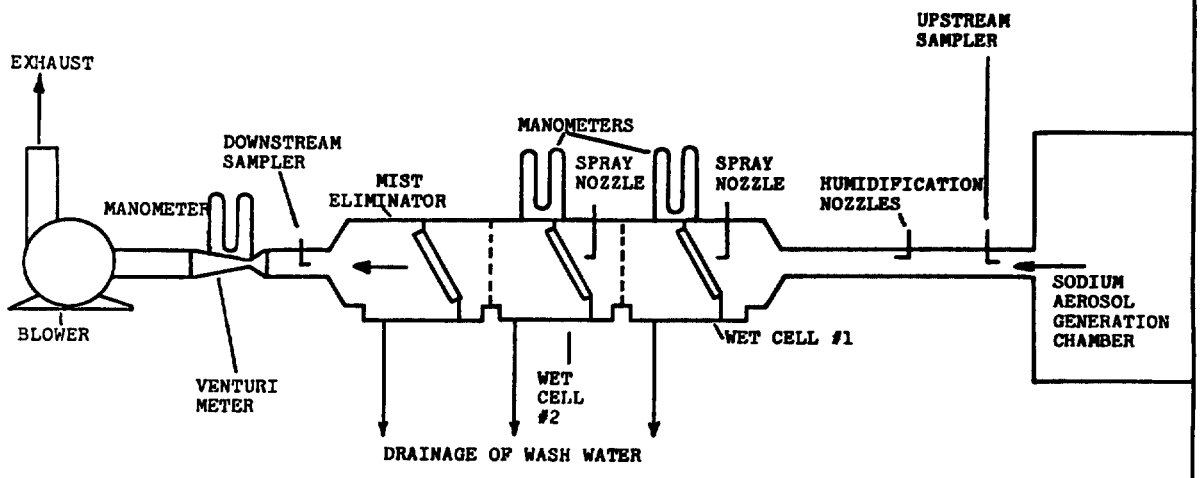

FIGURE 1. WET CELL WASHER

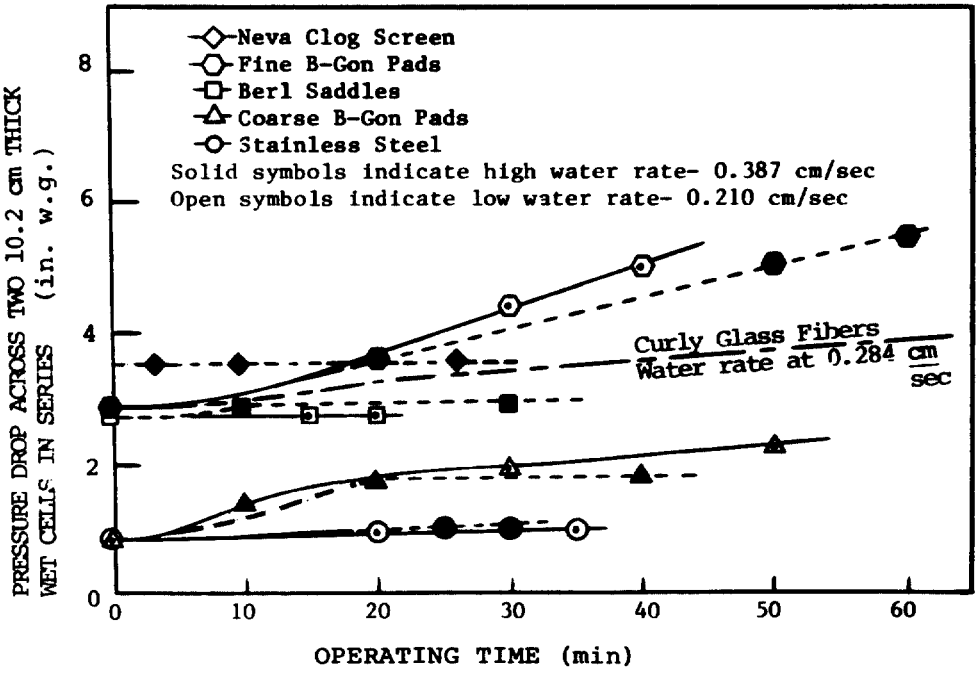

FIGURE 2. LOADING CHARACTERISTICS OF SIX PACKING MATERIALS AT 185 cm/sec

the humidification section and the scrubber unit. A Venturi meter, located downstream of the scrubber unit, measured air flow rate and liquid manometers were used to measure pressure drop across the cells. The upstream sampling port was located between the 90 m^3 aerosol generation chamber and the humidification section and the downstream sampling port was located after the mist eliminator cell. Cells up to 4" thick were mounted in a support frame sealed to the scrubber unit at a 45 degree angle to provide a 12" x 15" filter face area (820 cm^2 active area) in a 12" x 12" (30 cm x 30 cm) scrubber cross section. System air flow rates were 0.151 and 0.236 m^3/sec, giving filter face velocities of 185 and 289 cm/sec.

Experimental variables were cell construction, cell face velocity, spray water flow rate, option of prehumidification, and aerosol concentration. Experiments were conducted using a factorial design for each filter medium and two levels for system variables. A total of 30 runs were made providing 151 efficiency and pressure drop measurements. Tests were done in a random order and analyzed statistically to show the significance of each variable or combination.

Cells were filled with the packing materials at the porosities indicated in Table I.

Table I. Characteristics of cell packings.

Cell packing	Fiber Size	Packing Density	Porosity
curly glass fibers	35 μm	16 kg/m^3	.99
stainless steel fibers	50 μm	30 kg/m^3	.99
coarse B-GON* pads	410 μm	26 kg/m^3	.96
fine B-GON* pads	208 μm	31 kg/m^3	.96
ceramic Berl saddles	1/4" nominal	678 kg/m^3	.72

In addition to packed cells, a Neva-clog** screen was tested. It is constructed from two thin perforated stainless steel plates each having an array of 0.025 cm diameter holes on 0.075 cm centers with the holes in one plate offset from the other so that aerosol flow must bend twice. This induces interception and impaction of aerosol particles on and between the plates.

Two Spraying Systems 1/4 J atomizing nozzles, each spraying 45 cm^3/min, were used to humidify the sodium aerosol before it entered the first wet cell. These are two-fluid nozzles that use water and air pressure to produce a fine water spray with a high concentration of droplets in the 1-10 μm range.[2] Retention time in the humidification chamber was 1 sec.

Each wet cell is sprayed with a single Spraying Systems type 3/8" HH27W nozzle that produces a wide angle (120 degrees) solid cone

*Monofilament polypropylene fibers manufactured by Kimre Inc., Perrine, Florida 33157.
**Buffalo Forge Co., Buffalo, N.Y.

spray that covered the entire cell face. Water flow rates were 170 and 320 cm^3/sec to give a water rate per unit area of cell face of 0.210 to 0.390 $cm^3/sec/cm^2$. Water drained to a sump at the bottom of each cabinet from which it could be recirculated or sent to waste. The final stage was an unsprayed, 2" thick mist eliminator cell to remove entrained water droplets.

Sodium aerosols were generated in a 90 m^3 chamber. Elemental sodium was burned continuously in a heated steel pot to produce an aerosol of controlled concentration. A feed chute, 5 cm in diameter and 1.2 meters long and slanted 45 degrees from outside of the chamber to the sodium burning pot, was used to add small increments of sodium metal periodically throughout the course of each run. The rate of sodium addition was determined by monitoring the aerosol mass concentration in the chamber at ten minute intervals. In this manner, sodium fires were sustained for several hours and the sodium aerosol concentration maintained at 1 ± 0.2 gm/m^3 by the addition of 35 to 50 g/min to the pool fire. For aerosol concentrations greater than 1.0 g/m^3, sodium was added at the rate of 85 to 110 g/min and 1600 cm^3/sec of compressed air was directed onto the surface of the burning sodium pool to increase the burning rate by providing additional oxygen and turbulent mixing. Thermocouples were used to monitor the temperature of the sodium in the burning pot. Initially the burning pot was heated electrically, but rapid heater element failures led to the later use of a gas burner.

Sodium aerosol was withdrawn from the 90 m^3 aerosol chamber through a 25 cm diameter port that led to the prehumidification section upstream of the scrubber unit. Ports in the opposite chamber wall provided make up air. Other ports, located at mid-chamber height, were used to sample the chamber aerosol concentration. Chamber aerosol mass concentrations agreed with concentrations measured upstream of the scrubber unit, indicating negligible loss in the ductwork leading from the aerosol chamber to the scrubber unit.

Simultaneous isokinetic samples of the sodium aerosol concentration were collected up and downstream of the scrubber unit on all-glass absolute filter paper (MSA* 1106-B). After sampling was completed, and before the scrubber system was set to the next operating condition, the spray water rate to the cells was increased to about 0.5 $cm^3/sec/cm^2$ to clean the packing until the pressure drop across the filter had stabilized.

The deposit on sample filters was dissolved in 100 ml of deionized distilled water and the solution analyzed for sodium content by atomic absorption spectrophotometry. Because the all-glass filter paper contains some leachable sodium, measurements were corrected for filter blank which was less than a 0.5% correction. By careful dilution to the most sensitive range of the atomic absorption spectrophometer**, the sodium concentration was measured to an accuracy to ±

*Mine Safety Appliances, Pittsburg, PA
**Perkin-Elmer Model 360

0.03 µg/ml. From dilution calculations and the precision of the analysis the accuracy of the total sodium collection efficiency measurements was determined to within ±6%.

Eight stage Anderson 2000* cascade impactors were used at 28.3 lpm to determine the particle size distribution of the sodium aerosol upstream and downstream of the scrubber and the fractional efficiency for each cell packing. The cascade impactor measurements provided nine particle size ranges from 0.4 to 9.0 µm.

Results and Discussion

Pressure drop across two wet cells in series was measured at two water spray rates (0.210 and 0.387 $cm^3/sec/cm^2$) and at two face velocities (185 and 289 cm/sec). Pressure drop across the wet cells increased with increasing water rate, increasing face velocity, and, for some packing materials, with time of operation. Figure 2 presents pressure drop data at a face velocity of 185 cm/sec for each of the wetted cell packing materials as a function of exposure duration. The pressure drop of the fine and coarse B-GON pads increased more rapidly at the lower water spray rate than at the higher spray rate, but there was very little change in pressure drop at either water spray rate for the Berl saddles and stainless steel fiber packings.

In Figure 3, pressure drop across two wet cells as a function of scrubbing time is shown for the higher face velocity of 289 cm/sec. Again, the B-GON pads showed a greater pressure drop increase with time at the lower water spray rate, whereas Berl saddles and stainless steel fibers leveled off at a constant pressure drop after a small initial build up. Measurements of the pressure drop across individual cells indicated that an increase in pressure drop with time was a result solely of the increased resistance of the first cell.

Results of efficiency measurements for six packing materials are summarized in Table II in terms of the three dichotomous system variables: face velocity, water rate, and humidification. Except for one outlyer, the efficiencies ranged from 59 to 92% with a maximum range for any packing material of 20%. Because of the narrow range and the high variability of the results, no clear patterns emerge. This fact was confirmed by the factorial analysis which failed to show significance for any of the system variables or interactions. The most important, though non-significant, effect came from face velocity, followed by water rate, and then, by humidification. The results for the stainless steel fibers, based on the largest number of measurements, showed consistent but modest increases in efficiency with face velocity and humidification. It is noteworthy that prehumidification had a weak and inconsistent effect on efficiency. Apparently, these hydroscopic particles grow so rapidly that they reach full growth in the region of the cell spray water and prehumidification is unnecessary. The curly glass fibers deterioriated

*Andersen 200, Atlanta, GA

Table II. Sodium removal efficiencies in percent for 7 cell packing materials.

Cell Packing	185 cm/sec Face Velocity				289 cm/sec Face Velocity			
	Water Rate 0.210 $cm^3/sec/cm^2$		0.387 $cm^3/sec/cm^2$		0.210 $cm^3/sec/cm^2$		0.387 $cm^3/sec/cm^2$	
	Humidification		Humidification		Humidification		Humidification	
	No	Yes	No	Yes	No	Yes	No	Yes
Curly Glass Fibers	*86 (3)	*89 (17)	———	** 89 (10)	———	———	———	———
Neva Clog Screen	———	———	57 (4)	70 (5)	———	———	51 (4)	65 (6)
Neva Clog Screen and Curly Glass Fibers	———	———	———	** 90 (35)	———	———	———	———
Coarse B-GON Pads	61 (1)	63 (1)	59 (1)	70 (1)	60 (1)	66 (1)	68 (1)	73 (1)
Fine B-GON Pads	89 (1)	88 (1)	89 (1)	82 (1)	92 (1)	87 (1)	88 (1)	89 (1)
Stainless Steel Fibers	70 (3)	75 (4)	70 (3)	81 (5)	81 (3)	83 (3)	81 (3)	80 (7)
Porcelain Berl Saddles	62 (1)	49 (1)	81 (1)	68 (1)	63 (1)	68 (1)	72 (1)	61 (1)

number of observations shown in parentheses
*Water rate was 0.210-0.284 $cm^3/sec/cm^2$
**Water rate was 0.318-0.340 $cm^3/sec/cm^2$

Table III. Aerosol particle size characteristics.

Scrubber Run #	Chamber Aerosol Concentration (g/m^3)	Mass Median Diameter (μm)	Geometric Standard Deviation
19	0.75	1.58	2.03
20	0.96	1.63	1.90
21	0.85	1.57	2.01
22	0.88	1.50	2.37
23	1.05	1.58	2.10
25	0.82	1.70	2.12
26	1.02	1.33	1.95
27	0.88	1.38	2.14
28	4.75	1.48	1.84
29	4.75	1.41	1.56
30	0.96	1.37	2.09
Average of 11 measurements		1.50	2.01

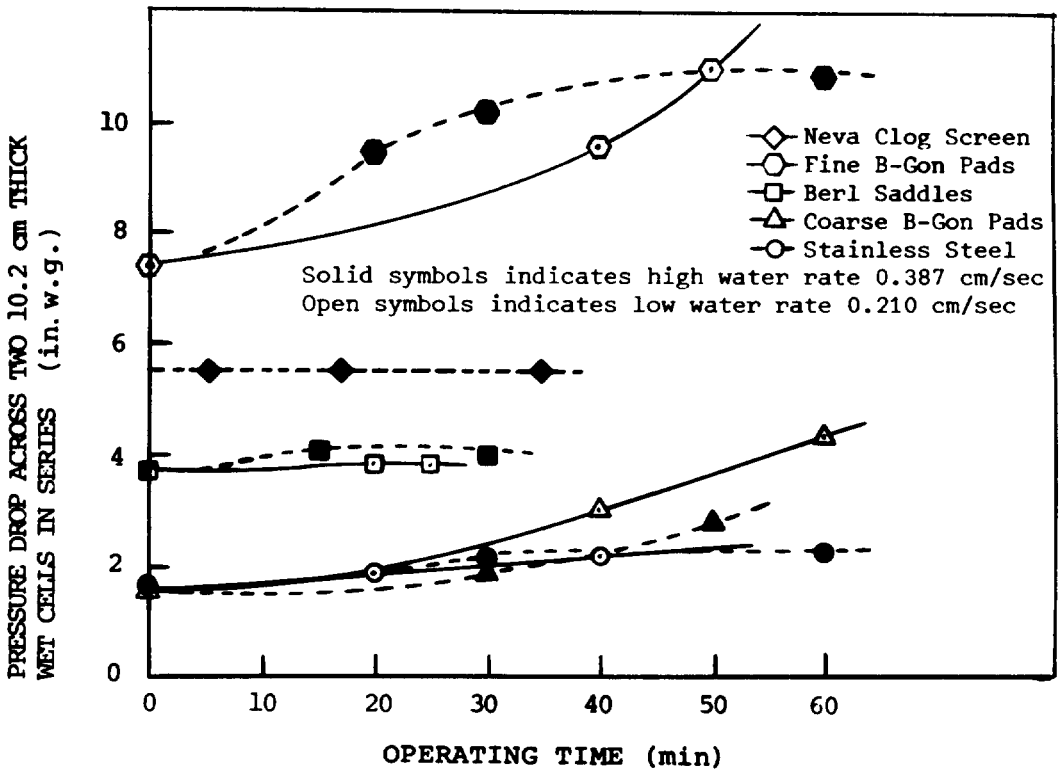

FIGURE 3. LOADING CHARACTERISTICS OF FIVE PACKING MATERIALS AT 289 cm/sec

noticeably after 90 minutes of exposure to the strong caustic scrubging solution whereas other materials showed no visible change after 8 hours of exposure.

A typical particle size distribution of the sodium fire aerosol upstream of the scrubber system is shown in Figure 4. All upstream size distributions showed a good fit to the log normal size distribution. Table III presents size distributions for several scrubber runs. The average Mass Median Diameter (MMD) was 1.50 μm with an average Geometric Standard Deviation (GSD) of 2.01. These particle size distributions are in reasonable agreement with data reported by Viles et al.[3] (i.e., MMD = 1.26 to 1.74 μm and GSD = 2.65 - 3.36 in a nitrogen atmosphere) and Lauben et al.[4] (MMD = 1.4 μm and GSD = 1.95).

Collection efficiency as a function of particle size was determined using up and downstream Anderson impactor sampling. Table IV presents the efficiency for 9 particle size ranges for each of the cell packing materials tested. In general, collection efficiency was near 100% for particle sizes larger than 2 or 3 μm. As shown in Figure 5, the lowest collection efficiency was found in the 0.40 μm to 1.1 μm particle size range. The increased efficiency for particles less than 0.5 μm shown in Figure 5 is not a result of diffusion of particles to collector surfaces. Although this mechanism becomes more effective as particle size decreases, it is comparatively weak for submicrometer particles. As shown in Table V, the predicted system efficiencies due to diffusion and impaction continue to decline as particle size decreases in the submicrometer range.

Table V. Calculated* scrubber efficiency due to diffusion and impaction for cells each packed with 10 cm of 50 μm diameter fibers.

Particle Size, μm	Eff. due to diffusion	Eff. due to impaction	Total eff.**
0.25	2.0%	0.05%	2.0%
0.55	1.1	4.5	5.5
0.9	0.8	34.7	35.4
1.6	0.6	98.6	98.6

*Efficiencies calculated using the methods described in reference (5).
**Assumes single fiber efficiencies for diffusion and impaction are additive.

The apparent increase in collection efficiency for particles less than 0.40 μm is thought to result from depletion of particle mass in this size range as a result of particle growth in the humid atmosphere rather than from collection. Growth by water adsorption occurs for all sizes of particles passing through the scrubber and shifts the size spectrum upward with a net reduction in the numbers of particles in the smallest sizes. This means that the smallest particles are depleted by growth to larger sizes and the larger particles are depleted by inertial removal, leaving an intermediate size

Table IV. Fractional efficiency of 5 packing materials

Cell Packing Material	Face Velocity cm/sec	Aerosol Particle Size Range, μm								
		<.40	0.4-0.7	.7-1.1	1.1-2.1	2.1-3.3	3.3-4.7	4.7-5.8	5.8-9.0	>9.0
Neva Clog Screen**	185	48	28	29	51	94	94	77	74	64
	289	67	58	49	67	67	100	67	83	95
Coarse B-GON	185	68	51	22	43	55	98	100	89	75
Fine B-GON	289	94	69	66	96	99	98	100	100	81
Stainless Steel	185	62	22	*	*	96	96	100	100	100
	289	71	39	42	85	100	100	100	100	100
Berl Saddles	185	95	57	*	*	95	100	100	100	100

* Unreliable data.

** Evaluated without mist eliminator stage.

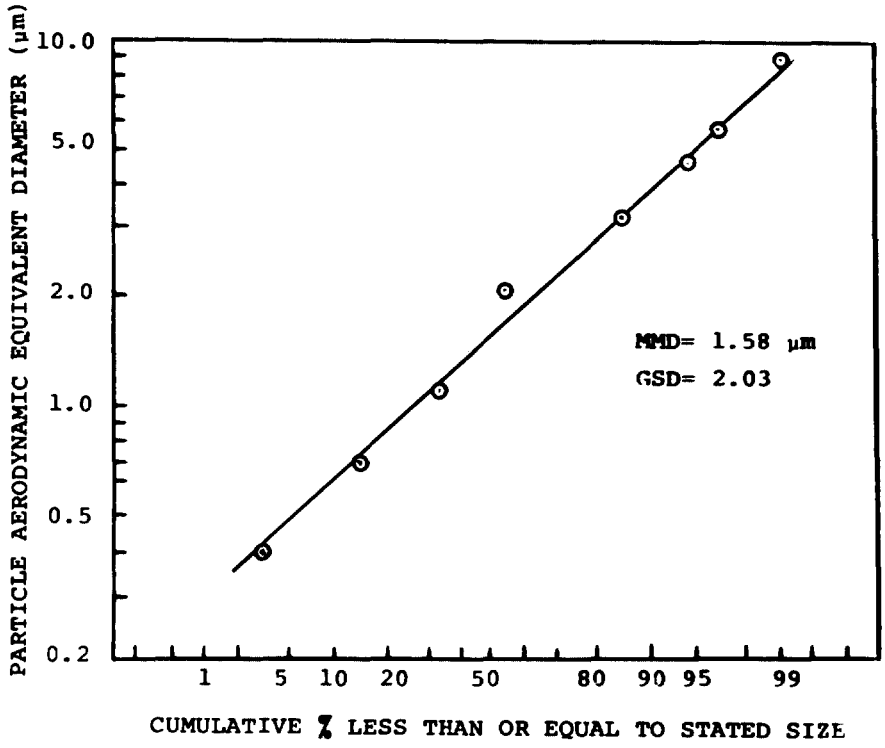

FIGURE 4. SODIUM FIRE AEROSOL INLET PARTICLE SIZE DISTRIBUTION

Figure 5
Fractional Efficiency

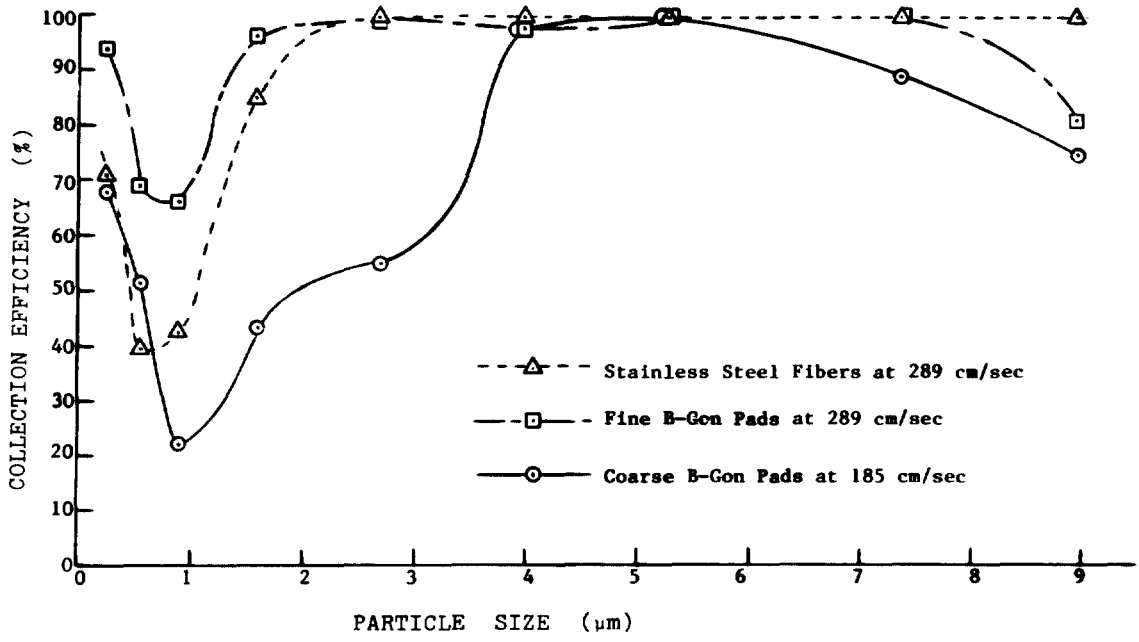

FIGURE 5. FRACTIONAL EFFICIENCY

of maximum penetration. The size of maximum penetration depends on the inertial removal characteristics of the scrubber, the particle size distribution, and the particle size growth that occurs in the scrubber. For this particular system, i.e., a sodium pool fire in a normal atmosphere and a wet cell scrubber operated as described above, the apparent particle size for maximum penetration occurred between 0.5 and 1.0 μm.

Conclusions

Based on the results presented here, it may be concluded that it is feasible to use a wet cell scrubber upstream of a HEPA filter to reduce the loading of sodium combustion aerosol reaching the HEPA filter by a factor of ten or more (depending on scrubber size) for a period of many hours. A satisfactory design requires at least three cells in series, a face velocity of 200-300 cm/sec, and a water rate of .400 $cm^3/sec/cm^2$.

The most satisfactory single packing material studied was 50 μm diameter stainless steel fibers at a face velocity of 289 cm/sec. This material gave the lowest pressure drop and showed little tendency to clog when operated at a water rate of 0.387 $cm^3/sec/cm^2$. At this operating condition, typical sodium fire aerosols were removed by two 10 cm deep beds in series at efficiencies in the 80-90% range. Although the fine B-GON pads gave higher efficiencies than the stainless steel fibers, they were unsatisfactory because the flow resistance of the B-GON pads increased with time for all operating conditions as a result of incomplete wetting.

Combinations of packing materials may provide better performance than the use of a single material. Because the cell packings that gave the highest efficiencies tended to clog with time, they should be preceded by non-clogging, though lower efficiency, cells in a manner similar to a graded fiber diameter deep bed filter, i.e., the upstream cells would reduce the loading on the high efficiency cell so that the latter would never clog or would clog at an acceptably slower rate. Such a system might consist of a Neva-clog screen or ¼" Berl saddles for the first cell (which would remove about 60% of the particulate mass but would not clog under any realistic conditions), a second cell of 50 μm stainless steel fibers which would capture an additional 25 to 30%, and a final cell of 35 μm stainless steel fibers which would ensure an overall efficiency in excess of 90%. Such a system would operate for 7 to 10 hours at a face velocity of 185 cm/sec and an inlet concentration of 1 gm/m^3 before it increased in resistance by one inch of water.

The curly glass fibers displayed inadequate chemical resistance to sodium fire aerosol after 90 minutes exposure, but other materials showed no visible change after 8 hours of exposure.

It was found that there is little advantage to using a prehumidification stage. This space could be used more profitably by installing a low resistance, non-clogging stage to reduce the possibility of clogging of subsequent stages.

Packing materials that were non-clogging at an aerosol concentration of 1 gm/m^3 were also non-clogging at 5 gm/m^3.

Because cells clog rapidly without continuous application of water, the water system must be designed to preclude even momentary interruptions of water and the water spray must be initiated prior to aerosol flow.

Although the use of a high water rate, 0.387 $cm^3/sec/cm^2$, had little effect on system efficiency, it prevented or reduced the rate of clogging.

The combined effect of particle growth by humidification and particle capture in the scrubber resulted in a most penetrating particle size. For the conditions evaluated, this size was between 0.5 and 1.0 μm.

Acknowledgement

Support for this research was provided by the U.S. Department of Energy under contract No. EY-76-S-02-2801.

References

1. Dennis, R., Kristal, E., and Silverman, L., "Fibrous Filters for NaK Fume Removal," USAEC Report NYO-4811, Harvard Air Cleaning Laboratory, May 1960.

2. First, M.W. and Leith, D.H., "Entrainment Separator Performance," Fourteenth Air Cleaning Conference, Sun Valley, Idaho, August, 1976, NTIS CONF-760822.

3. Viles, F.J., Jr., Himot, P., and First, M.W., "High Capacity-High Efficiency Filters for Sodium Aerosols," USAEC Report NYO-841-10, HACL, August, 1967.

4. Lauben, G.N., Koontz, R.L., Greenfield, M.A., and Nelson, C.T., "Study of Sodium Fires and Particle Release as Applied to the FRCTF," NAA-SR-MEMO 11403, Atomics International, June, 1965.

5. Davies, C.N., "Air Filtration," Academic Press, New York (1973).

DISCUSSION

BURCHSTED: The efficiencies shown are mass efficiencies, are they not?

HINDS: Yes, they are sodium mass efficiencies determined by atomic absorption measurements of up- and downstream filters.

ALVARES: When you turned the water off and you got plugging, were you able to unplug by turning the water back on again?

HINDS: When we turned the water off, it wasn't intentional; the line broke and we paid complete attention to getting the line fixed. We ended up abandoning the whole test from then on. I don't think we ever made that particular test, but I believe it would be successful.

ALVARES: Did you ever run a HEPA filter downstream?

HINDS: No.

ALVARES: Why have no downstream HEPAs been installed to validate the performance of the scrubber?

HINDS: The objective of this study was to test only the performance of the scrubber. I believe tests such as you are asking for are planned at Hanford Engineering Development Laboratory.

HILLIARD: I suggest that your test aerosol was actually prehumidified in the test cell since high humidity air existed due to inflow and also to the gas-heated sodium system.

HINDS: We did allow room air to go into the chamber at about 40% relative humidity. Also, we had a burner that produced both CO_2 and water vapor, so there was significant moisture present.

HILLIARD: It looked from your slide as if you took the water exit streams and put them into a common pool. Did you ever measure the concentration in the liquid from the separate stages?

HINDS: We never measured it from the separate stages.

HILLIARD: I am interested in the carryover from the demister. Did you measure its efficiency as a function of the concentration in the water? Did you recirculate the scrubber liquid?

HINDS: No, we did not recirculate the scrubber liquid, except during some preliminary trials. For the rest, we used a once through water system and did not measure the sodium concentrations in the waste water downstream. I should mention that we measured efficiency by atomic absorption based on the amount of sodium atoms present, rather than by mass, to avoid the quantification problems associated with moisture pickup by the sodium oxide particles.

HILLIARD: I would comment that you were right when you said a wet scrubber can take a larger sodium oxide loading than a filter system. But, I think the loading is probably not infinite because you have to have a supply of water and even if you recirculate, there is a limit to solubility, especially for sodium carbonate. It requires a rather large water storage capacity.

BROWN: Did you prepare a particle growth model which would account for the minimum in your curve or did you just hypothesize that particle growth occurred?

HINDS: We based the growth on work done by Clough and Garland (AERER 6460, 1970) in the UK in which they traced out curves of expected growth for different compositions of particles at different humidities from 50 to 100%. It is about a factor of three growth in diameter for our conditions.

BROWN: So the small particles grow at a rate so fast that it accounts for the minimum in the curve? I could see how they would change the shape of the curve, but the minimum seems unusual.

HINDS: The minimum is a result of the way we measure efficiency, i.e., measuring upstream and downstream of the whole system. The fact is that there aren't any of these little particles left because they have all grown to be big particles. They haven't been collected in the traditional sense.

BROWN: I understand that but I would also think that intermediate sized particles would grow at a somewhat slower rate.

HINDS: All particle sizes grow very rapidly and the difference in rate is not enough to conclude that the largest particles are not going to grow very much.

BROWN: Solution of the set of differential equations for lumped particle size groupings should be done to verify the hypothesis of a minimum in your collection efficiency. Does a mathematical model of particle growth predict the observed minimum in collection efficiency?

HINDS: Such an analysis was not done and is not necessary. The paper by Clough and Garland (AERER 6460 (1970)) shows that particles less than 2 μm in diameter, the particles of interest here, grow to an equilibrium size at a relative humidity of 99% in 0.01 sec. This growth is about three-fold for all particle sizes and is completed prior to a particle's arrival at the first wet cell.

ENHANCED FILTRATION PROGRAM AT LLL - A PROGRESS REPORT*

W. Bergman, R. D. Taylor, H. H. Miller, A. H. Biermann,
H. D. Hebard, R. A. daRoza, and B. Y. Lum

Lawrence Livermore Laboratory, Livermore, California

Abstract

As part of Lawrence Livermore Laboratory's Enhanced Filtration Program, we are investigating the use of an externally applied electric field to improve the performance of fibrous filters. Our objective in this program is to develop filtration systems for the nuclear industry that will reduce the cost and volume of nuclear waste associated with present systems.

We have developed a new theory of the electrostatic filter that is consistent with experimental tests made during transient and steady-state conditions. For these tests, we used ac and dc electric fields, insulated and noninsulated electrodes, and conducting and nonconducting filter media; all tests were conducted in our small-scale 25 l/s test system, using sodium chloride aerosols. Our theory employs a new mechanism based on the attraction between charged particles and charged fibers in addition to the previously proposed mechanism based on the attraction between charged particles and polarized fibers. In this theory, fibers are charged when charged particles deposit on them.

We have also developed a theoretical model that explains the increase in filter efficiency and pressure drop when particles load on the filter. The filter loading tests we conducted to evaluate this model verify its accuracy to a remarkable degree. By using the model equations, we are thus able to explain the observed increase in filter efficiency as a function of particle mass loading, particle size, and particle-particle collection efficiency. The increase in filter pressure drop also agrees quantitatively with experiments involving different air flow velocities and particle sizes. We have also conducted experimental loading tests using external electric fields with insulated and noninsulated electrodes. In both cases, our test results showed that application of an electric field increases filter efficiency and reduces pressure drop compared to similar tests without an electric field.

Two systems we developed for use in the nuclear industry use electric fields to increase the performance of fibrous filters. One is designed for use inside glove boxes to control radioactive particles at their source; the other is designed for use in ventilation systems. Here we report the results of laboratory and field evaluations for the glove box system.

I. Introduction

The high-efficiency particulate-air (HEPA) filters used in the nuclear industry to remove radioactive airborne contaminants are extremely effective and practical devices and will continue to be so despite the large number of new control devices presently available. However, HEPA filters generate a significant volume of radioactive waste and are costly to purchase and operate. The actual cost of materials and labor to buy, change, test, and dispose of a HEPA filter is several times its initial purchase price.

*This work was performed under the auspices of the U.S. Department of Energy by the Lawrence Livermore Laboratory under contract No. W-7405-ENG-48.

In an effort to reduce the HEPA's operational cost and the volume of radioactive waste it generates, the Nuclear Fuel Cycle and Production Division of the Department of Energy (DOE) has contracted with Lawrence Livermore Laboratory (LLL) to develop an enhanced filtration system that will extend the service life of HEPA filters. The approach selected by LLL consists of using an electrostatic prefilter to take the load off the HEPA filter since it appears to have a greater potential for success than such methods as scrubbers and electrostatic precipitators. The total cost of and volume of radioactive waste generated by the prefilter-HEPA filter system were assumed to be significantly less than the corresponding cost and waste from a system consisting of only a HEPA filter.

II. Previous Studies

Electrostatic filters are relatively old air cleaning devices that have been investigated since 1930. Although they can have a number of different configurations, all are based on charging or polarizing filter fibers to generate an electric force between the fibers and charged particles.

The first electrostatic filter was developed in 1930 by Hansen, who found that mixing a powdered resin with wool fibers greatly improved the resulting filter efficiency[1]. The resin particles that coated the fibers were highly charged in the mixing process thereby, in effect, producing charged fibers. This type of electrostatic filter is widely used today, especially in respirators. Unfortunately resin filters are ruined when they are exposed to organic vapors that dissolve the resin or to ionizing radiation that neutralizes the resin charge.

Recognizing the problem of charge dissipation in the resin filter, a number of investigators have developed methods to continuously recharge the filter by generating charged aerosols upstream of the filter. In a method developed by Rossano and Silverman in 1954, an electric corona was used to charge particles before they entered the filter[2]. These charged particles were initially trapped in the filter by image forces until the fibers acquired a high charge density. Further particle trapping occurred primarily from Coulombic forces between charged fibers and charged particles. Reid and Browne have recently repeated these experiments and have shown high filter efficiencies[3]. Another method for continuously recharging the filter was proposed by Mazumder and Thomas in 1967[4]. Instead of charging the aerosols to be filtered, they injected a charged mist into the air stream in front of the filter. The charged mist would then be trapped by the filter fibers and effectively charge them. Oncoming aerosols would then be collected by Coulombic forces between the aerosols and the charged fibers. In another method, developed by Silverman et al, electrostatic charges were generated on fibers by rubbing the downstream side of the filter with a windshield wiper[5].

Electrostatic filters can also be generated by polarizing the fibers with an external electric field. Although these electrostatic filters have been commercially available since the early 1950's, they have not been widely used. In 1954, Silverman et al evaluated several commercial electrostatic filters that consisted of glass fiber matts sandwiched between a high voltage and a ground screen[5]. Since that time, a large number of theoretical and experimental investigations have been made on the electrostatic filter. In 1961, Havlicek reported he was able to increase the filter efficiency for potassium dichromate particles from 55% to 99.98% by applying an electric field of 10 kV/cm[6]. The pressure drop across the filter at 20 cm/s was 150 Pa.

An excellent review of electrostatic filters up to 1972 was given by Davies[1]. The theoretical investigations showed the increase in filter efficiency with an applied electric field resulted from two electrical forces that arose from both polarized particles and fibers and from charged particles and polarized fibers. A good elementary description of these two forces was given by Rivers[7].

In recent years, the number of studies dealing with electrostatic filters generated by an external electric field has significantly increased. These studies have become international with research groups in Russia (Kirsch[8]), Germany (Walkenhorst and Zebel[9]), Japan (Iinoya[10]), and the United States (Bogardus[11], Lamb[12], Ariman[13], Hill[14], Frederick[15], and Penney[16]) investigating various aspects of the electrostatic filter. Most of these studies are concerned with parameters that affect the well-established increase in filter efficiency due to the external electric field. However, Frederick reported in 1975 that the electrostatic filter also had a significantly lower pressure drop than the same filter without an applied electric field[15]. Lamb and Costanza[12] and Penney[16] have also observed large reductions in filter pressure drop with an external electric field. These results indicate electrostatic filters have a longer service life than standard filters.

Electrostatic filters have also been developed with a combination of particle charging and an external electric field. Thomas and Woodfin filled the space between plates of an electrostatic precipitator with glass fiber medium and observed a large increase in performance compared to the precipitator or to the filter alone[17]. In this configuration, applied high voltage generates an external electric field; it also generates ions in the same region by a corona discharge. This complicates system analysis because polarized and charged fibers now fill the normally open regions of an electrostatic precipitator.

Hybrid electrostatic filters can also be built by having separate regions for both particle charging and filtration. Inculet and Castle have evaluated a two-stage electrostatic filter having a concentric geometry[18]. Particles charged by a corona discharge in the first stage are then trapped in a second stage that consists of a filter medium with a superimposed electric field.

Although any of the variety of electrostatic filters discussed above could be used in our Enhanced Filtration Program, we selected a method using a fibrous filter with a superimposed electric field because it, unlike the other methods, did not involve a corona discharge. Systems that use a corona discharge have a much higher energy consumption and pose a greater fire risk than the electrostatic filter we selected.

We have been investigating the use of applied electric fields on fibrous filters since October 1975 and presented the first results of our investigation at the 14th ERDA Air Cleaning Conference[19]. Similar to a previous study by Bogardus et al, our investigation dealt with the empirical effects of air flow, electric field strength, and different filter media on filter efficiency[11]. We then made a more extensive analysis of the theoretical and experimental effects of face velocity, particle charge and size, filter void volume, and fiber size[20]. We found most of our experimental measurements qualitatively agreed with Zebel's theory on charged particles and polarized fibers[21]. The results of our most recent work cover a period from January 1977 to June 1978 and are presented in this paper. Since the Enhanced Filtration Program at LLL is a continuing effort, many of the topics presented here are still under investigation.

III. Theory and Small-Scale Experiments

A review of the test results from our early investigations shows we have treated the electrostatic filter as an oversimplified static system[19,20] when it is, in fact, a very complex dynamic system that involves both mechanical and electrical forces. Perhaps the most well-known dynamic process is the increase in filter efficiency and pressure drop that occurs during filter clogging. A good understanding of the detailed filtration mechanisms that control filter efficiency and pressure drop is essential for designing an optimum electrostatic filter. In Table I, we qualitatively summarize the relative effort expended on and the level of understanding of the mechanical and electrical filtration mechanisms.

We have made separate entries for clean and clogged filters to emphasize the significant changes that occur when the filter becomes clogged.

Table I. State of the Art in Filtration

Filter Condition	Filtration Mechanism	
	Mechanical	Electrical
Clean	Extensively studied Moderately understood	Moderately studied Poorly understood
Clogged	Moderately studied Poorly understood	Negligibly studied Not understood

Table I shows the level of understanding of filtration mechanisms reflects the extent of investigation.

Although we are concerned with developing an electrostatic filter, we must understand the mechanical and electrical mechanisms to optimize filter design. The effect of face velocity on filter efficiency illustrates this point. Increasing the face velocity increases filter efficiency for mechanical mechanisms (primarily inertia) but decreases filter efficiency for electrical mechanisms. Since the efficiency of an electrostatic filter depends on both mechanical and electrical mechanisms, both must be considered in developing an optimum design.

The objective of our theoretical studies and small-scale experiments was to understand the mechanical and electrical filtration mechanisms for both clean and clogged filters in sufficient detail to optimize the electrostatic filter. A survey of Table I shows the only reasonably well understood filtration mechanisms are the mechanical mechanisms for clean filters. Therefore, to reach our objective, we had to investigate and develop theories for the remaining filtration mechanisms shown in Table I. We have already met our objective for the electrical mechanisms for a clean filter and the mechanical mechanisms for a clogged filter. The results of these investigations are presented in this paper. We are currently investigating the electrical filtration mechanisms for a clogged filter.

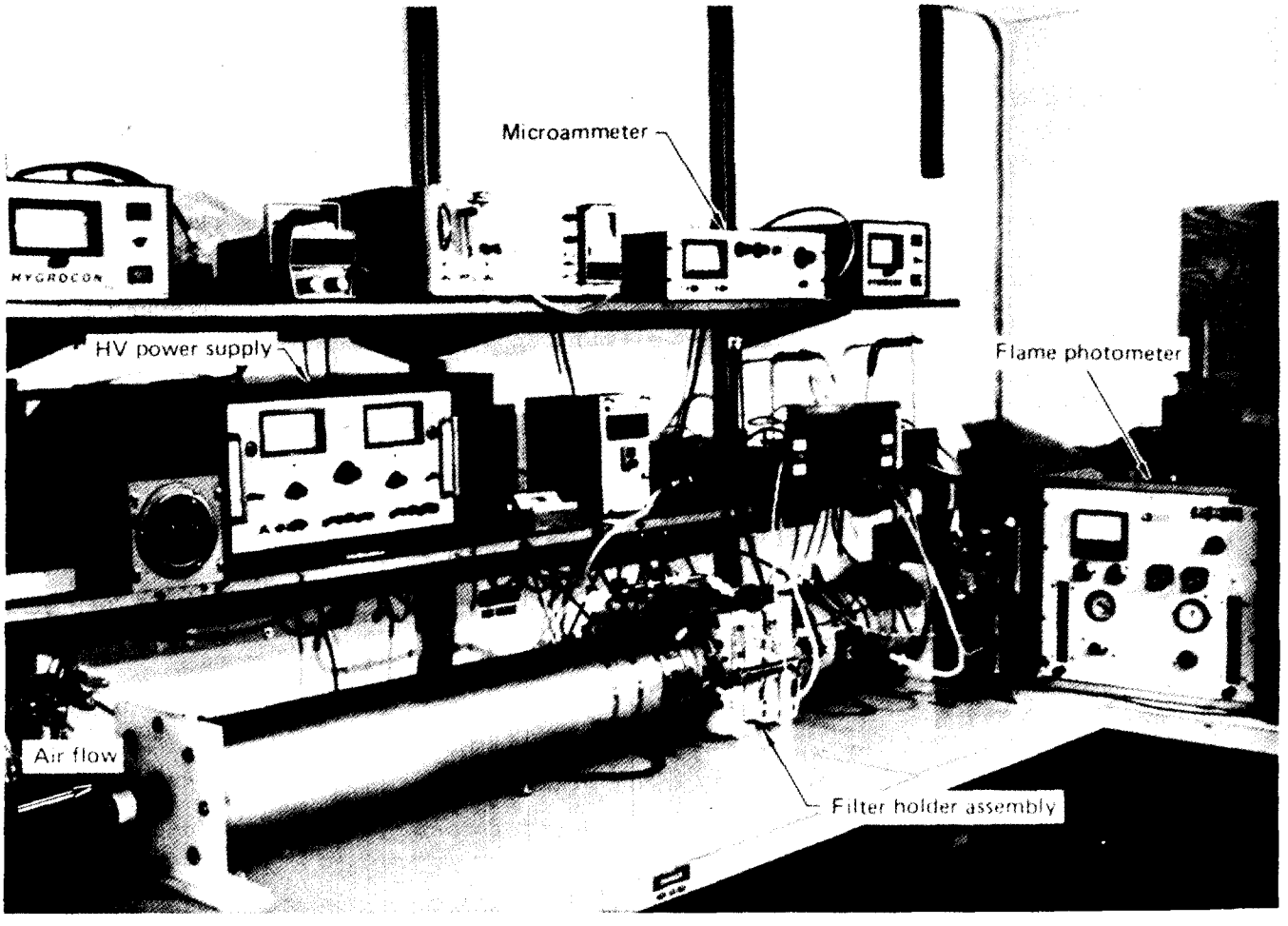

Figure 1 Small-scale filter test facility.

Experimental apparatus

The experimental apparatus used to generate the data presented in this section is shown in Fig. 1. Sodium chloride aerosols (ammd = 1.0 μm, σ_g = 2.0) were generated using Wright nebulizers (not shown) and were passed through a flexible hose into a 20.3 cm-i.d. tube[19]. A Stairmand disk installed at the tube entrance promoted uniform mixing of the aerosols. The relative humidity of air in the duct generally fell between 40-60%. Measurements of air velocity and salt concentrations were taken across the duct and indicated a uniform distribution.

The electrostatic filter unit was mounted in the filter holder assembly and was energized with the high-voltage power supply. Efficiencies were determined by measuring the salt concentration before and after the filter with the flame photometer. Pressure drop measurements were also taken across the filter for each test. In certain experiments, a microammeter was used to measure current bleeding from the electrostatic filter. A more detailed picture of the filter holder assembly is shown in Fig. 2; here the filter holder is partially removed from the assembly to expose the electrode. Figure 3 shows the filter holder disassembled, with the perforated electrodes, glass-fiber filter, and spacer arranged in the same sequence as in the assembled unit. High voltage was applied to the rear electrode and the front electrode was grounded.

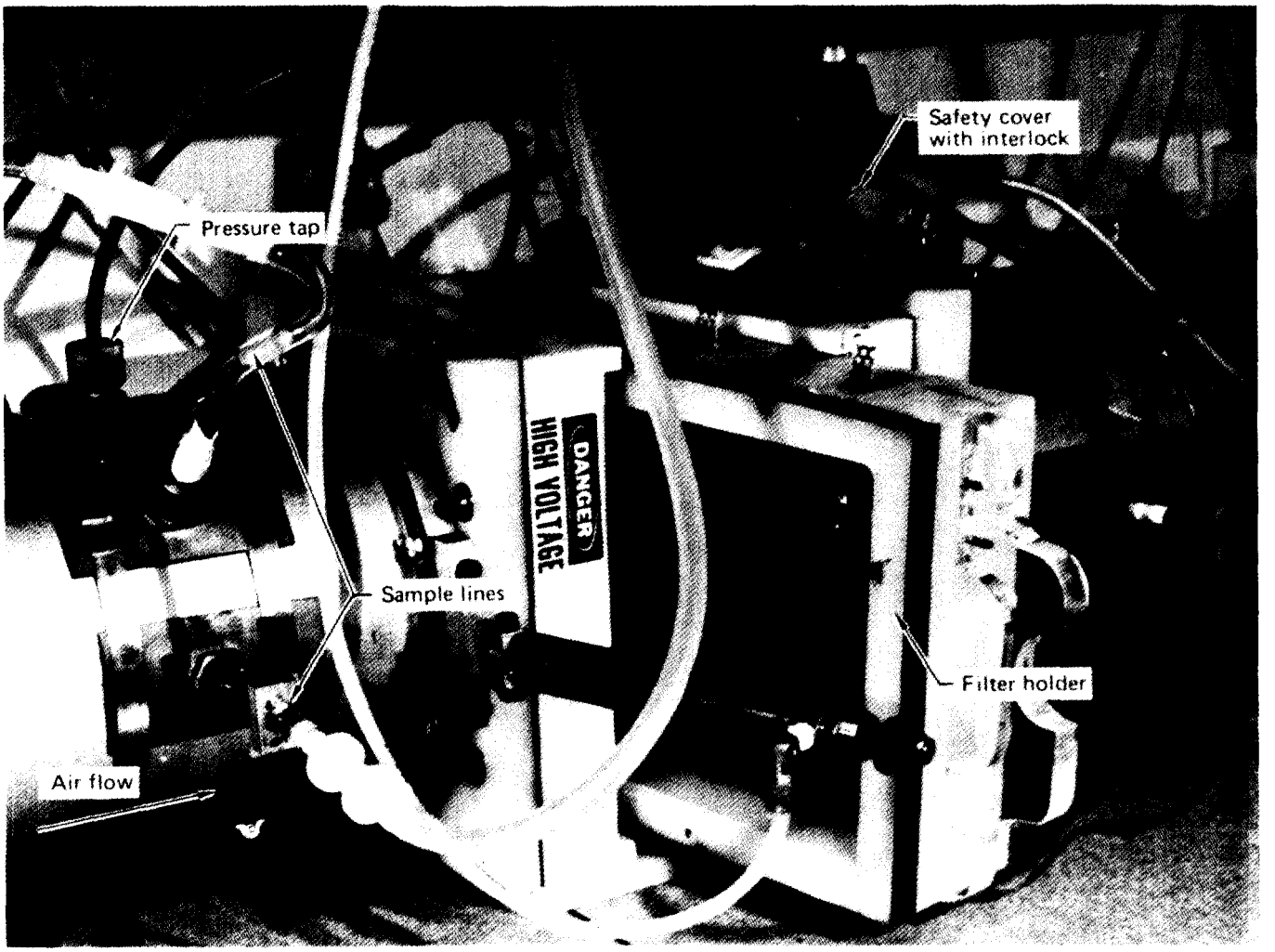

Figure 2 Filter holder assembly showing the filter holder partially removed.

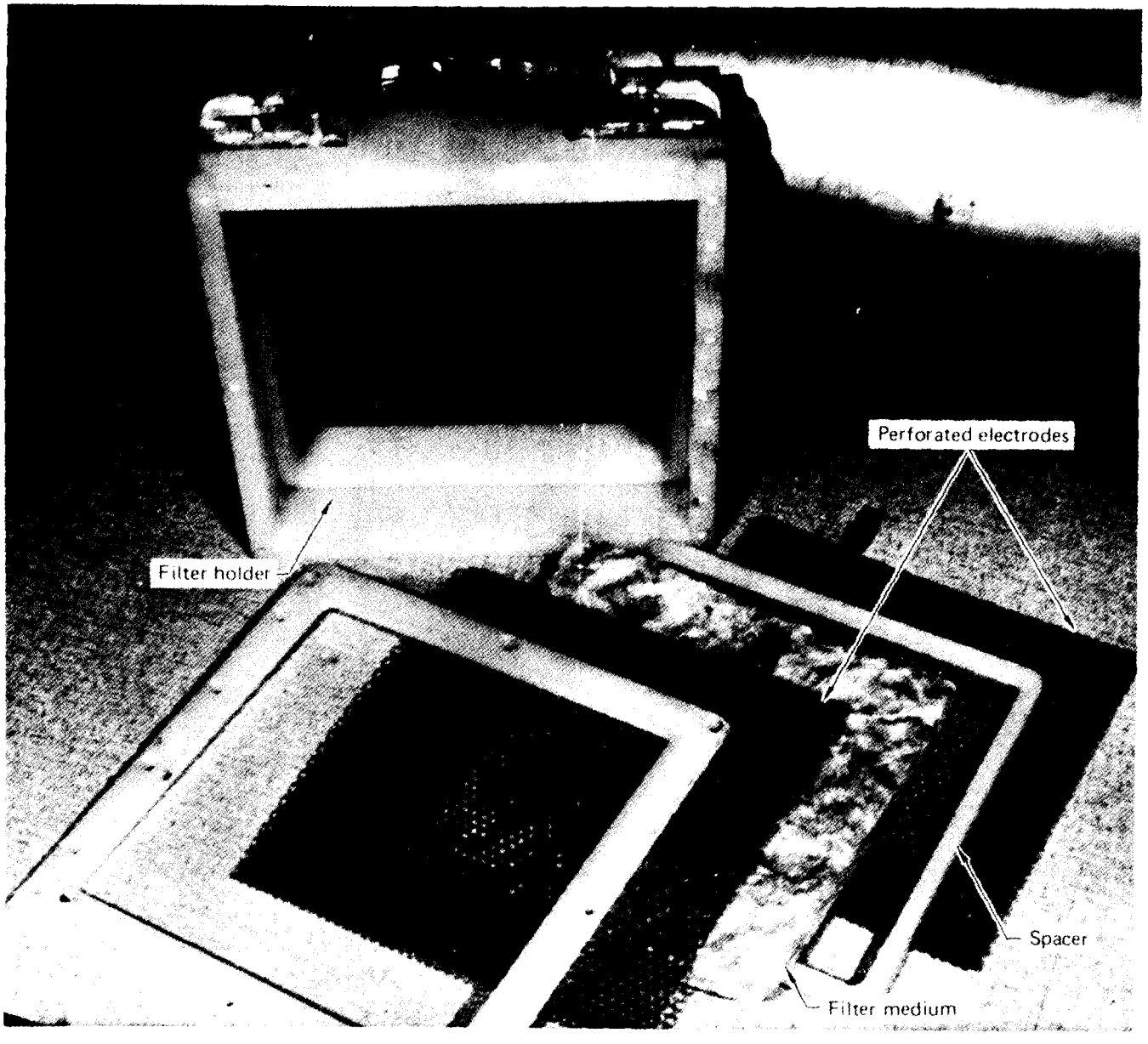

Figure 3 Disassembled filter holder.

Extension of Filtration Theories for Fiber Size Distribution

Filtration theories are based on the premise that all filtration parameters such as fiber and particle size are monodisperse. However, in laboratory experiments most, if not all, filtration parameters have a distribution of values. The most common exception is particle size, which can be frequently treated as a monodisperse distribution. This is possible because modern particle size analyzers are able to measure small size intervals independently of other particle sizes. Measurements of filter efficiency within this size interval are, therefore, independent of efficiencies at other sizes. Efficiencies can also be determined with monodisperse aerosols because of commercially available latex particles in a wide range of monodisperse sizes. However, in spite of the availability of accurate particle size analyzers and monodisperse aerosols, most filter efficiencies are determined with heterodisperse aerosols using instruments that measure an unknown average of the size distribution.

The common practice is to take an arbitrary* average of the distribution for each parameter and treat this average as a monodisperse value. Even if the correct average were obtained, it may still be wrong to treat the average value of a parameter as a monodisperse value since products and quotients of parameters are generally involved in filtration equations. It is well known in mathematics that the average of a product is not equal to the product of the averages. Recognizing the problems that may occur when treating parameters having a distribution of values as a single value, we have been investigating how these distributions affect filter efficiencies and pressure drops.

Since fiber size is the most difficult filtration parameter to control in experimental systems, we began our distribution studies by determining the effect of fiber size distributions on filter pressure drop. Pressure drop was selected rather than efficiency because no particle parameters were involved in the equations. The objective of this study was to modify the pressure drop equation for monodisperse fiber sizes to allow for a distribution of fiber sizes.

Pressure Drop Theories

Although a number of pressure drop theories could be used as the basis for our heterodisperse model, we have considered only those theories that agree with Darcy's law, which states the pressure drop per unit flow velocity is a constant at any velocity[1]. Theories based on flow around isolated fibers, like the frequently used Lamb's theory, do not agree with Darcy's law and were, therefore, not considered in our investigation. The problem with these theories is their failure to account for the influence of neighboring fibers on flow patterns.

Several models have been developed that include the interaction from neighboring fibers. The most popular of these models, e.g., the Kuwabara[22] and Happel[23] models, are called "cell models" because the streamlines form closed cells around each fiber within the filter mat. Spielman and Goren have developed a flow model wherein neighboring fibers create a dampening force on the fluid passing around each fiber[24]. This model is less popular than the cell models presumably because Spielman and Goren's complicated equations involve Bessel functions.

* The average of the distribution selected is usually arbitrary because it is based on the device used to generate the distribution. For example, the average fiber size obtained from an electron microscopy study is normally chosen to be a number average without considering whether this average is the correct one for predicting filter efficiency or pressure drop.

The pressure drop for all the models can be described by Eq. (1)

$$\Delta P = \frac{4\alpha\mu VX}{R^2}\Phi(\alpha), \tag{1}$$

where:

ΔP = pressure drop (Pa)

α = vol fraction of fibers

μ = viscosity (Pa•s) of gas

V = velocity (cm/s) of gas

X = filter thickness (cm)

R = fiber radius (cm)

$\Phi(\alpha)$ = function of α (varies with model)

The function Φ represents a dimensionless pressure drop that has been normalized for all variables except α.

Pressure Drop Theory with Fiber Size Distribution

The pressure drop for a filter mat with a heterodisperse fiber size distribution can be derived by taking weighted averages of Eq. (1) subject to certain constraints. Although the specifics will be presented elsewhere, the physical basis for this derivation can be readily explained. Beginning with a filter mat having a uniform fiber size, one decreases and increases individual fibers until the desired distribution is obtained. The constraint in this process is that the total length of the fibers within the filter remain constant. In terms of the cell models, this constraint requires that the total number of flow cells remain constant. The weighting factors are then the fraction of the total fiber length or the fraction of the total number of flow cells having a given fiber size.

We have used an empirical pressure drop equation obtained by Davies to illustrate how the pressure drop changes for a distribution of fiber sizes[25]. Davies' equation was chosen over other theories because it is simpler, obeys Eq. (1), and represents experimental data. Although any of the other theories could also be used as a starting point for the heterodisperse model, the resulting equation would be much more complex.

$$\frac{\Delta P}{\mu VX} = 16\,\frac{\alpha^{3/2}}{R^2}\,. \tag{2}$$

For a distribution of fiber sizes, we can show that

$$\frac{\Delta P}{\mu VX} = 16\,\alpha^{3/2}\,\frac{\int_0^\infty N(R)R\,dR}{\left(\int_0^\infty N(R)R^2\,dR\right)^{3/2}}\,, \tag{3}$$

where N(R) represents the number of fibers having a radius R. This equation is useful for calculating pressure drops when the distribution of fiber sizes is obtained from electron microscopy. By combining Eqns. (2) and (3), we can calculate the effective fiber radius R_{EF} if the number-size distribution is known.

$$R_{EF}^2 = \frac{\left(\int_0^\infty N(R)R^2dR\right)^{3/2}}{\int_0^\infty N(R)RdR}, \tag{4}$$

However, if the mass distribution of different size fibers is known, Eq. (5) is more useful.

$$\frac{\Delta P}{\mu VX} = 16\left(\int_0^\infty \frac{\alpha dR}{R^2}\right)^{1/2}\int_0^\infty \frac{\alpha dR}{R}. \tag{5}$$

Equations (3) and (5) are different forms of the same equations.

If the number (or mass) distribution of fibers is known to obey the log-normal distribution, we can integrate Eq. (3) or (5) analytically, yielding

$$R_{EF} = R_{NMR}\exp(1.25\ \ell n^2\sigma_g) \tag{6}$$

where R_{NMR} is the number median radius and σ_g is the geometric standard deviation of the distribution.

Comparing Experimental Measurements with Theory

We took a series of electron micrographs of three filter media to determine fiber-size distributions. Figure 4 shows typical electron micrographs of filters AF-4, -11, and -18* at the same magnification. Note the AF-4 filter resembles tangled string while the AF-11 and -18 filters look like log jams. Using a Zeiss counter, we did a detailed size analysis of a large number of fibers and plotted the results on a log-probability graph. Since the data for AF-4 fell on a straight line, they can be represented by a log-normal distribution. The data for AF-11 and -18 did not fall on a straight line; however, a reasonably good straight line fit can be made for the central portion of the distribution. The number median diameters NMD and geometric standard deviations σ_g were obtained from the three lines.

An alternate method of displaying the fiber-size distribution is seen in Fig. 5, where the relative number of fibers per unit-size interval is plotted as a function of fiber diameter. The number median diameter D_{NMD} and the effective diameter D_{EF} (calculated from Eq. 6) are shown on the histograph. When distributions do not obey a standard equation, fiber-size statistics can only be determined from histographs (as shown in Fig. 5) or corresponding tabulated data.

* The filters designed at AF numbers represent commercially available filters from Johns Manville. The suffix number is a relative indication of the fiber size, which increases for larger numbers.

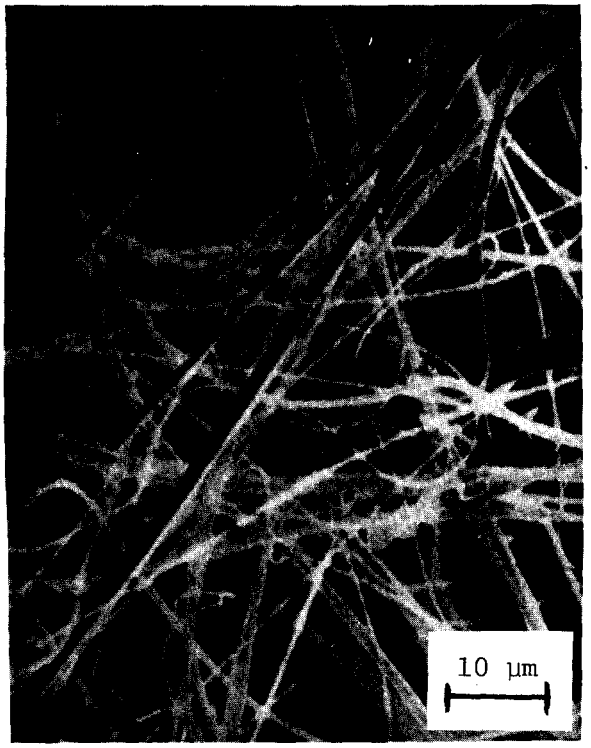

AF-4

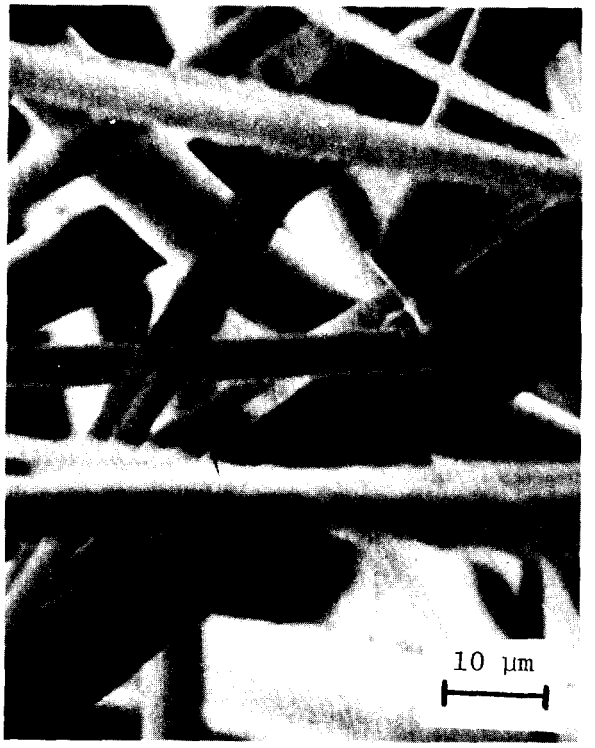

AF-11

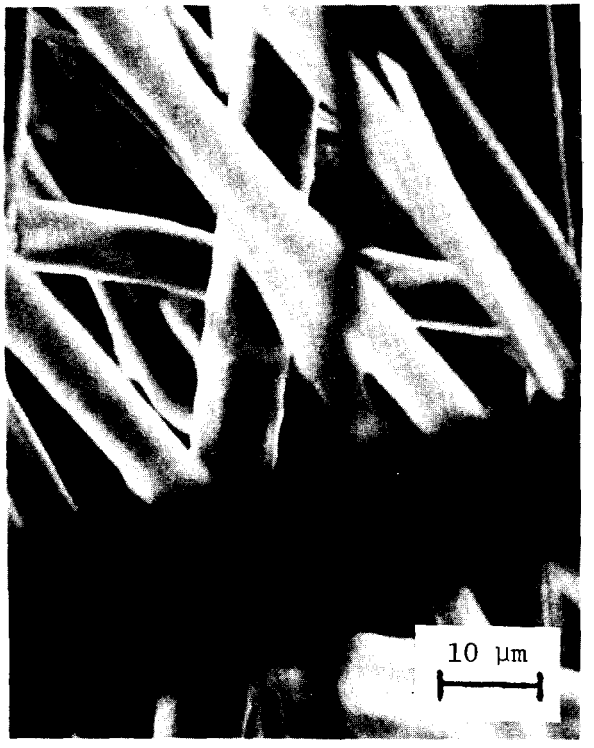

AF-18

Figure 4

Electron micrographs of filters AF-4, -11, and -18.

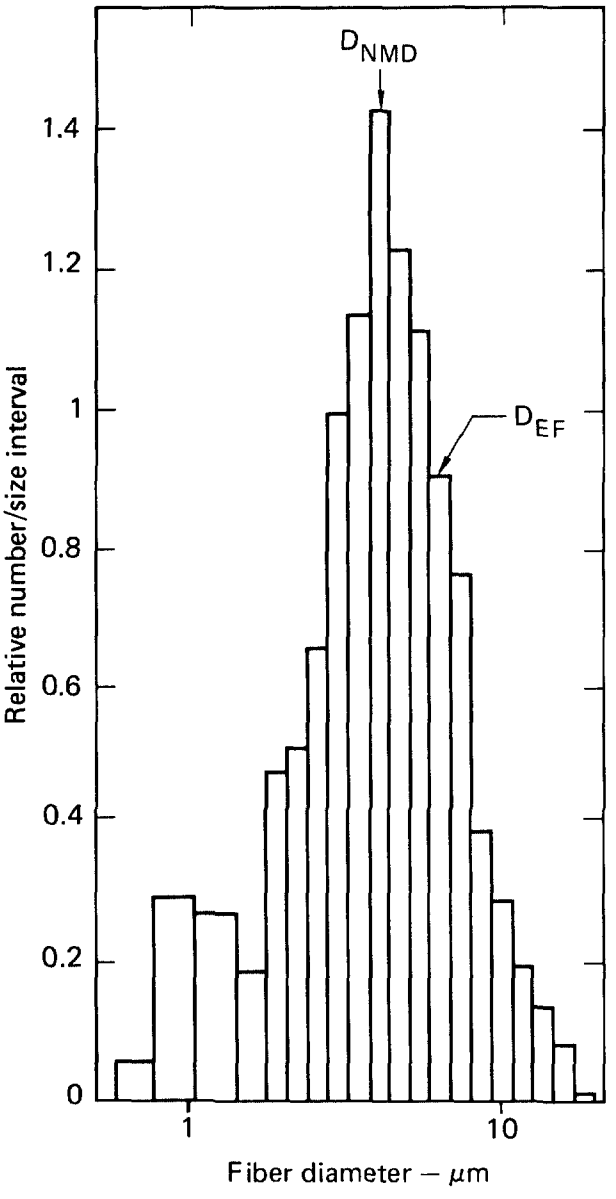

Figure 5

Histograph of number-size distribution as a function of fiber diameter for filter AF-11.

We then measured the pressure drop across the AF-4, -11 and -18 filters at various face velocities to compare the experimental values of Φ to the values predicted by Davies' empirical equation and the three theoretical models. The experimental values were determined from Eq. (3) using the fiber-size distributions obtained from electron microscopy. These data are shown in Fig. 6 as a function of α along with the Φ values from Davies' equation and the three flow theories. The Kuwabara and Happel theories are very similar cell models, while the Spielman and Goren theory is a fluid-dampening model. Curves for these models show fibers oriented transverse and parallel to the air flow. The Spielman and Goren model also shows a curve for a three-dimensional random orientation of fibers with respect to the air flow. As one would expect, the parallel orientation gives the lowest values for normalized pressure drop while the transverse orientation gives the highest values; the curve for the random orientation has an intermediate value. Note the curve representing a three-dimensional orientation almost matches Davies' empirical curve.

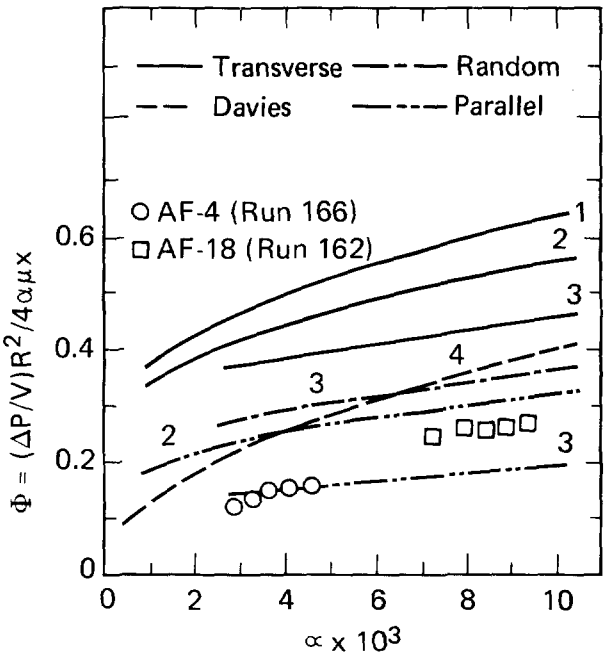

Figure 6

Comparison of 1) Kuwabara, 2) Happel, 3) Spielman and Goren, and 4) Davies Empirical flow theories with experimental filters AF-4, and AF-18 at flow rates of 12.3-65.4 cm/s. The normalized pressure drop, Φ, is plotted as a function of fiber volume fraction α.

The circles and squares in Fig. 6 represent experimental measurements at flow rates from 12.3 to 65.4 cm/s for filters Af-4 and -18, respectively. Each set of these data points show that α increases with increased flow velocity. This occurs because the filters compress to smaller thicknesses at higher flow rates, thus increasing the volume fraction of the fibers. If filter thickness remained constant at different flow rates, all points would fall on the same α value.

The most disturbing aspect of the experimental data points is the low values of the normalized pressure drop compared to Davies' empirical equation . The Φ values obtained from Davies' equation for AF-4 and -18 filters are approximately 40% and 28% higher than those obtained in our experiments. Although several possibilities for this discrepancy exist, the primary cause is believed due to the nonuniform distribution of fibers in the filter mat.

An equivalent method for comparing experimental pressure drop measurements with Davies' equation is based on measured and derived fiber diameters. A summary of fiber-size statistics for filters AF-4, -11, and -18 is given in Table II.

Table II. Comparison of fiber diameters calculated from pressure-drop equations

Filter	D_{NMD}, μm	σ_g	D_{EF}[Eq. (6)], μm	D[Eq. (2)], μm	Increase, %
AF-4	0.73	2.0	1.34	1.78	33
AF-11	3.3	1.7	4.70	5.12	9
AF-18	3.5	1.7	4.98	5.86	18

Using Eq. (6), we calculated the effective fiber diameter for each filter with the D_{NMD} and σ_g obtained from the log-probability graphs. The D_{EF} diameters should, in principle, have agreed with the diameters obtained from Davies' empirical equation,

Eq. 2, that relates filter pressure drop measurements to fiber radius. However, a comparison of the two diameters in Table II indicates the diameters obtained from Davies' equation were always higher than the corresponding diameters calculated from fiber-size distributions. This discrepancy was seen earlier in Fig. 6 where the experimental Φ values for AF-4 and -11 were considerably lower than the values predicted from Davies' equation. We plan to investigate the cause of the discrepancy in our future studies.

Clean Filter Efficiency With an Electric Field

We have shown that previous investigators were able to greatly improve filter efficiency by applying an external electric field across the filter medium. The increased efficiency was believed to be the result of electrostatic forces arising from polarized particles and polarized fibers and from charged particles and polarized fibers. The former force was called dielectrophoresis by Bogardus et al[11].

A careful review of these previous studies has shown that dielectrophoresis makes a negligible contribution to increased filter efficiency. Fielding has acknowledged "the dielectrophoresis effect is minor" in discussing their paper[11]. We also concluded in a previous study that the dielectrophoresis term in negligible[20]. These conclusions were based on observations that the logarithm of the penetration was a linear function of the applied electric field rather than of the square, as predicted for dielectrophoresis. Two factors are responsible for dielectrophoresis' negligible contribution to the increase in filter efficiency with an applied electric field: 1) nearly all aerosols are charged, and 2) dielectrophoresis is only important for large particles. Since most filters already have very high efficiencies for large particles, any improvement in filter efficiency would not be seen. In contrast, small charged particles that normally penetrate the filter can be attracted to polarized fibers when an electric field is applied.

The previous studies on electrostatic filters were conducted under steady-state conditions, using noninsulated electrodes. A relatively simple static model developed by Zebel could explain nearly all of the experimental results from these studies[21]. Our previous results on the effect of electric field, face velocity, fiber volume fraction, and fiber size were in good qualitative agreement with the Coulombic force in Zebel's model[20].

However, our recent experiments with transient electric fields and insulated electrodes have shown the electrostatic filter is a complex dynamic system involving two electrostatic forces. One is the well-established Coulombic force between charged particles and polarized fibers; the other, while also a Coulombic force, involves charged particles and charged fibers. Although this additional force makes a large contribution to the increase in filter efficiency with an applied electric field, it had not been recognized before our investigation.

Theory of Electrostatic Filter

The electrostatic filter exhibits a very dynamic behavior with two opposing processes: the increasing fiber charge due to charged particles collected on the fibers, and the dissipation of this charge due to the conductivity of the fibers. We have incorporated these dynamic processes into our efficiency model for clean filters. The filter efficiency model used in our investigation is based on the standard single fiber efficiency[1]. The differential form of the equation for this model is

$$-\frac{\partial N}{\partial X} = \frac{2\alpha N \eta_T}{\pi R (1-\alpha)} \tag{7}$$

where:

N = conc (cm^{-3}) of particles

α = vol fraction of fibers

X = filter thickness (cm)

η_T = total single fiber efficiency

R = fiber radius (cm)

Equation (7) describes the fractional decrease in the number concentration, -dN, across a differential filter element, dX. The mechanical and electrical filtration mechanisms are incorporated into the total single fiber efficiency η_T.

One commonly used method for combining all the different filtration mechanisms is to calculate the single fiber efficiency from each mechanism separately and add these values together. Unfortunately, this procedure does not yield the correct results because it neglects the interaction terms between different mechanisms[1]. Nonetheless, the summation of separate efficiency mechanisms has been used in our theoretical model because it provides trends and gives approximate values for this relatively simple model. We plan to develop a rigorous mathematical model of our electrostatic filter in future investigations.

The total single fiber efficiency used in our model is

$$\eta_T = \eta_M + \eta_{Pq} + \eta_{Qq} \tag{8}$$

where:

η_M = single fiber efficiency for mechanical mechanisms

η_{Pq} = single fiber efficiency for polarized fibers and charged particles

η_{Qq} = single fiber efficiency for charged fibers and charged particles

We have dropped the single fiber efficiency for polarized fibers and polarized particles (dielectrophoresis) used in our previous models because that term was insignificant. The term η_{Qq} represents a new term in our theoretical model and allows the charge to build up and dissipate on the fibers. Replacing η_T in Eq. (7) with Eq. (8) and substituting the expressions for η_{Pq} and η_{Qq} we have:

$$-\frac{\partial N}{\partial X} = \frac{2\alpha N}{\pi R(1-\alpha)} \left\{ \eta_M + \frac{qEC}{6\pi\mu rV} \left(\frac{1 + \frac{\varepsilon_f - 1}{\varepsilon_f + 1}}{1 + \frac{qEC}{6\pi\mu rV}} \right) + \frac{qQ}{3\pi\mu RrV} \right\} \tag{9}$$

where:

q = particle charge (C)

E = electric field strength (V/cm)

C = Cunningham slip factor[1]

μ = viscosity (Pa•s) of gas

V = velocity (cm/s) of gas

r = particle radius (cm)

ε_f = dielectric constant of fiber

Q = fiber charge (C)

The last term in braces represents the term η_{Qq}. The fiber charge Q in this term is responsible for the dynamic nature of the electrostatic filter. Equation (10) gives the rate at which the fiber charge increases or decreases:

$$\frac{\partial Q}{\partial t} = -\frac{\gamma Q}{\varepsilon} + q\frac{\partial m}{\partial t} \qquad (10)$$

where:

γ = fiber conductivity (S)

ε = permittivity (F/m) of fiber

m = conc (cm^{-3}) of particles in the filter

t = time (s)

This equation shows that increasing the fiber charge increases the rate of charge dissipation. Similarly, increasing the rate of particle accumulation in the filter increases the rate of charge accumulation on the fibers.

The rate of particle accumulation in the filter is given by:

$$\frac{\partial m}{\partial t} = \frac{2\alpha N V \eta_T}{\Pi R(1-\alpha)} \qquad (11)$$

This equation assumes that previously trapped particles cannot trap new particles.

Using Eqns. (9)-(11) and assuming a steady state for the fiber charge, we can show that

$$\ln P = \ln P_o - \frac{2\alpha q}{3\Pi^2(1-\alpha)\mu R r}\left\{\frac{N_o\, q\varepsilon(1-P)}{R\gamma} + \frac{ECX}{2V}\left(\frac{1+\frac{\varepsilon f-1}{\varepsilon f+1}}{1+\frac{qEC}{6\Pi\mu r V}}\right)\right\} \qquad (12)$$

where:

P = particle penetration with mechanical and electrical mechanisms

P_o = particle penetration with only mechanical mechanisms

N_o = conc (cm^{-3}) of particles at filter inlet

Details of this derivation will be given elsewhere. Equation (12) allows us to calculate the filter penetration for our electrostatic filter under steady-state conditions. Since the filter efficiency equals 1-P, we can also determine the filter efficiency.

Of the several observations that can be made from Eq. (12), the most prominent is the decrease in filter penetration due to the electrical terms. However, if the aerosols have no charge (q = 0), the filter penetration reduces to the penetration involving only mechanical mechanisms. This is an unlikely condition since almost all aerosols, either natural or artificially generated, have a particle charge. Equation (12) also shows that the charged fiber mechanism is favored by increased particle charge, whereas the polarized fiber term is favored by increased electric field. Increasing the air velocity decreases the effect of the polarized fiber mechanism but has no effect on the charged fiber mechanism. Another important observation from Eq. (12) is the decrease in the charged fiber mechanism due to increasing fiber conductivity. In fact, when the fiber conductivity increases sufficiently, the charged fiber mechanism disappears and Eq. (12) reduces to our previous electrostatic equation[20]. Also, note that the filter penetration, P, occurs in two terms that cannot be combined. Solutions of the penetration in Eq. (12) therefore require numerical methods. However, for high filter efficiencies, $P < 0.1$, the P can be dropped from the right side of Eq.(12) with little error.

Transient Filtration Measurements

The theory of electrostatic filters presented in this paper can be used to explain the major experimental findings of our investigation. The experiments actually preceded our theoretical work and served as the basis for our model. Figure 7 shows the concentration of NaCl aerosols penetrating two electrostatic filters as a function of time. The major difference between the two filters was their conductivity. The filter on the left was relatively nonconducting (10^{10} ohm/cm) while the filter on the right was relatively conducting (10^{8} ohm/cm). A dye, added to the filter on the right for identification purposes, was responsible for the increased conductivity. The two filters did not have the same steady-state penetration values because of slightly different fiber size and fiber volume fractions.

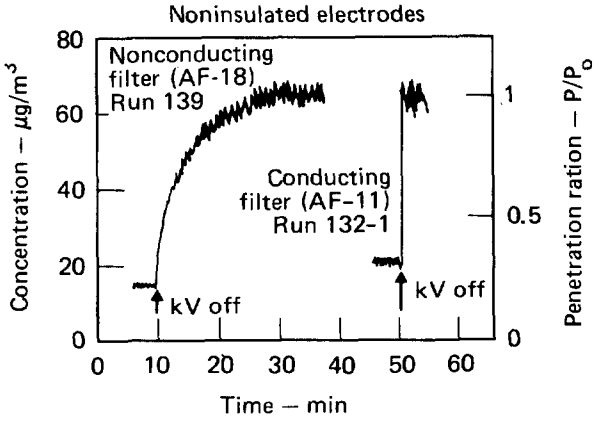

Figure 7

Aerosol concentration measurements downstream of the filter during transient conditions when the electric field is turned off for a nonconducting and conducting filter using noninsulated electrodes.

Figure 7 shows that when the electric field is turned off, the aerosol penetration increases very slowly for the nonconducting filter and very fast for the conducting filter. As these observations involve transients, we cannot interpret them using Eq. (12) because it only applied to steady-state conditions. The complicated transient equations will be presented elsewhere.

We can still make a qualitative explanation of the two transients using Eq. (10). For the nonconducting filter (small γ), a significant charge can build up on the fiber before the charge dissipation term ($-\gamma Q/\varepsilon$) reaches equilibrium with the charge accumulation term ($q\partial m/\partial t$). However, the charge dissipation term for the conducting fiber (large γ) is so large that equilibrium between charge dissipation and accumulation is established with a negligible charge on the fibers. Since the conducting fiber cannot develop a charge, the penetration will instantly increase to the P_o level when the electric field is turned off. In contrast, the nonconducting filter has a significant fiber charge which bleeds off very slowly when the electric field is turned off. As a rough approximation, the accumulation term in Eq. (10) becomes zero* and the resulting equation is integrated to yield

$$Q = Q_o e^{-\frac{\gamma t}{\varepsilon}}, \tag{13}$$

where Q_o is the fiber charge before the electric field is removed. Although the polarized fiber mechanism disappears immediately when the electric field is removed, the charged fiber mechanism persists until all of the charge bleeds off.

In a similar experiment, we measured transient aerosol penetrations for the same nonconducting filter using electric fields generated by ac (60 H_z) and dc voltages. Figure 8 shows dc and ac electric fields generate the same filter behavior when the field is turned off as the nonconducting and conducting filters in Fig. 7, respectively. Although the results in Fig. 8 were obtained with insulated electrodes, similar results were obtained with noninsulated electrodes. The explanation for the transient behavior using a dc field was given previously for the nonconducting filter in Fig. 7. A comparison of the results using an ac field in Fig. 8 with those from the conducting filter in Fig. 7 suggests the same explanation would apply in both cases. This is not the case, since the conducting filter in Fig. 7 cannot support a fiber charge whereas the nonconducting filter in Fig. 8 can. However, the instantaneous increase in filter penetration for both cases when the electric field is shut off suggests that neither filter has developed a fiber charge.

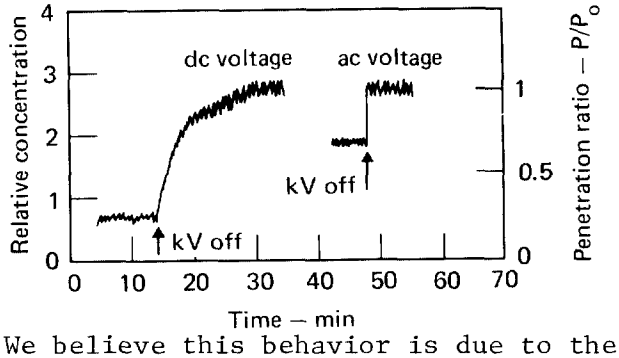

Figure 8

Aerosol concentration measurements downstream of a nonconducting filter during transient conditions when the electric field is turned off for a dc and an ac field using insulated electrodes.

We believe this behavior is due to the NaCl aerosols, which have equal positive and negative charges. When the electric field is in one direction, aerosols of a given charge are trapped on the fibers. When the electric field is reversed, aerosols of the opposite charge are deposited on the same fiber location, thereby cancelling the first charge. Repeated field reversals will continue this charge cancellation and, therefore, never develop a net charge on the fiber. Figure 8 also shows the aerosol penetration of a filter with an ac field is much higher than with a dc field. The higher penetration is due to the absence of the charged fiber mechanism, which lowers the penetration [see Eq. (12)].

* In a rigorous analysis, the accumulation term in Eq. (10) does not reduce to zero because it is a function of the fiber charge. This results in a longer time for the charge to bleed off.

The preceding explanation with ac fields provides a brief glimpse of the complex dynamics of the electrostatic filter. Except for the case involving ac fields, we have ignored the aerosol and fiber charge and have assumed in our simple model that we always have attractive forces. However, in a real electrostatic filter, both the aerosols and fibers have a distribution of plus and minus charges. Depending on the conductivity of the fiber, these charges may migrate and cancel. Clearly both attractive and repulsive forces are involved in this system.

Effect of Fiber Conductivity and Electrode Insulation on Filter Efficiency

The conductivity of the fiber is an important variable in electrostatic filtration since it determines the amount of charge that can be accumulated on the fibers and the associated increase in filter efficiency. In field applications, the fiber conductivity may increase as particles load up the filter or acid mists coat the fiber surface. Both effects may lower filter efficiency. The effect of fiber conductivity on filter efficiency also depends on the insulation of the high-voltage electrodes. Experimental results can only be interpreted when the effects of both fiber conductivity and electrode insulation are included in our theoretical model.

Figure 9 shows the results from efficiency tests on a conducting filter using both insulated and noninsulated electrodes. The logarithm of the penetration ratio is plotted against the applied electric field to linearize the resulting curve and eliminate the initial filter efficiency with no external field. A larger value of $-\ell n(P/Po)$ means a greater filter efficiency. We see that increasing the electric field improves the filter efficiency when noninsulated electrodes are used but has no effect when insulated electrodes are used.

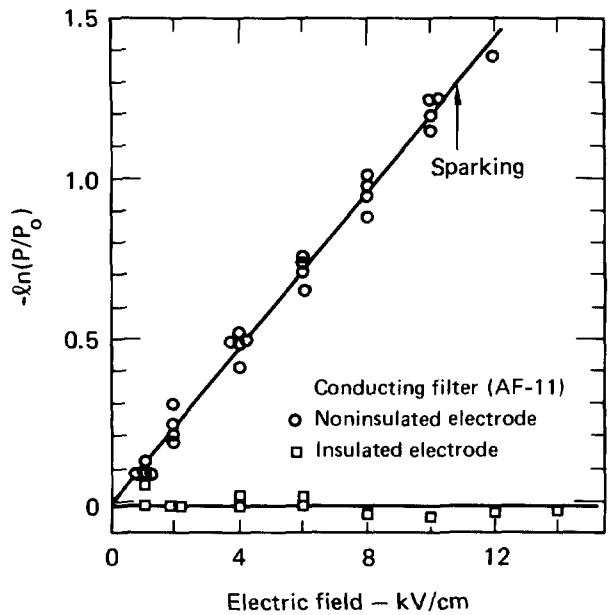

Figure 9

Effect of electrode insulation on the enhanced filtration for a conducting filter.

For tests on a less conductive filter (Fig.10), both insulated and noninsulated electrodes show an increase in filter efficiency when the applied electric field is increased. However, filter efficiency is lower when an insulated electrode is used instead of a noninsulated electrode. Based on Figs. 9 and 10, we would expect that in the limit of zero conductivity, the filter efficiency would be the same for either insulated or noninsulated electrodes.

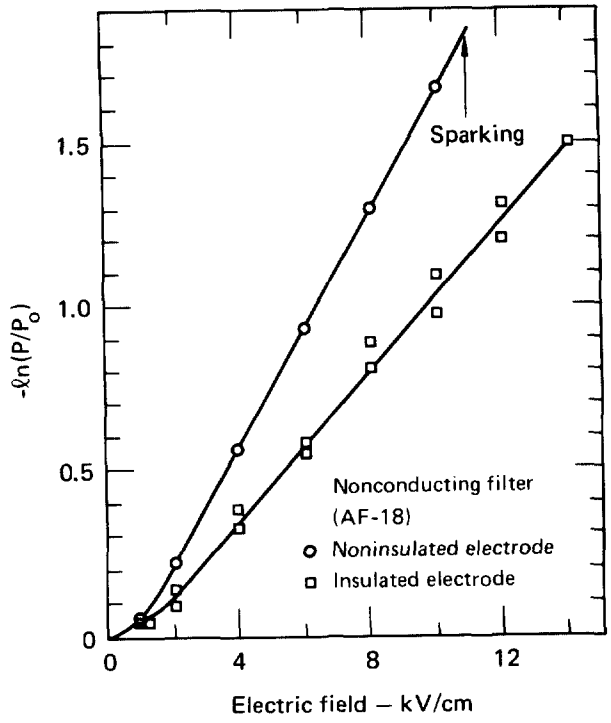

Figure 10

Effect of electrode insulation on the enhanced filtration for a nonconducting filter.

The conductivity of the fibers does not have to be very large for the filter to behave as seen in Fig. 9. The resistivities of the conducting and nonconducting filters were 10^8 and 10^{10} ohm/cm, respectively. Figures 9 and 10 also show that sparking across the electrodes occurs at 11 kV/cm for the noninsulated electrodes while no sparking occurs for the insulated electrodes up to 14 kV/cm.

The experimental results shown in Figs. 9 and 10 can be explained in terms of a charged fiber mechanism, using a schematic of our electrostatic filter system shown in Fig. 11. This figure shows a filter mat of fibers sandwiched between two electrodes that are connected to a high-voltage source. The high voltage produces an electric field E_o within the filter bed that polarizes the individual fibers.

Charged aerosol particles will then be attracted to the polarized fibers and, if the fibers have a low conductivity, accumulate a net charge on the fibers. However, since all materials have a finite conductivity, the charge on the fibers will migrate in the direction of the electric field and dissipate over a time period according to Eq. (13). The positive and negative charges will migrate along the fibers to the electrode of opposite charge and build up an induced charge as shown in Fig. 11.

If the electrodes are not insulated, these induced charges will be neutralized on contact with the electrodes. However, if the electrodes are insulated, the induced charge cannot be neutralized. These induced charges will then generate an electric field that is opposed to the external field created by the high-voltage electrodes. The net effect is a reduction of the electric field within the filter medium.

The extent of this field reduction depends on the magnitude of the induced charge. For the filter shown in Fig. 10, the low conductivity allows only a small charge to build up next to the insulated electrode. This small charge buildup generates a small opposing electric field that consequently reduces filter

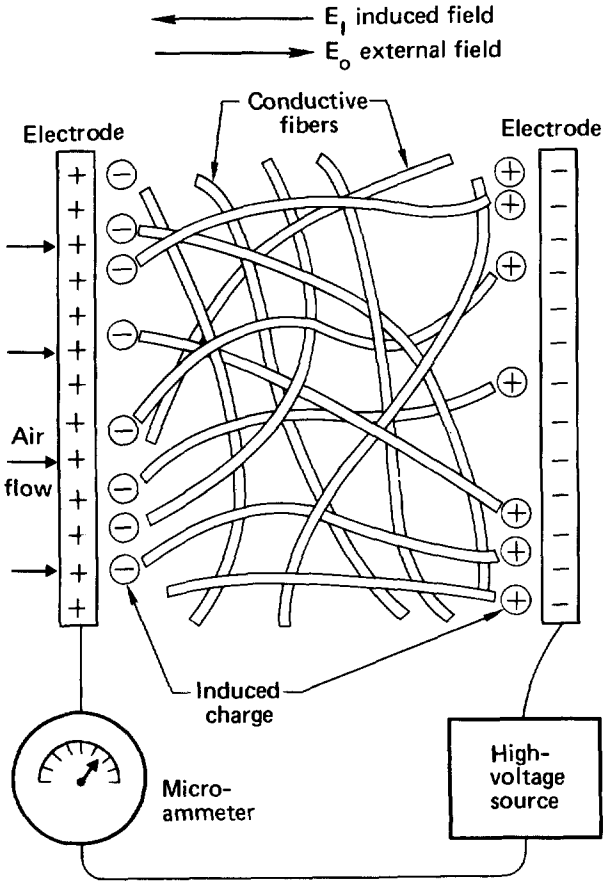

Figure 11

Schematic of the induced charge build-up that cancels the applied electric field when a conducting filter is used with insulated electrodes.

efficiency by only a small amount. In contrast, the conducting filter shown in Fig. 9 allows a significant charge to build up next to the insulated electrodes. The magnitude of this induced charge is large enough to cause a net cancellation of the external electric field within the filter medium. An applied electric field in this case does not increase filter efficiency.

Filter-Loading Model

We recently developed a filter-loading model [28] that avoids the problem of determining the detailed capture mechanism of particles in a loaded filter [27]. Our approach is an extension of the theoretical treatment of filter efficiency and pressure drop for unloaded filters. It treats captured particles within the filter as new fibers. Filter efficiency and pressure drop are then derived in the same manner as for clean filters except that additional fibers are included to represent trapped particles. Details of the derivation will be presented elsewhere.

The expression for the concentration of particles penetrating a filter is given by

$$N = \frac{N_0 \exp -\left(\frac{2\alpha X\eta_F}{\pi R(1-\alpha)} + \frac{\pi V tr^2 N_0 \eta_p}{2}\right)}{1 - \frac{\pi V tr^2 N_0 \eta_p}{2} \exp -\left(\frac{2\alpha X\eta_F}{\pi R(1-\alpha)} + \frac{\pi V tr^2 N_0 \eta_p}{2}\right)}, \quad (14)$$

where:

N = conc(cm^{-3}) of particles penetrating filter

N_o = conc(cm^{-3}) of particles entering filter

α = vol fraction of fibers

X = filter thickness (cm)

η_F = single fiber efficiency

R = fiber radius (cm)

V = velocity (cm/s) of air

t = time (s)

r = particle radius (cm)

η_p = collection efficiency for one particle by previously trapped particles

Equation (14) can, without too much error, be approximated by the following equation:

$$N = N_0 \exp -\left(\frac{2\alpha X\eta_F}{\pi R(1-\alpha)} + \frac{\pi V t r^2 N_0 \eta_p}{2}\right), \tag{15}$$

or, in terms of penetration (P),

$$P = P_0 \exp -\left(\frac{\pi V t r^2 N_0 \eta_p}{2}\right), \tag{16}$$

where $P = N/N_o$ at time t and $P_o = N/N_o$ at time 0.

Since experimental data showing filter efficiency as a function of the mass of trapped particles are often available, the appropriate theoretical equation should relate efficiency or penetration to particle mass. This relationship is obtained from a particle mass balance. The rate of particle mass accumulation in the filter equals the rate of particle mass entering the filter times the filter efficiency or

$$\frac{dm}{dt} = (N_0 V A m_p)E, \tag{17}$$

where:

m = mass (g) of particles trapped in filter

A = filter area (cm^2)

m_p = mass (g) of a single particle

E = filter efficiency ($E = 1-P$)

The mass of particles trapped after a given time can be obtained by integrating Eq. (17) with respect to time and by using Eq. (16) for penetration. The result is

$$m = \left(\frac{8\rho rA}{3\eta_p}\right)(-\ell n(P/P_0) + P - P_0) , \tag{18}$$

where ρ = particle density (g/cm^3). If ψ represents the term $-\ell n(P/P_0) + P - P_0$, then experimental data plotted as ψ vs m should fall on the same curve for any filter media and experimental conditions provided the aerosol properties remain constant.

If we consider a filter loaded with particles as a mixture of two types of fibers, one representing the original clean fibers and the other representing the trapped particles, we can use Eq. (5) to describe the pressure drop across loaded filters. The effect of neighboring fibers or particles is already included in Eq. (5). If we further assume all the original filter fibers are the same size and that trapped particles (now treated as fibers) also have a constant size, we can reduce Eq. (5) to

$$\frac{\Delta P}{\mu V X} = 16\left(\frac{\alpha_F}{R^2} + \frac{\alpha_p}{r^2}\right)^{1/2}\left(\frac{\alpha_F}{R} + \frac{\alpha_p}{r}\right), \tag{19}$$

where:

α_F = vol fraction of original fibers

α_p = vol fraction of trapped particles

R = radius (cm) of original fibers

r = radius (cm) of particle fiber

Note the radius (r), of the particle fiber is not necessarily the same as the single particle radius. Equation (19) can be directly compared with experimental data.

Experimental Evaluation of Model

Although much additional work is still needed to develop accurate theoretical models of filter loading, our present model agrees reasonably well with experimental data, as can be demonstrated with the data shown in Fig. 12, where filter efficiency and pressure drop are plotted as a function of the particle mass trapped in the filter. These data were obtained in our small-scale test system, using sodium chloride aerosols. The filter media for both data sets in Fig. 12 is the same. The primary difference between the two is the airflow velocity used to load up the filter.

To test the accuracy of our theoretical equations, we plotted the experimental data as a dependent function of particle mass loading. The particular dependent function used was obtained from Eq. (18) for comparisons of filter efficiencies and from Eq. (19) for comparisons of filter pressure drops. A perfect agreement between theory and experiment was reached whenever curves of the particular dependent function vs particle mass loading coincided for widely different experimental conditions.

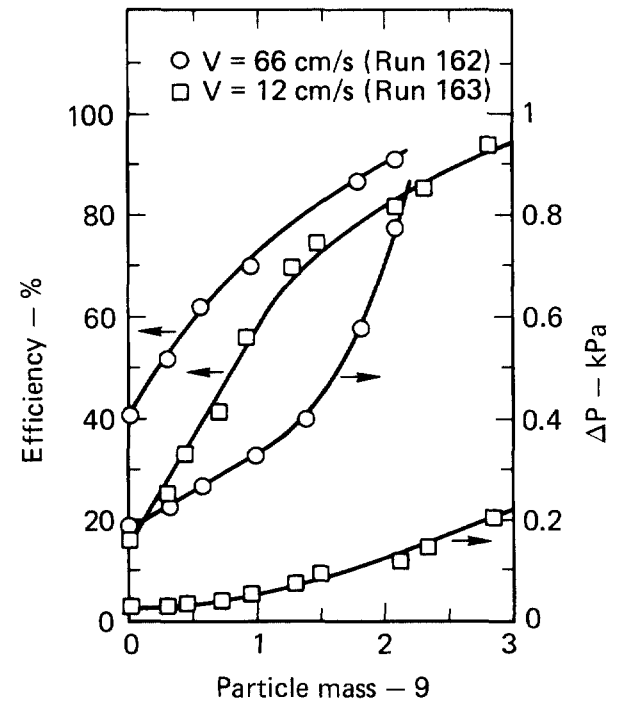

Figure 12

Efficiency and pressure drop as a function of particle mass loading for filter loading tests at different flow velocities.

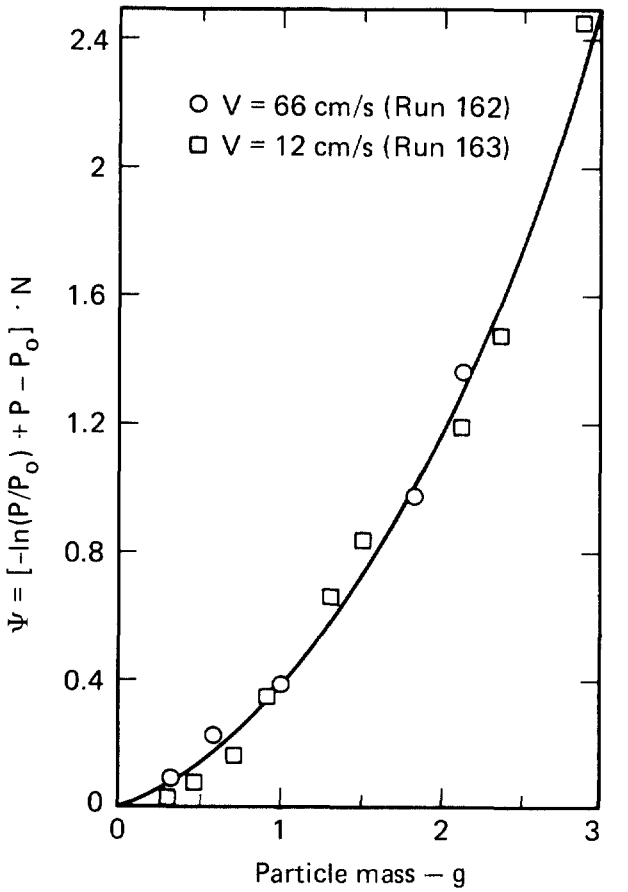

Figure 13

Normalized penetration Ψ as a function of particle mass loading for filter loading tests at different flow velocities.

The efficiency data for the two experiments shown in Fig. 12 are shown replotted in Fig. 13, with the dependent variable ψ as a function of the particle mass. We multiplied the ψ values of the two experiments with a factor N to account for changes in particle-particle collection efficiency, η_p. The excellent agreement between the normalized ψ values seen in Fig. 13 indicates the accuracy of Eq. (18) for predicting filter efficiency values at different mass loadings.

A similar analysis of the pressure drop for the two experiments shown in Fig. 12 could be performed with Eq. (19). We plotted the data as $(\Delta P-\Delta P_o)/V$, where ΔP_o is the pressure drop across the filter with zero mass loading, so the resulting curve would pass through zero at zero particle mass loading. The resulting data in Fig. 14 show good agreement between the two experiments. An even better fit could be obtained by normalizing both sets of data to the same value of filter thickness (X) and fiber volume fraction (α_F); however, the normalization is complicated by the compression of the filter at higher flow rates. This compression increases the value of $\Delta P/V$ by decreasing the filter thickness and increasing the fiber volume fraction.

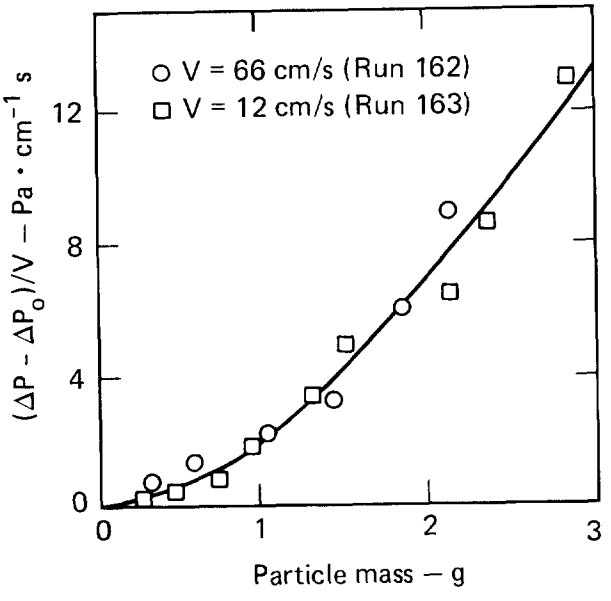

Figure 14

Pressure drop increase per unit flow velocity as a function of particle mass loading at different flow velocities.

Another illustration of the accuracy of Eq. (19) to predict the pressure drop for loaded filters can be made with experimental data obtained by Adley and Wisehart[29]. They measured the pressure drop across a HEPA filter as a function of particle loading for three particle sizes. Their results are shown in Fig. 15(a) The equations developed to describe the very loose filters used in the Enhanced Filtration Program should be equally applicable for characterizing HEPA filters. The primary difference between HEPA filters and loosely packed filters is the higher fiber volume fraction (α_F) and the smaller fiber size (R) for HEPA filters. This difference allows us to simplify Eq. (19) by making a Taylor series expansion of the square root term and dropping small terms.

$$\frac{\Delta P}{\mu V X} = 16\left(\frac{\alpha_F}{R^2}\right)^{1/2}\left(\frac{\alpha_F}{R}+\frac{\alpha_p}{r}\right). \qquad (20)$$

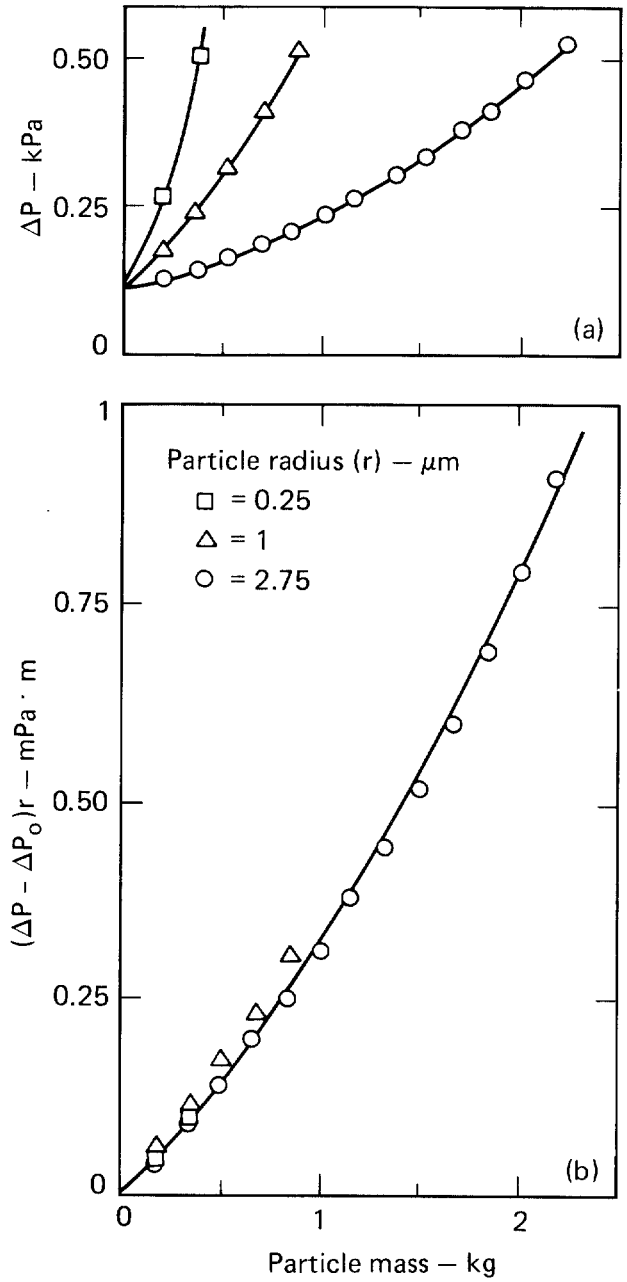

Figure 15

(a) Loading test on HEPA filters using different size particles.

(b) Loading data replotted to normalize pressure drop increase for different size particle diameters.

Then, we can subtract the initial pressure drop to yield

$$\frac{\Delta P - \Delta P_0}{\mu V X} = 16 \frac{\sqrt{\alpha_F}\ \alpha_p}{R\ \ r} \tag{21}$$

Equation (21) predicts the increased pressure drop due to particle loading will be inversely proportional to the particle size r. A plot of $(\Delta P-\Delta P_o)r$ will, therefore, be independent of the particle size and will increase in direct proportion to the particle loading or α_p. The data from Fig. 15(a) were replotted in this fashion in Fig.15(b), where one can see all the data fall on a nearly straight line, thus confirming the validity of Eq. (21).

One series of experiments in our filter loading program is aimed at understanding how airflow velocity and the mass of trapped particles affect measured pressure drop. Figure 16 shows experimental pressure drop measurements versus particle mass at different air velocities for an AF-18 filter. Note the data in Fig. 16 were obtained in the same experiment (Run 162) shown in Fig. 12. However, the pressure drop measurements in Fig. 12 were taken at only one flow rate while Fig. 16 shows a complete map of the pressure drop resulting from various particle masses and flow rates.

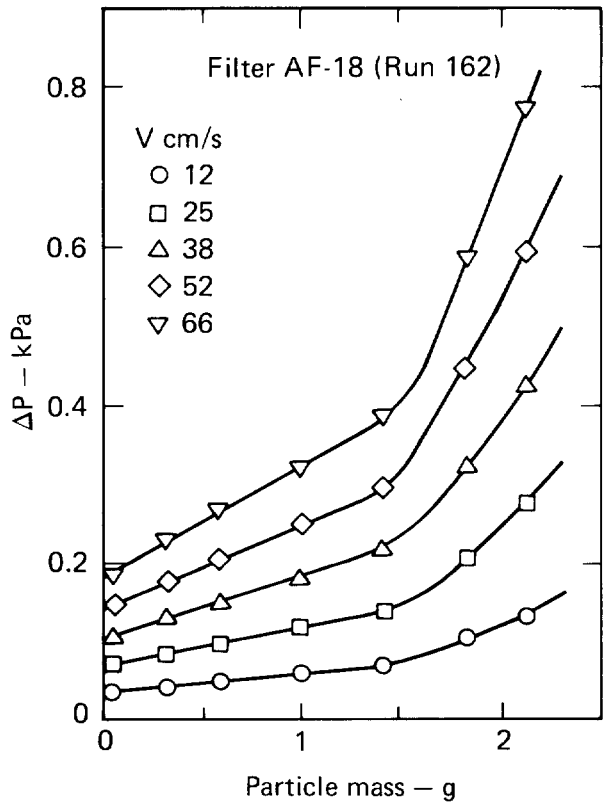

Figure 16

Pressure drop for filter AF-18 as a function of particle mass loading at various flow velocities.

If the same data are replotted as $\Delta P/V$ in Fig. 17, the primary influence of air flow velocity is removed. This agrees with Darcy's Law, which predicts that $\Delta P/V$ is a constant independent of the airflow rate[1]. However, a detailed analysis of the data indicated $\Delta P/V$ increased slightly as the velocity increased. Moreover, this increase became greater for larger particle loadings. The reason for the observed increase in $\Delta P/V$ values with increasing velocity is primarily due to the compression of the filter at higher flow rates.

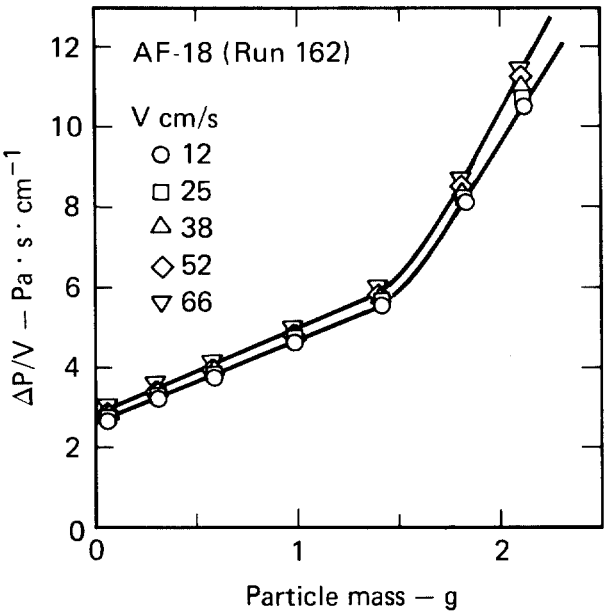

Figure 17

Pressure drop per unit flow velocity for filter AF-18 as a function of particel mass loading at various flow velocities.

Morphology of the Particle Deposits

Another important aspect of our filter loading study is the use of electron microscopy to characterize the particle deposit within the filter. We plan to study the morphology of the particle deposit under various conditions to discover if there is any relationship between the macroscopic observable properties and the microscopic nature of the deposit.

Figure 18 shows electron micrographs of the particle deposit on the top surface of an AF-18 filter, corresponding to a particle loading at 66 cm/s. The macroscopic properties of filter efficiency and pressure drop were seen earlier in Fig. 12.

Figure 19 shows electron micrographs taken on the surface of an AF-4 filter loaded with aerosols at a 66 cm/s flow velocity. Comparison of this figure with Fig. 18 shows the effect fiber size has on particle deposition.

The main difference between the particle depositions shown in Figs. 18 and 19 is the depth of the deposition. Although nearly the same mass of NaCl aerosol was trapped in both filters, the AF-4 filter had a surface deposition while the AF-18 filter had a major deposition at some depth within the filter. The deposition on HEPA filters would be similar to that seen in Fig. 19 since the fiber sizes would be comparable. Our theory predicts the concentration of deposited aerosols will be highest on the front face of the filter and will decrease exponentially with increasing filter depth. To account for the differences in particle deposition, we must add a sticking factor to our single fiber efficiencies[1].

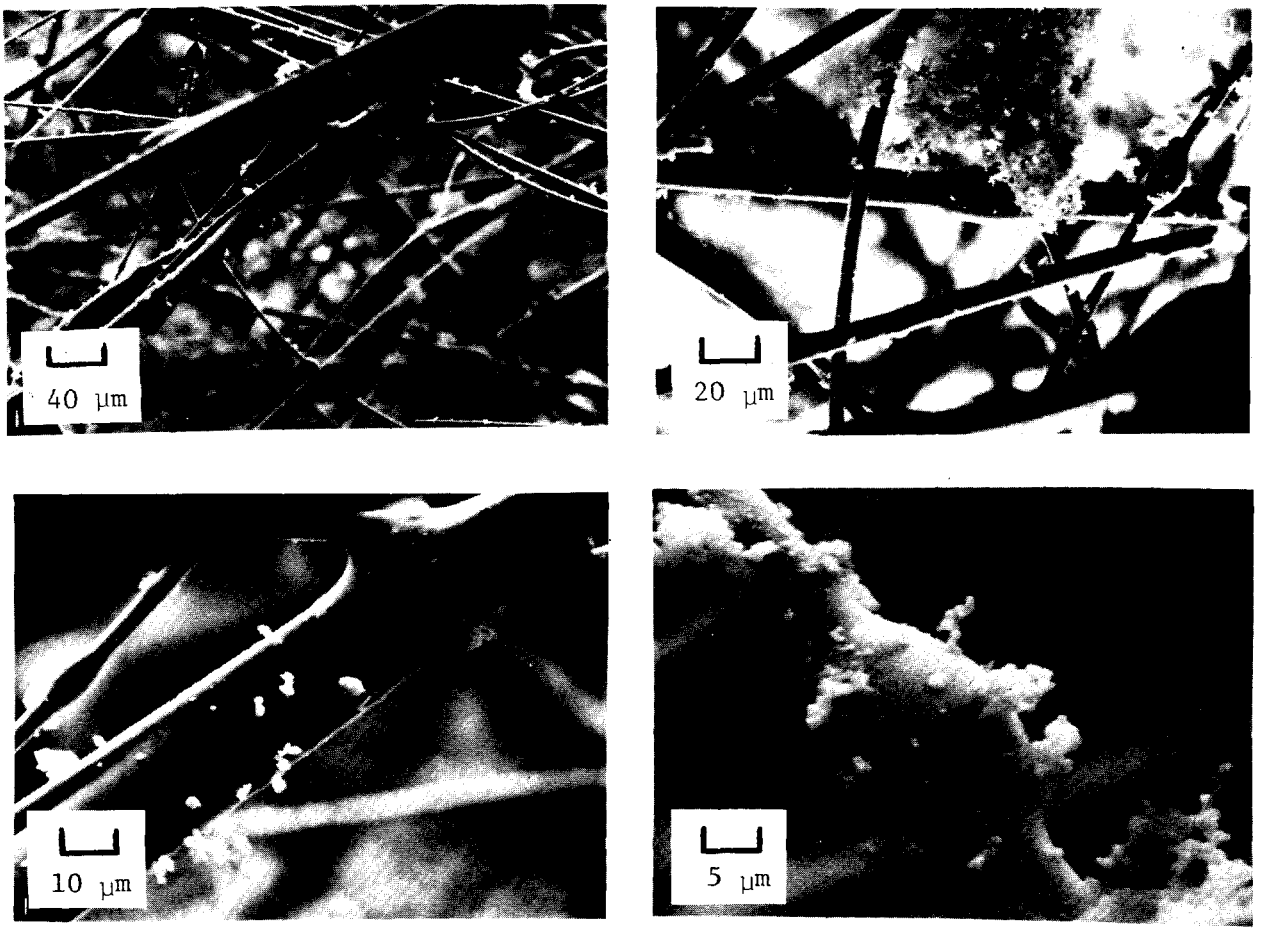

Figure 18 Electron micrographs of particle deposits on a AF-18 filter from a loading test conducted at a 66-cm/s flow velocity.

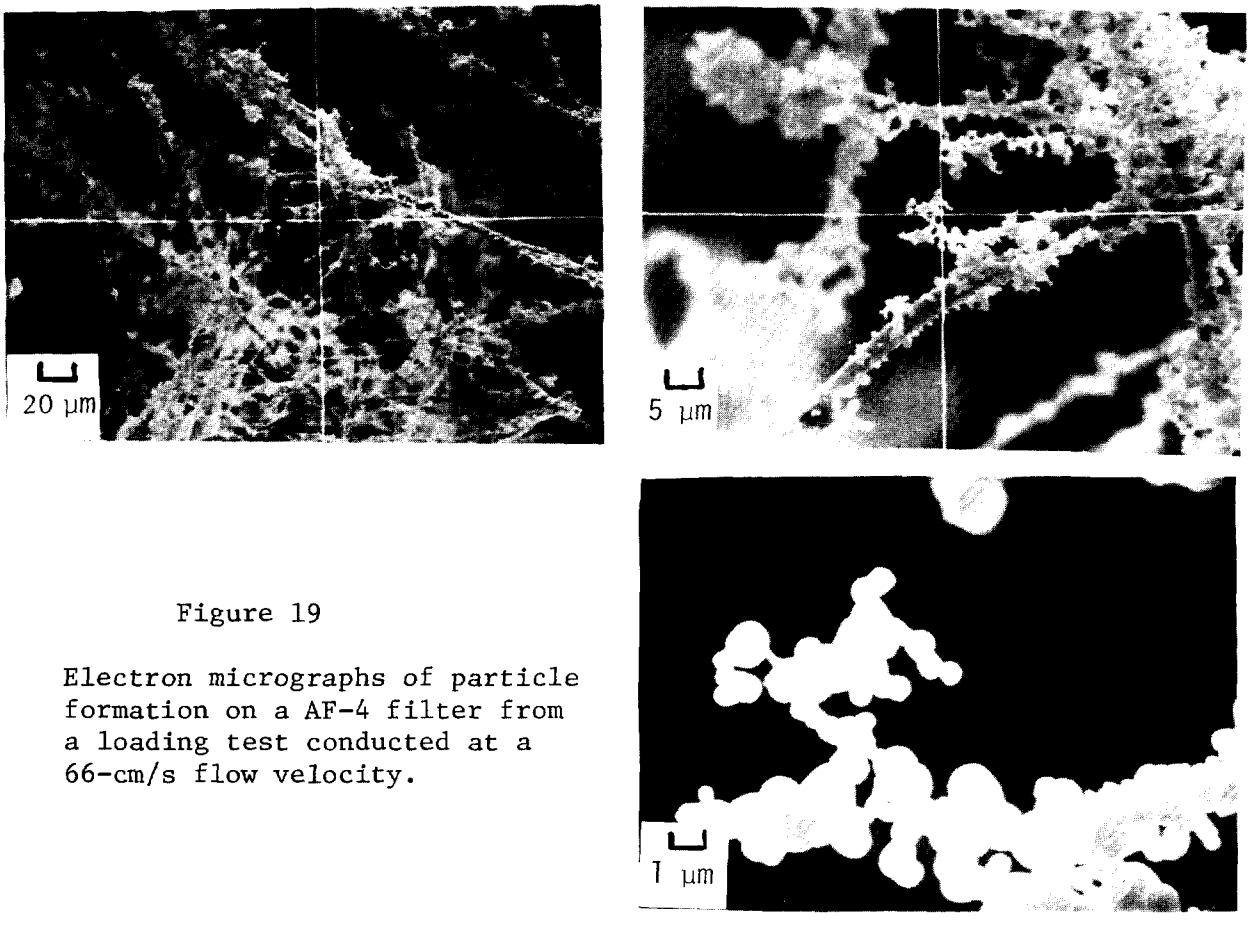

Figure 19

Electron micrographs of particle formation on a AF-4 filter from a loading test conducted at a 66-cm/s flow velocity.

Particle Loading Experiments Using Electric Fields

Test results from a preliminary filter-loading test with a 10-kV/cm applied electric field are shown in Fig. 20. Here an AF-18 filter was sandwiched between the front and rear screens used to generate the electric field. This figure shows three curves; one represents filter efficiency with an applied electric field of 10 kV/cm, one represents filter efficiency with no electric field, and the third represents pressure drop across the filter. We plotted these curves as a function of time instead of particle mass because we could not measure the mass until the end of the test.

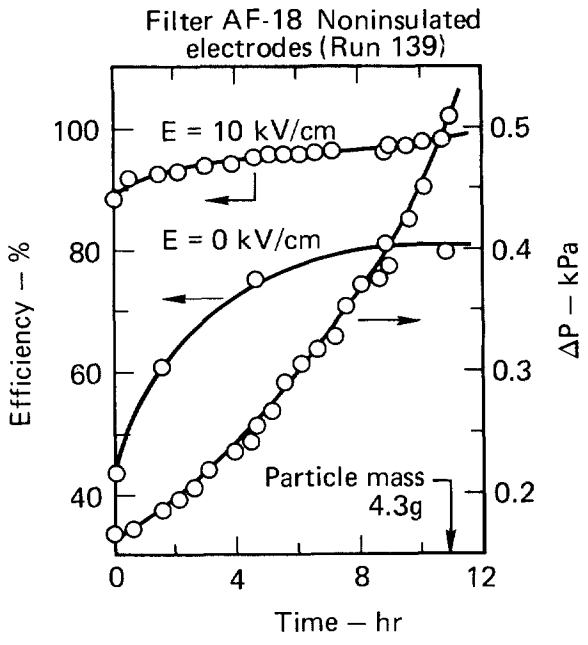

Figure 20

Filter loading test on an AF-18 filter using noninsulated electrodes to generate an electric field.

We have conducted three tests on the AF-18 filter to determine the effect of electric field and electrode insulation on the particle loading. These test results are summarized in Table III. All of these tests had the same initial pressure drop and were terminated when the pressure drop reached 500 Pa. The particle mass collected by the filters is shown in the last column.

Table III. Electric field and electrode insulation effects on filter efficiency and particle mass loading for the AF-18 filter.

Test	Efficiency at zero particle mass loading, %	Efficiency at ΔP = 500 Pa,%	Particle mass loading at ΔP = 500 Pa,g
No electric field	41	84	1.70
10-kV/cm insulated electrode	82	95	2.45
10-kV/cm noninsulated electrode	89	98	4.30

Several important trends are seen in Table III. The filter efficiency increased as particles loaded the filter for all cases. Applying an electric field increased the filter efficiency at all particle loadings for both insulated and noninsulated electrodes. The slightly lower efficiency seen for the insulated electrodes resulted from the slight cancellation of the applied electric field by the induced charge as previously seen in Fig. 11.

Using theory presented in this paper, we are able to explain the increase in filter efficiency with particle loading and with an applied electric field. However, we have not yet developed a theory to explain the significantly higher loading capacity for a filter with an applied electric field. Instead of comparing the particle loadings at a given pressure drop, we can compare the pressure drops at a given particle mass loading. Such a comparison shows the electrostatic filter has a

significantly lower pressure drop then the same filter with no electric field. Previous investigators have also reported significantly lower pressure drops with other electrostatic filters[12,15,16].

We believe the reason for the lower pressure drop resulting from an electric field is due to a less restrictive particle deposit on the fibers. Since the electric field attracts particles to the fibers, the particle deposit would also tend to build up along the fibers. In contrast, ordinary filters do not have this electric force attracting the particles to the fibers. The particle deposit would thus form a greater number of dendrites to bridge between the fibers and block the air passage. Figure 21 illustrates this hypothesis. We are currently taking electron micrographs of particle deposits with and without an electric field at various stages of particle loading. Once we determine the nature of the particle deposit, we will then develop a model to explain the lower pressure drop for electrostatic filters.

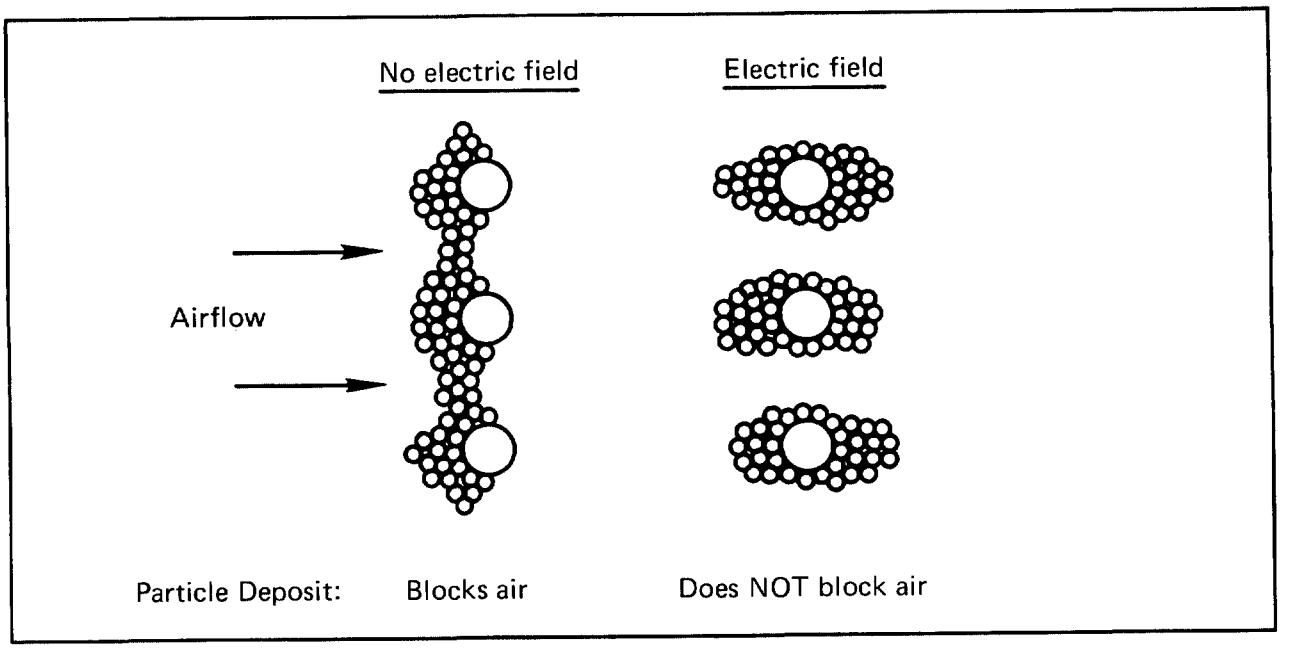

Figure 21 Schematic of possible explanation for decreased pressure drop observed when electric fields are used to enhance filtration.

IV. Application of the Electrostatic Filter in the Nuclear Industry

The objective of LLL's Enhanced Filtration Program is to develop an enhanced filtration system for HEPA filters that will extend their service life. To meet this objective, a large fraction of our effort during the past year has been devoted to developing practical hardware that can be evaluated in field environments. We have two prototype units under development: one for glove box installations and the other for installations in ventilation systems.

Application of electric filter concepts to glove boxes was not an original objective; however, the advantages from this spin-off contribute significantly to the management of radioactive waste and improve our ability to control radioactive particles at their source. Figure 22 shows a detailed schematic of our first prototype electric filter installed in a glove box. This prototype unit consists of a polyethylene main body supported near the ceiling of the glove box, a high-

voltage electrode mounted within the main body, a grounded electrode connected to a lever arm on the main body, and a handle that opens and closes the filter assembly for changing filters. Figure 22 shows the fiberglass filter medium in the filter holder; a tab allows for easier filter replacement.

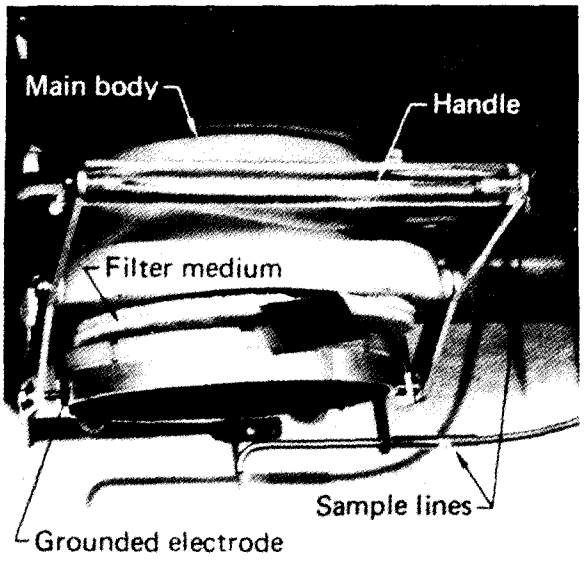

Figure 22

Prototype electric filter holder installed in glove box.

The design of the filter unit shown in Fig. 22 gives it several advantages over a conventional HEPA filter design. First, and most important, this prototype unit facilitates filter change. Figure 23 shows an operator removing the filter medium. Filter replacement takes about 30 s, can be done with one hand, and does not interrupt work inside the glove box. (We have assumed exhaust from the glove box is filtered by a HEPA filter at all times before being discharged into the atmosphere.)

The glove box unit's other advantages include a reduction of the contamination hazard normally encountered with filter changes and the possibility of recovering material from the filter. Use of this filter unit should also result in a reduction of nuclear waste volume since the typical filter medium has over 99% empty space and can be easily reduced in volume.

We have also examined the safety features of the prototype glove box filter and have incorporated the following features in it to reduce the possible high-voltage hazard:

- All high-voltage lines and electrodes have been well insulated to prevent current leakage.

- An interlock mechanism has been placed on the filter holder to shut off the high voltage when the filter holder is opened to replace filters.

- The high-voltage power supply has been set to automatically shut off when the current exceeds a preset level.

These prototype filter units will be installed in a number of glove boxes for radioactive material handling to evaluate their performance under field conditions.

Figure 23

Operator removing filter medium from the filter unit.

We have completed evaluating the electrostatic filter installed in a glove box used to grind chunks of UO_2/BeO into a fine powder. By taking filter samples of the aerosols before and after the electrostatic filter and by measuring the activity on a proportional counter, we determined filter efficiency. Berylium analysis on the same filter samples gave us identical results. Figure 24 shows the sample filters mounted in a specially designed chamber that allowed us to measure filter efficiencies without contaminating the environment.

The efficiency of the electrostatic filter with no particle loading is shown in Fig. 25 for both UO_2 and NaCl aerosols as a function of the applied electric field. The tests with NaCl aerosols were conducted in a different glove box under controlled laboratory conditions and provided a reference for the field evaluation. Since efficiency measurements of the electrostatic filter with UO_2aerosols would be determined using in-line filters, we used both in-line filters and a flame photometer in these reference tests. Figure 25 shows good agreement between these two measurement techniques. The NaCl tests also agreed with previous tests generated in our small-scale system in Fig. 1.

Compared to the NaCl tests, the measurements with UO_2 aerosols showed higher efficiencies and had considerable scatter. We found that the variation in filter efficiency was due to different operations within the glove box. Low efficiencies were obtained during grinding operations, and high efficiencies were obtained during powder handling operations. The variation in filter efficiency was probably due to differences in the aerosol properties during the different operations.

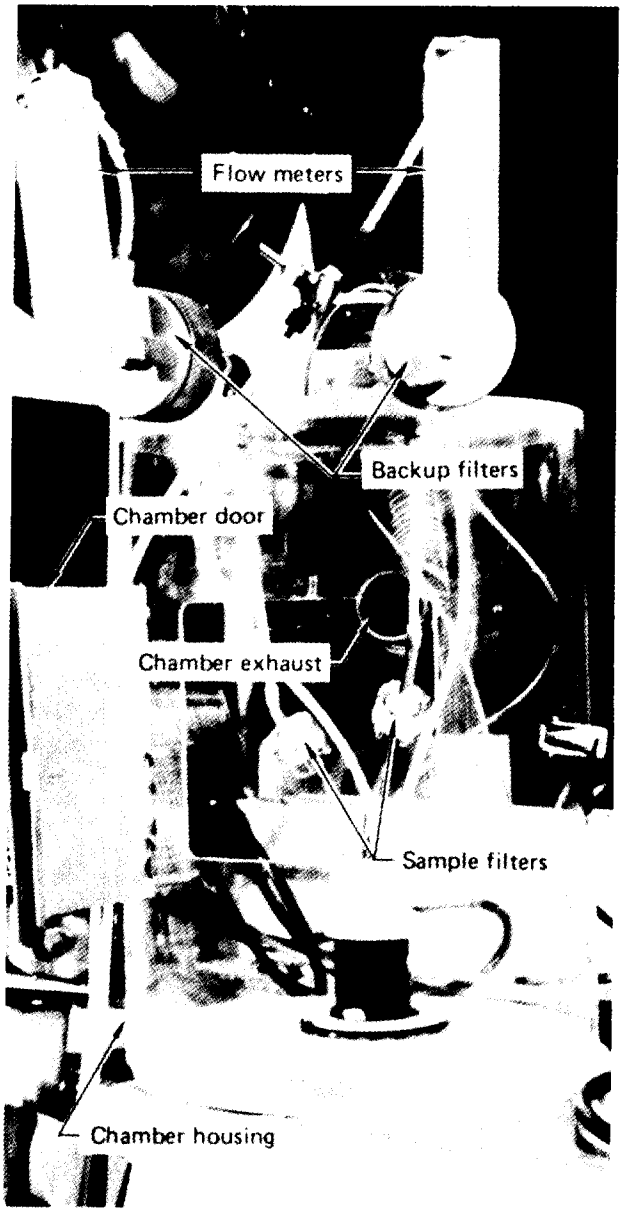

Figure 24

Sampling chamber containing filters for efficiency measurements.

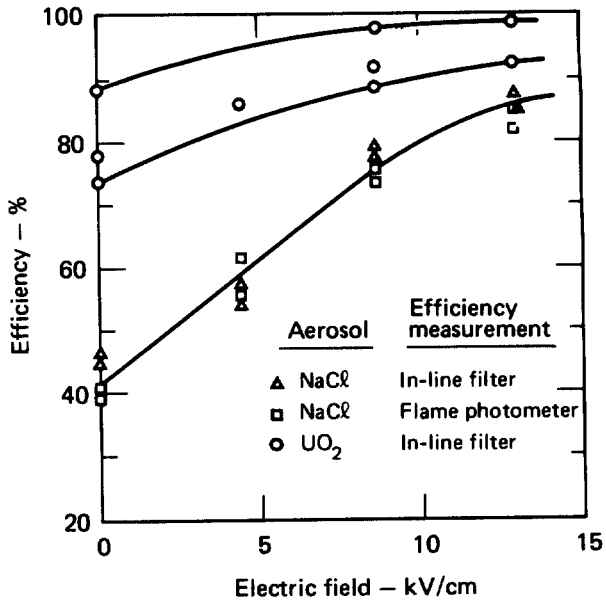

Figure 25

Efficiency of the prototype glove box filters for NaCl and UO_2 aerosols as a function of the applied electric field.

We measured the size distribution of the UO_2 aerosols with an Andersen impactor and found the activity median aerodynamic diameter (AMAD) was 5.4 μm. Figure 26 shows the size distribution of the UO_2 and NaCl aerosols with the cumulative percent of mass or activity plotted as a function of the aerodynamic diameter. The NaCl distribution was determined from mass measurements, while the UO_2 distribution was determined from activity measurements. The larger size of the UO_2 aerosols accounts for the higher efficiency compared to the NaCl aerosols in Fig. 25.

The effect of the electric field on filter efficiency is hard to see in Fig. 25 because both the mechanical and electrical filtration mechanisms contribute to the observed efficiencies. Figure 25 implies that the electric field has a much greater effect on the NaCl test than on the UO_2 test. However, replotting the data for UO_2 and NaCl as $\ell n(P/P_o)$ versus the electric field would remove the mechanical mechanisms and show the electric field has the same effect on both aerosols. The decrease in the average filter penetration is 72% for both UO_2 and NaCl aerosols when the electric field is increased from 0 to 12.8 kV/cm.

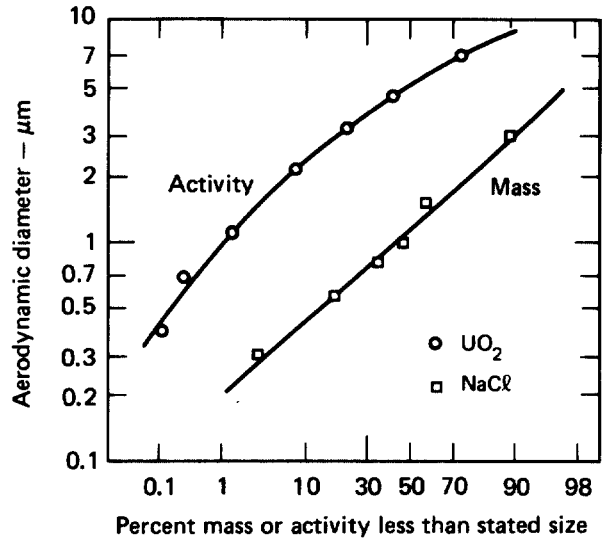

Figure 26

Particle size distribution for UO_2 and NaCl aerosols.

The same decrease in filter penetration for both UO_2 and NaCl aerosols with increasing electric field appears to contradict our previous statement that the electric field (via dielectrophoresis) has no measurable effect on the filtration of large particles. This apparent contradiction can be resolved by noting in Fig. 25 that 80-90% of the UO_2 particles are trapped by the filter with no electric field. Most of the trapped particles are large, whereas those penetrating the filter are small. This does not contradict our previous statements since the electric field decreases the penetration of the small UO_2 particles.

We also conducted filter loading tests on the electrostatic filter installed in the UO_2 glove box. Figure 27 shows the filter efficiency and pressure drop for two loading tests, with and without an applied electric field, as a function of the particle mass trapped on the filter. These field data illustrate all the major trends seen in the laboratory tests with NaCl aerosols summarized in Table III. Figure 27 shows that filter efficiency increases with particle mass and with an applied electric field. The lower pressure drop at the high mass loading is also seen for the filter with an electric field. Although Fig. 27 implies there is little difference in filter efficiency with and without an electric field at a high particle mass, this is not true. The UO_2 penetrations at 6 g are 0.22% with and 0.72% without an electric field. Thus, the electric field significantly reduces penetration.

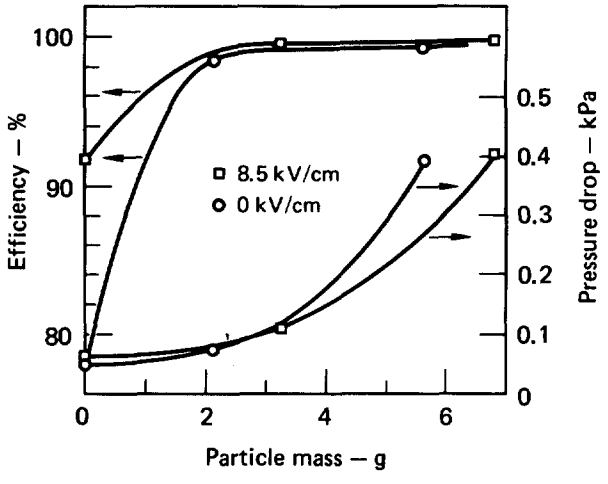

Figure 27

Filter efficiency and pressure drop for the prototype glove box filters during filter loading with and without an applied electric field.

An important finding of our field evaluation was the recovery of material normally lost in the ventilation system or in a HEPA filter. We found over 70% of the particle mass trapped on the filter could be recovered by gently shaking the filter and reusing it in normal operation. The pressure drop on this semi-clean filter was only slightly higher than the initial value. We successfully completed two cycles of filter loading and cleaning and believe repeated loading and cleaning may be possible.

In addition to our glove box applications, we are developing an electrostatic filter unit for installation in typical ventilation systems in the nuclear industry. To accomplish this objective, we have completed construction and calibration of the large-scale test system shown in Fig. 28. This system is designed to test prototype electrostatic filters at flow rates up to 0.472 m^3/s (1000 cfm). Our test results with the flat screen design and NaCl aerosols are in good agreement with comparable tests in our small-scale and glove box systems. We are building and will soon evaluate extended area prefilters using electric fields.

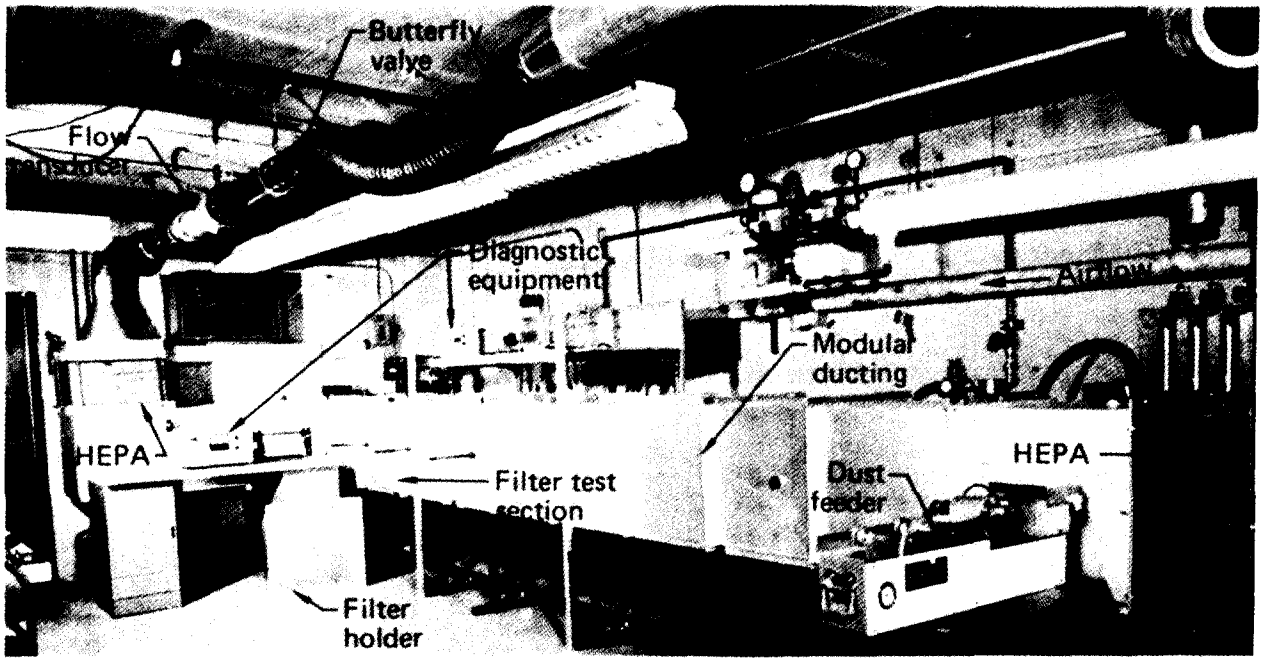

Figure 28 Large-scale test system.

V. Conclusions

The objective of LLL's Enhanced Filtration Program is to increase the service life of HEPA filters, thereby reducing filtration costs and the volume of nuclear waste. To reach this objective, we used an electrostatic filter to take the load off the HEPA filter. The electrostatic filter consists of a fibrous filter mat having a superimposed electric field generated by high-voltage electrodes that sandwich the filter. Investigation of this electrostatic filter is continuing, and the results presented in this paper represent a progress report of most of our work from January 1977 to June 1978. A number of additional investigations were not sufficiently advanced to be presented here. The major findings of this investigation were:

- Dielectrophoresis (the electric force between polarized particles and polarized fibers) makes a negligible contribution to the observed increase in filter efficiency with an applied electric field.

- Pressure drop theories for fibrous filters were extended to allow for distributions of fiber size. The predicted fiber diameter values for filter media were 9-33% lower than those calculated from pressure drop measurements and Davies' empirical equation[1].

- A new filtration mechanism based on the interaction of charged fibers and charged particles was responsible for much of the increased filter efficiency with an applied electric field.

- The electrostatic filter is a complex, dynamic system involving the buildup and dissipation of charge on the fibers.

- Fiber conductivity and electrode insulation have a large effect on filter efficiency. A filter with conducting fibers (10^8 ohm/cm) and insulated electrodes

had no improvement in filter efficiency with an applied electric field. The same filter showed a large increase in filter efficiency when noninsulated electrodes were used.

- A theoretical model was developed that successfully explains the electrostatic filter efficiency.

- A theoretical model was developed that successfully explains the increase in filter efficiency and pressure drop that occurs during filter loading. Experimental data with different face velocities, particle size, and particle mass loading agreed with theoretical predictions.

- Filter loading tests with an applied electric field showed higher efficiencies and lower pressure drops than comparable tests without an applied electric field.

- Prototype electrostatic filters for glove box applications were built and evaluated in both laboratory and field tests. The evaluations were very successful.

VI. Acknowledgements

The authors take great pleasure in acknowledging the help of D. E. Salmi, H. L. Tasto, W. J. Kadi, and S. W. Wilson of LLL for the design and construction of the filter test facilities and prototype electrostatic filters shown in this report.

We are also indebted to Dr. J. C. Dempsey of DOE for his suggestions and for important information on new developments in the filtration field.

VII. Bibliography

1. Davies, C. N., Air Filtration, Academic Press, New York (1973).

2. Rossano, A. T., and Silverman, L., "Electrostatic effects in fiber filters for aerosols," Heating and Ventilating, Ref. Sect. 102 (1954).

3. Reid, D. L., and Browne, L. M., "The electrostatic capture of submicron particles in fiber beds," Proc. 14th ERDA Air Cleaning Conf. (Sun Valley, Idaho, 1976).

4. Mazumder, M. K. and Thomas, K. T., "Improvement of the efficiency of particulate filters by superimposed electrostatic forces," Filtration and Separation, 25, (1967).

5. Silverman, L., Billings, C. E. and Dennis, R., Performance of the Model K Electro-Polar Filter, USAEC Report NYO 1592, Harvard University (1954).

6. Havlicek, V., "The improvement of efficiency of fibrous dielectric filters by application of an external electric field," Int. J. Air and Water Poll., 4, 225 (1961).

7. Rivers, R. D., "Operating principles of non-ionizing electrostatic air filters", J. ASHRAE, 37, (1962).

8. Kirsch, A. A., "The influence of an external electric field on the deposition of aerosols in fibrous filters," J. Aerosol Sci., 3, 25 (1972).

9. Walkenhorst, W., "Reflections and research on the filtration of dust from gases with special consideration of electrical forces," J. Aerosol Sci., 1, 225 (1970).

10. Iinoya, K. and Makino, K., "Applications of electric field effects to dust collection filters," J. Aerosol Sci., 15, 357 (1974).

11. Bogardus, H. F., Clark, R. C., Thompson, J. K., and Fielding, G. H., "Enhancement of filter media performance by corona-free electric fields," Proc. 13th AEC Air Cleaning Conf. (San Francisco, Calif., 1974).

12. Lamb, G. E. R. and Costanza, P. A., "Electrical stimulation of fabric filtration," J. Textile Res., 372 (1977).

13. Ariman, T. and Tank, L., "Collection of aerosol particles by fabric filters in an electrostatic field," Atmos. Envir.,10, 205 (1976).

14. Nielsen, K. A. and Hill, J. C., "Collection of inertialess particles on spheres with electrical forces," Ind. Eng. Chem. Fundam,15, 149 (1976).

15. Frederick, E. R., "Some effects of electrostatic charges in fabric filtration," Fine Particulate Control Technology, H. M. Englund and W. T. Beery eds., Air Pollution Control Association, Pittsburgh, PA (1975).

16. Penney, G. W., "Using electrostatic forces to reduce pressure drop in fabric filters," Powder Tech.,18, 111 (1977).

17. Thomas, J. W. and Woodfin, E. J., "Electrified air filters," J. AIEE, 275 (1959).

18. Inculet, I. I. and Castle, G. S. P., "A two-stage concentric geometry electrostatic precipitator with electrified media," J. ASHRAE, 47, (1971).

19. Nelson, G. O., Richards, C. P., Biermann, A. H., Taylor, R. D., and Miller, H. H., "Air filtration enhancement using electronic techniques," Proc. 14th U.S. ERDA Air Cleaning Conf. (Sun Valley, Idaho, 1976).

20. Nelson, G. O., Bergman, W., Miller, H. H., Taylor, R. D., Richards, C. P., and Biermann, A. H., "Enhancement of air filtration using electric fields," J. AIHA,39, 472 (1978).

21. Zebel, G., "Deposition of aerosols flowing past a cylindrical fiber in a uniform field," J. Colloid. Sci.,20, 522 (1965).

22. Kuwabara, S., "The forces experienced by randomly distributed parallel circular cylinders or spheres in viscous flow at small reynolds numbers," J. Phys. Soc. Japan, 14, 527 (1959).

23. Happel, J. "Viscous flow relative to arrays of cylinders," J. AICHE, 5, 174 (1959).

24. Spielman, L. and Goren, S. L., "Model for predicting pressure drop and filtration efficiency in fibrous media," Env. Sci. Techol., 2, 279 (1968).

25. Davies, C. N., "The separation of airborne dust and particles," Proc. Inst. Mech. Eng., 1B, 185 (1952).

26. Pich, J., "Theory of aerosol filtration by fibrous and membrane filters," Aerosol Science, C. N. Davies, ed., Academic Press, New York (1966).

27. Payatakes, A. C., "Model of the dynamic behavior of a fibrous filter. Application to case of pure interception during period of unhindered growth," Powder Technology, 14, 267 (1976).

28. Nelson, G. O., Bergman, W., Taylor, R. D., Miller, H. H., Biermann, A. H., and Richards, C. P., Enhanced Filtration Progress Report, July-September 1976 Lawrence Livermore Laboratory, Rept. UCID-16949-76-3 (1977).

29. Adley, F. E. and Wisehart, D. W., "Filter loading tests on certain filter media," Proc. Seventh AEC Air Cleaning Conf. (Office of Technical Services, Washington, 1961).

DISCUSSION

BURCHSTED: Are the efficiencies you cited mass or number efficiencies?

BERGMAN: They are mass efficiencies.

BURCHSTED: An observation: we may be developing a nomenclature problem in calling these electrostatic filters, perhaps causing confusion with the better known plate-and-electrode electrostatic precipitator. I suggest the term "charged/polarized fiber filter" or "electrostatically charged/polarized fiber filter."

BERGMAN: I agree that there may be confusion. I like Dr. Rivers' term: "a nonionizing electrostatic filter." George Lamb, at Princeton Textile Institute, has called them "electrostatic filters, ESF."

RIVERS: Early in your talk you mentioned that the dielectrophoretic force was considerably less than the coulombic. I agree, and since this is the case, it would seem advantageous to increase the coulombic force by pre-charging the aerosol. Since all the elements for an ionizer (dust charger) are present, and the additional power consumption is quite trivial, have you considered adding an ionizer? In my experience, this results in sharply increased efficiency over the non-ionizing case.

BERGMAN: I mentioned a couple of references in the paper where people such as Don Reed (14th ERDA Air Cleaning Conference) have used aerosol precharging instead of just having an aerosol deposit naturally by image forces and charged fiber-charged particle interactions. You can also increase performance by having an electric field superimposed. So you see, you can use quite a variety of different combinations. We did not attempt to precharge the aerosols because electrical means require a high power consumption and a corona discharge. The system I described employs approximately 15 kilovolts and less than one microamp of current. This will give you an idea of how little power consumption is involved. We envisage an entire HEPA filter bank being operated by the equivalent of the power of a light bulb.

RIVERS: I agree that an ionizer requires a lot more current, but it is still trivial.

T. F. ALLEN: We did some work on polarizing DOP and we experienced a lot of arcing in the system. You mentioned the use of polypropylene in the frame material of the filter. Polypropylene is a combustible material, and would not be allowed in a ventilating system. I wonder about this.

BERGMAN: This is our first prototype unit. We have a joint program with a group at Rocky Flats to explore additional versions. We don't consider the materials that we are using now to be the final design. In other words, we are primarily interested in insulation and preventing sparking and we have not seen sparking when we insulate the electrodes. When we do not insulate the electrodes, we do see significant sparking.

ALLEN: What voltage are you using?

BERGMAN: We are using 10,000 volts.

DYMENT: This is a fascinating paper and especially authoritative in respect to the fact that you use sodium chloride aerosols for your evaluations. Seriously, I have two questions; first, you state in your paper that for a uniformly thick filter medium, assuming particles stick at the first impact, one would expect the particle deposition density to tail away exponentially from the upstream face. Do any of your observations support this?

BERGMAN: It did and it did not. The smaller fibers show a heavy deposit on the surface which is what you'd expect from exponential decay by the standard filtration theories. For the filters composed of larger fibers, the heaviest deposit is somewhere in the center of the filter, rather than one the front surface. This is due to inefficient adhesion between particle and fiber after a collision. So, the theoretical models have to incorporate a sticking efficiency factor, whether you use van derWaal's forces or some other appropriate sticking factor. Thus, in some cases, you do see exponential decay whereas in others, you do not, but these differences can all be explained by rational means.

DYMENT: The second question: have you investigated the performance of your enhanced filter using a standardized test method such as ASHRAE 52-76 so that performance characteristics can be compared directly with commercially available filters of other types?

BERGMAN: The report shows our large scale 1000 CFM system. We have a standard ASHRAE dust feeder, we have a standard UK sodium chloride generator, and DOP generators, and we plan to make a thorough comparison with all of these aerosols.

STUDIES ON PROLONGING HEPA FILTER SERVICE IN CHEMICAL APPLICATIONS

R. W. Woodard, K. Terada, O. I. Buttedahl
Rockwell International
Energy Systems Group
Rocky Flats Plant
Golden, Colorado
Work Funded by the Department of Energy

Abstract

The report presents information on activities directed toward gaining a better understanding of the performance of materials used in the construction of HEPA filters. The report discusses experiments in which materials were exposed to nitric and hydrofluoric acid vapors under controlled conditions in a specially constructed test chamber. In addition, observations are presented on filters tested in actual service. Finally, work on cleanable prefilters is reviewed.

I. Introduction

High Efficiency Particulate Air (HEPA) filters are relied upon to clean the air from chemical glovebox operations used in plutonium recovery. It is the objective of the work on this project to acquire information which will permit development of improved filters for chemical service.

II. Description of Chemical Exposure Tests

Test Chamber

A test chamber has been designed and constructed for the exposure of filter media to corrosive chemical vapors. The chamber is a stainless steel glovebox measuring 2 1/2 x 3 x 7 ft. with an atomizing nozzle and filter sample holders at opposite ends. A solution containing about 50 ppm hydrofluoric acid (HF) by weight and 8000 ppm of nitric acid (HNO_3) is atomized into the chamber atmosphere and drawn through the filters. These concentrations were selected in order to obtain an exposure level of about 50% relative humidity. There are holders for four filter handsheets, each with exposure dimensions of 8 x 8 inches. Flow rate through each filter was adjusted at 2 cfm to approximate the maximum flow rate of 1000 cfm through a 2 x 2 x 1 ft. HEPA filter. Dry air was added to the atomized solution to achieve the desired atmospheric concentrations.

A schematic diagram of the test chamber is shown in Figure 1. The amount of acid sprayed into the chamber is controlled by the air pressure in the atomizer. Dry instrument air is piped into the chamber to maintain the 50% relative humidity at 68°F. The relative humidity is allowed to fluctuate with temperature but the atomizing pressure is kept constant to maintain a steady rate of acid flow. Very little change in relative humidity is recorded as the laboratory temperatures in the past have ranged from a maximum of 77°F to a minimum of 68°F. Normal daily fluctuation range is about 4°F.

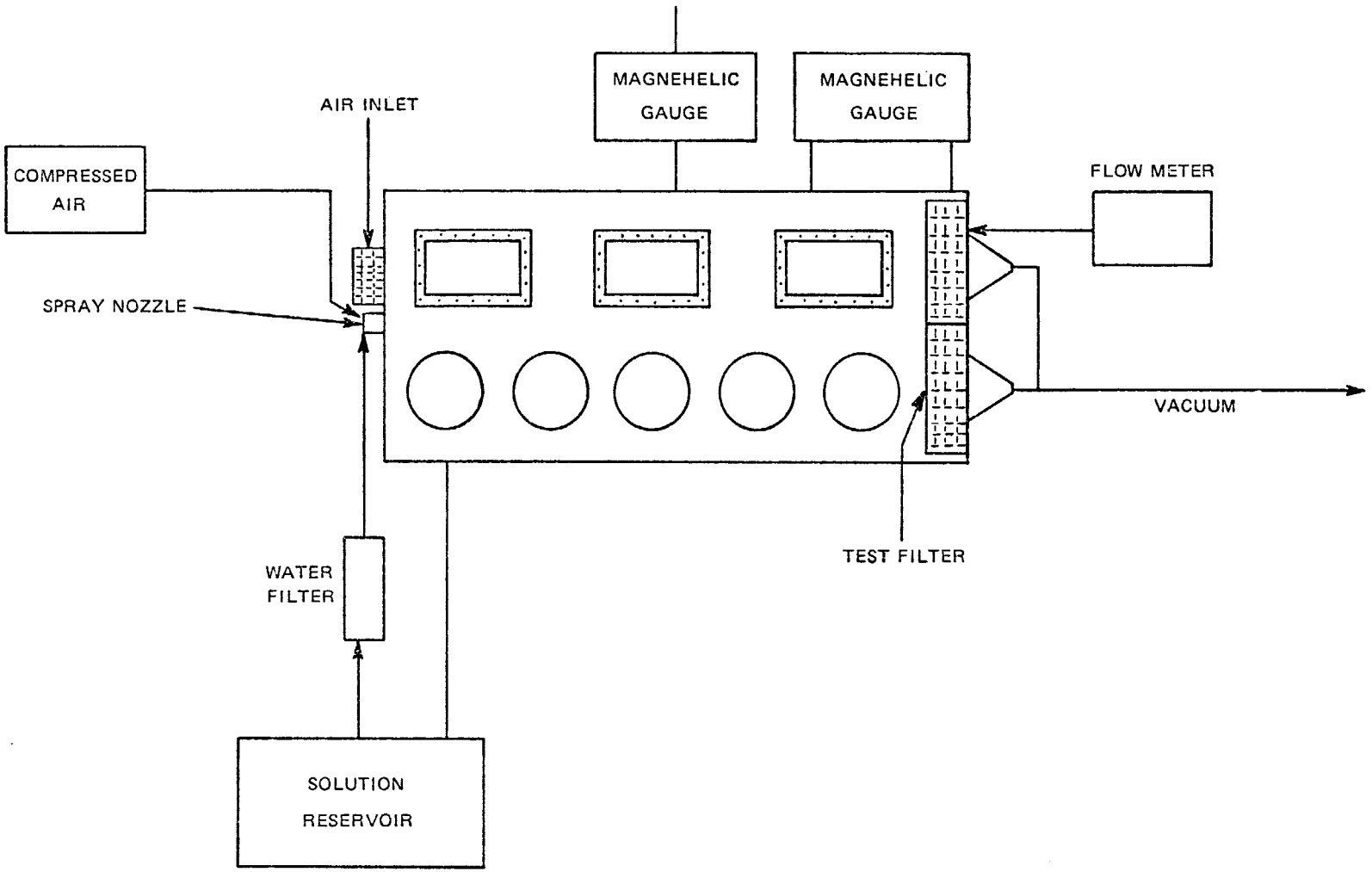

Figure 1. Schematic Diagram of Test Chamber

Air is drawn through the chamber and filter media using the house vacuum line. An automatic control valve was placed in the line to compensate for any change in pressure.

A data acquisition system was installed to record information every hour. Data are currently being gathered on room humidity, room temperature, test chamber atmosphere temperature, house vacuum, NO_x concentration and total flow rate. Figure 2 shows a schematic diagram of the instrumentation of the chamber. The wet and dry bulb hygrometer data for the test chamber humidity is recorded on a separate chart. Thus far, attempts to interface a hygrometer with the data acquisition system have failed because of the corrosiveness of the chamber atmosphere.

Chemical Exposure of Filter Media

The initial experiments in the chamber were conducted to determine whether the small amount of crocidolite asbestos (~5%) improves the chemical resistance of the filter medium. Handsheets containing different concentrations of asbestos were exposed in the test chamber. Table I shows the data obtained in a series of tests. The results show that media with asbestos have greater retention of filtration efficiency after chemical exposure than the media without any asbestos. Under the conditions of the test there was no loss of chemical resistance when the asbestos contents were reduced to 4 and 3%.

When the asbestos was eliminated there was a significant increase in penetration. This is demonstrated where filter handsheets with and without asbestos were exposed to the same acid atmosphere simultaneously and for the same period.

Table I. $HF-HNO_3$ Exposure Tests on Filter Media
Exposure Time - 2 Weeks

*Sample #	% Asbestos	**% Penetration Before	After
57	4	0.008	0.006
58	4		0.006
59	4		0.005
60	4		0.008
61	3	0.009	0.004
62	3		0.006
63	3		0.008
64	3		0.010
69	0	0.008	0.036
70	0		0.080
71	4	0.008	0.006
72	4		0.010
73	0	0.005	0.012
74	0		0.060
75	4	0.005	0.012
76	4		0.008
79	0	0.010	0.044
80	4	0.006	0.006

* Samples in brackets were run simultaneously.
**The penetration test is destructive and the "before" tests were on

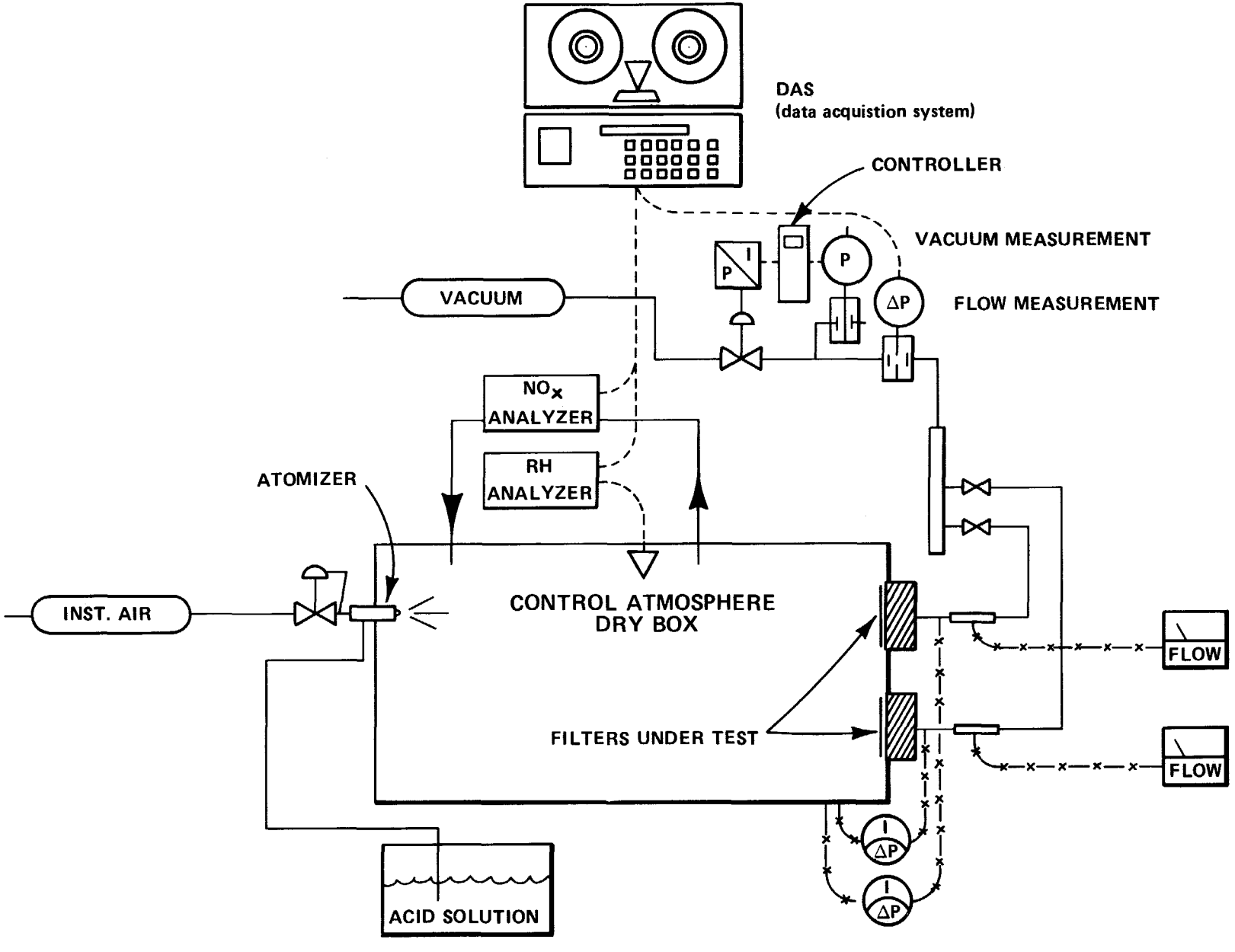

Figure 2. Diagram of Test Chamber Instrumentation

handsheets made at the same time the test sheets were prepared but were not exposed to the acid atmosphere in the chamber.

Further tests to determine the optimum amount of asbestos to maximize corrosion resistance of the filter media have been suspended because of the health concerns regarding the handling of asbestos. Filter manufacturers are converting to asbestos-free filter media which has made the effect of asbestos in filter media a moot question.

Scanning electron photomicrography of the filter media exposed to the acid atmosphere in the test chamber has shown the presence of two different types of formations resulting from chemical attack of the filter media. They were web-like films connecting two glass fibers and bead-like structures strung along individual fibers. Electron microprobe analyses showed iron, nickel, and chromium present in the beads. Figure 3 is a scanning electron photomicrograph at 5000 magnification of a filter medium exposed to acid vapors in the test chamber. The numbers on the photograph refer to the areas which were analyzed with an energy dispersive spectrometer (EDS). Figures 3 a, b, and c are photographs of CRT displays of EDS scans of areas 1 - 3 respectively. The scans were over a range of 0 to 10.230 Kev in 50 seconds. Energy dispersive analyses show that areas 1 and 3 have typically a glass fiber composition. In the bead (area 2), although the concentration of silicon is less than that in the fiber, it is sufficiently great to indicate the HNO_3-HF solution had attacked the glass fiber and left silicate beads as it dried. The presence of iron, nickel, and chromium is attributed to the mist of acid solution carrying a small concentration of corrosion products of the stainless steel acid reservoir. Acid mist, along with acid transported in the vapor state, corrodes the fiberglass. The finer fibers are preferentially corroded away resulting in loss of filter efficiency. Degradation of filters due to chemical exposure is likely to be basically by this mechanism.

Future work in the test chamber will be to establish whether some of the commercial, asbestos-free, acid resistant filter media are truly more chemically resistant and longer lived. Other experimental filter media which show a good filtration efficiency and other physical properties will be tested to evaluate their potential use in HEPA filters.

Chemical Exposure of Separators

The establishment of asbestos as a carcinogen has forced filter manufacturers, as well as users, to consider means to eliminate asbestos. Most of the asbestos used in HEPA filters is in the separators which serve to keep the filter media apart to maintain a free airflow.

There are several approaches to this problem with regard to separators. One approach is to design the filter so that separators are not required. A manufacturer already is marketing a separatorless filter which is being evaluated in use at Rocky Flats. Another manufacturer is producing filters using tapes or strings as separators.

Figure 3. Scanning Electron Photomicrograph of Filter Medium after Chemical Exposure - 5000X

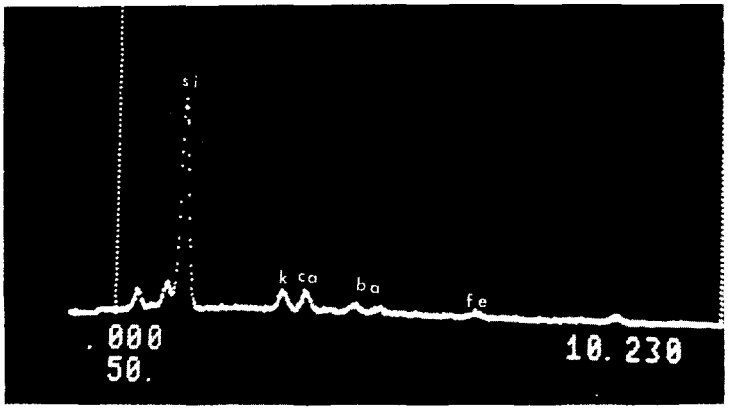

AREA 1

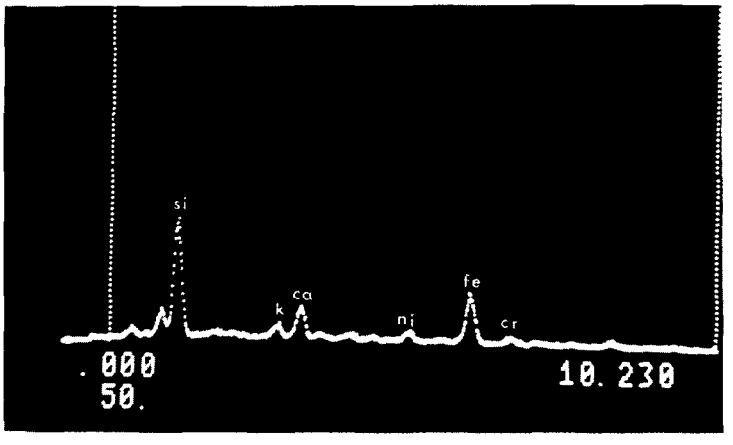

AREA 2

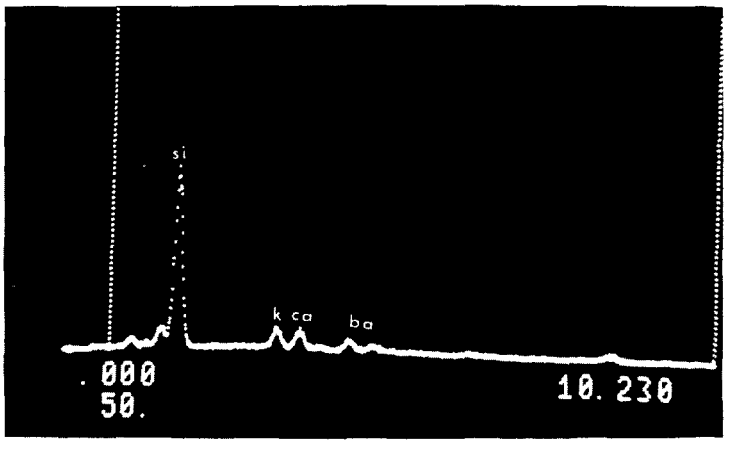

AREA 3

Figures 3a, 3b, 3c. Cathode Ray Tube Displays of Energy Dispersive Spectrometer Scans of Areas 1, 2, and 3 shown in Figure 3.

To insure a regular supply of filters which meet our specifications, Rocky Flats is investigating the possibility of using substitute materials to replace the asbestos separators.

Two general types of material were investigated or substituted for asbestos. They were plastics and metals. Three criteria used to screen candidate materials were flammability, chemical resistance, and cost.

It was found that the cost of plastic separators were at a minimum several factors higher than asbestos. For example, a polyvinylchloride (PVC) separator, 7 1/2 mil thick as shown in Figure 4, costs roughly 55¢ each in quantities in excess of 5000. Plastic material other than PVC tends to increase considerably above this cost. The cost of each asbestos separator is about 13¢. Another problem associated with the corrugation of plastics is that it can have memory which tends to return them to their original shape. This tendency can be reduced or eliminated by heating the material during corrugation. The memory of some polymers can also be destroyed by exposure to gamma irradiation. Gamma rays can break molecular chains and rearrange them so the material retains its new shape. The separators were fabricated from 7 1/2 mil thick PVC sheets by heating them in a mold. While the sheets exhibit little or no memory at room temperature, at about 150° they become pliable and sag.

Of the metal separators, aluminum was judged to be the most suitable. Its major shortcoming is a lack of acid resistance, especially to hydrofluoric acid. Attention was directed toward methods of protecting it from direct exposure to acid vapor. Two methods are being considered: one of them is the use of organic coatings such as fluorocarbon, epoxy, and phenolics which have good flame resistance as well as chemical resistance; the other is lamination with polymer films.

Polyvinylidene chloride and polyvinyl chloride laminated to aluminum were obtained from suppliers and suspended in the filter media test chamber for several months. Some delamination was more pronounced with the polyvinylidene chloride than the polyvinyl chloride. Exposure of the specimens whose edges were sealed with RTV silicone adhesives prevented any delamination or decomposition indicating that permeation of acid through the 0.5 and 1.0 mil polyvinylidene and polyvinyl chloride films is not a problem. Each vendor apparently uses his proprietary adhesive and will not reveal the formulation. One supplier's adhesive required that the aluminum foil be degreased before application and they did not have a practical process to accomplish this. When heat was used to degrease the aluminum, the heat treatment caused the aluminum to lose its temper. The alloy approved for use in the fabrication of HEPA filter separators requires a hardened grade.

Aluminum laminated with PVC by an aluminum company exhibited the greatest promise. Polyvinylidene laminate might be suitable if the plastic films were allowed to extend beyond the edge of the aluminum and sealed together. However, it was decided to use the PVC laminate for prototype studies since it exhibited only minor delamination in the test chamber.

Figure 4. Polyvinyl Chloride Separators

Preliminary work with fluorocarbon and silicone coatings and a polyimide laminate indicates lack of adequate adhesion in the coatings and excessive cost for the laminate.

Stainless steel sheets for separators appear to be suitable except the cost of the steel would exceed $500 per filter.

Future work planned is to continue testing and evaluation of coatings for aluminum.

III. In-Service Filter Testing

Chemical Studies

Chemical studies are made on components of HEPA filters which have been in service. The samples are taken from HEPA filters used in plenums to filter air exhausted from Production chemical glovebox lines. Figure 5 shows the location of the filters in the exhaust system. Note that six stages of filtration are used in booster plenums and two more stages in the main plenum. Most "in-service" tests are carried out by placing the test filters in the first stage of the four-stage booster.

The filters in the first stage bear the brunt of particulate and chemical vapors. The filters are highly contaminated during service and chemical tests can only be performed in a properly outfitted laboratory. However, in one instance, a filter removed from the sixth stage was not contaminated and could be handled without special precautions. Observations relating to the filter removed from the sixth stage are presented in Table III.

Table III. Data on HEPA Filter Removed from 6th Stage

Filter: Size 5, glass asbestos medium, asbestos paper separators
Manufacturer: Flanders Filters, Inc.

Tests on filter prior to service: Hanford Certification Lab(3/18/74)
Penetration: 100% flow .006% (.78" W.C. ΔP)
20% flow .004%
Gross weight (estimated): 21.4 kg (47 lbs.)

Tests after one year of service: Rocky Flats Filter Certification Lab
Penetration: 100% flow .004%
20% flow .020%
Gross weight: 30.4 kg (67 lbs.)

Test on medium taken from used filter:
Resistance: 42 mm W.C. @ 3.2 lpm thru 100 cm^2
Tensile strength: Machine direction 7.42 lbs. per sq. in.
Cross direction 5.27 lbs. per sq. in.
Bulk: (thickness) .023 inch

The weight of the filter as noted in Table III was 67 lbs. A new filter averages about 47 lbs. The increase in filter weight, estimated at 20 lbs., is attributed primarily to reaction of ingredients in the separator with nitric acid and/or NO_x fumes, along with

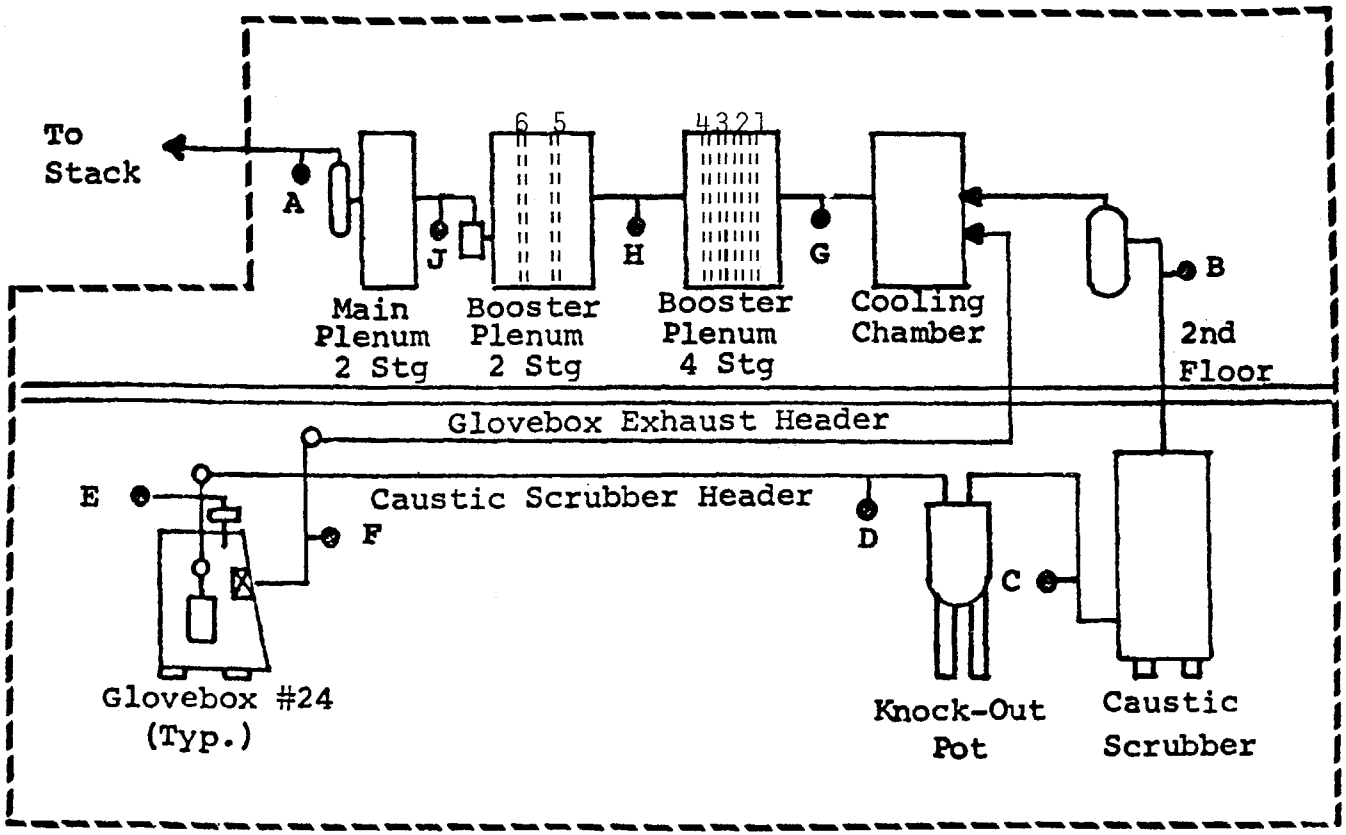

Figure 5. Exhaust System - Pu Chemical Recovery

absorption of water. Evidence of the nitration reaction is depicted in the photograph shown in Figure 6 where crystals of magnesium nitrate are evident on the surface of separator material viewed under low power magnification.

Analytical data on the sixth stage filter components are presented in Table IV.

Table IV. Chemical Analyses of HEPA Filter Removed from Sixth Stage

Sample Description	Wt. Loss (%) to (C°)	Water Soluble (%)	Fluoride (%)	Nitrate (%)
Medium	3.6 950	2.7	.10	1.0
Separator	61.0 840	68.3	.07	35.8

The analyses support the observation that the filter, particularly the separator, became heavily nitrated.

Separatorless Filters

In-service tests have been made on separatorless filters on three occasions. The filters were Flanders Super-Flow® (Super-Flow is a trademark of Flanders Filters, Inc., Washington, N.C.) and constructed using a medium identified as Y100 with additive.

The filters have been mounted in the first stage of the plenum and the length of the in-service test ranged from 3 1/2 to 8 months. There has been no visible sign of failure of these filters. In one instance, one of the separatorless filters removed from service was transferred to a glovebox and the frame cut away to permit closer inspection of the medium. The medium was dark and dusty on the upstream face but clean and white on the downstream side. The medium was pliable. Penetration tests of the medium could not be performed because of plutonium contamination.

Chemical Resistant Filter

Contacts were established with the C. H. Dexter Division of Dexter Corporation and Mine Safety Appliances Company in regard to constructing special filters. The filters requested were to be fabricated using Dexter 1236 medium and asbestos paper separators. Both the medium and the separators to be treated by Dexter's patented process (1).

Samples of the Dexter medium to be used in the filters were subjected to analyses to evaluate its properties. The details of the thermogravimetric analysis appear in Table V.

Analysis by mass spectrometry indicated the volatiles included water, diethyl phthalate, and organics suggestive of cellulose (CH_3OH, etc.) Infrared analysis of the residue obtained from an extraction of the medium by boiling carbon tetrachloride indicated polyphenylene oxide (PPO).

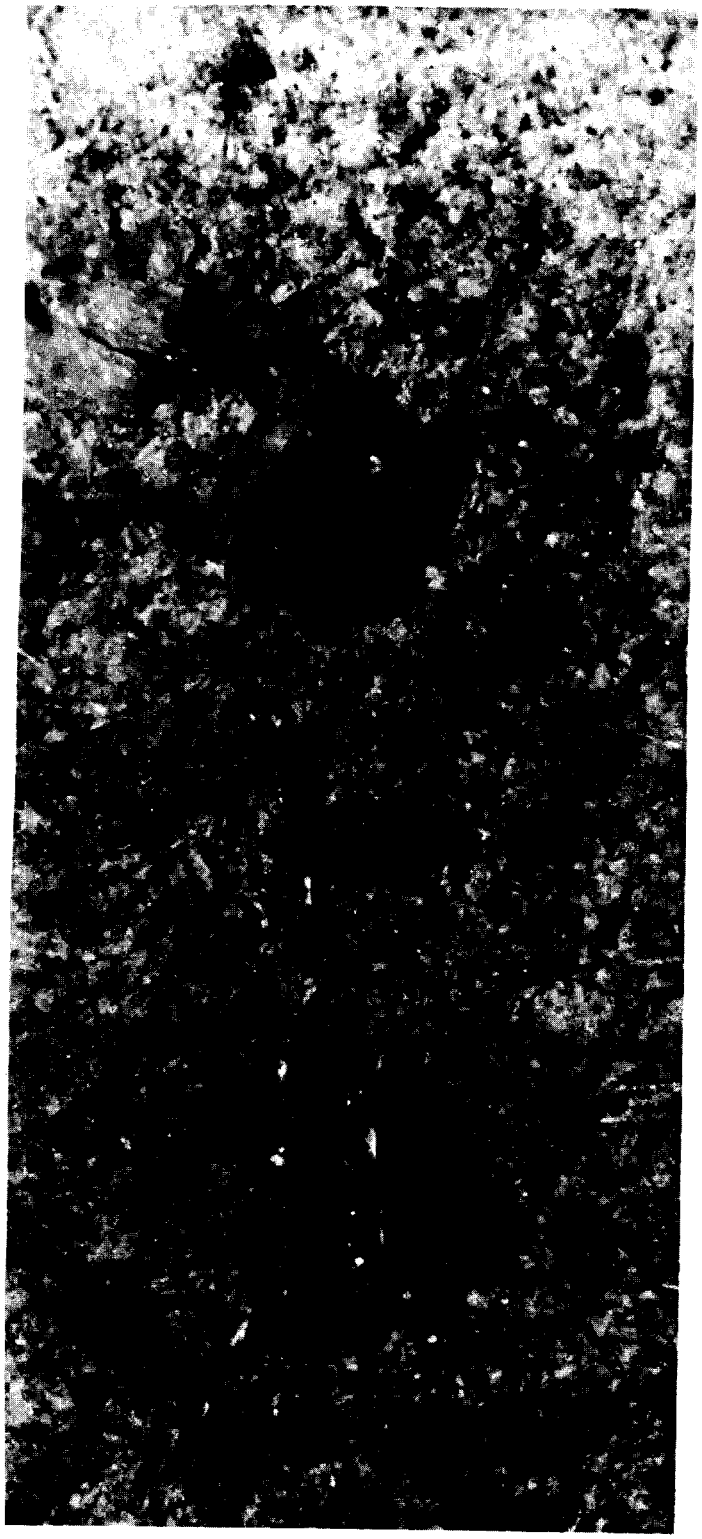

Figure 6. Photomicrograph (15X) of Magnesium Nitrate Crystals on Separator Sample from 6th Stage Filter

Table V. Thermogravimetric Analysis of Dexter 1236 Medium

Temperature Range (°C)	Weight Loss (%)	Comment
25-180	.43	Loss of H_2O
180-330	1.1	Attributed to loss of diethylphthalate but may include some PPO degradation.
330-490	2.8	Decomposition and oxidation of PPO
490-800	.08	Oxidation of residual carbon

Four special-built HEPA filters (2' x 2' x 1') were received from Mine Safety Appliance Company (MSA). The filters were constructed by MSA using Dexter 1236 medium and asbestos paper separators. Both medium and separators had been treated with polyphenylene oxide (PPO) as described in Dexter's patent (1).

The filters were tested at the Rocky Flats Filter Certification Laboratory. Test results were as follows:

Filter Serial No.	Resistance Water Gage (in.)	DOP Penetration (%) 100% Flow	20% Flow
66553	.97	.016	.014
66554	.97	.014	.014
66555	.98	.016	.014
66556	.98	.016	.012

The filtration efficiency is better than the required minimum of .03% penetration by DOP aerosol even though the filters were fabricated using special medium and separators.

Two of these filters were placed in service for five months. Samples of the exposed medium and separator were chemically analyzed. Analyses were also performed on a standard glass/asbestos filter exposed alongside of the "chemical resistant" filter. Results appear in Table VI.

Table VI. Chemical Analyses of Regular and Chemical Resistant Filters After 5 Months Service

Sample Description	Weight Loss (%) to (°C)		Water Soluble (%)	Fluoride (%)	Nitrate (%)
Standard glass/ asbestos:					
Medium	15.13	960	33.8	1.67	6.1
Separator	49.82	970	47.8	.22	18.7
Chemical Resistant:					
Medium	16.71	970	Lost	1.30	6.4
Separator	44.51	970	50.1	.12	22.9

The performance of the chemical resistant filter under the conditions of this test show it to be as good as the standard glass/ asbestos filter with which it was compared. Additional in-service testing is under way relating to the effect of exposure on penetration.

Test of Aluminum Separator Protected with Polyvinyl Chloride Film Laminate

Corrugated aluminum is frequently used as a separator in construction of HEPA filters. While aluminum is satisfactory in most applications, it is more vulnerable to attack by chemical vapors; e.g., nitric acid in the presence of hydrofluoric acid. Encouraging laboratory results on protection of aluminum with a polyvinyl chloride (PVC) film laminate was extended to an in-service test.

An aluminum company laminated about 200 yards of 10 1/2-inch wide and 0.0015-inch thick aluminum with 0.001-inch thick PVC film on both surfaces. The alloy conformed to Military Specification 51068C for aluminum separators. A filter manufacturer constructed the prototype filter and experienced no difficulty in the fabrication. Tests at the Rocky Flats Filter Certification Laboratory on the finished filter showed the following results:

Penetration

At 1000 cfm	0.024% (0.030% maximum allowable)
At 200 cfm	0.032% (0.030% maximum allowable)

For normal use, this filter would have been rejected on failure to meet the penetration requirements at 200 cfm. However, it was placed in the first filter bank of a plutonium processing facility where HEPA filters are exposed to the most corrosive chemicals on the plant site. It was possible to install this filter for in-service tests despite its nonconformance to specifications because there are six banks of filters in the filtration system where only four are required. Also, the cause of nonconformance of the filter was independent of the laminated aluminum separators and significant

information could be obtained by the in-service test. The filter was installed in the filter bank for over five months. Examination of the filter after its removal from the plenum showed no visible sign of degradation of the separators. However, a fire test at Edgewood Arsenal, N.J., where a prototype filter was exposed to a flow of hot air up to 750°F,demonstrated that the laminate was too flammable. Investigation of more temperature resistant materials is under way.

Cleanable Prefilters

An objective of the Filter Development Program is to increase the life of HEPA filters. The use of prefilters in conjunction with HEPA filters is one means whereby HEPA filter life can be extended. Many types of prefilters are available and incorporate a variety of fibrous materials such as glass, mineral, metal, and plastic.

Prefilters are usually constructed with a filter mat of rather loosely packed fibers. While in service, particulate matter collects in the fibrous medium and after the filter becomes sufficiently loaded the prefilter is removed and replaced. The used prefilter is discarded.

A logical objective in developing prefilter systems used in plutonium processing applications is to identify a means of cleaning the prefilter. A cleanable prefilter would offer the advantages of increased prefilter life and returning the plutonium to the process stream. Two materials have been investigated to determine the feature of cleanability.

Waterweb®

Waterweb® (Waterweb is the trademark of Heat Systems-Ultrasonics, Inc., Plainview, L.I., N.Y.) is a material developed for use as a demister and consists of plastic coated fiberglass screen which has been compressed into a rigid slab. Use of Waterweb as a prefilter is a departure from the use for which it was originally designed.

The first tests using this material were carried out by cementing a one-inch thick piece of Waterweb on a stainless steel frame which could be mounted in a holder normally used for a HEPA filter. Installation was made in a glovebox in which plutonium residues are leached. Exposure conditions include fine dust, moisture, hydrofluoric, and nitric acid fumes.

During the test the procedure was followed of exhausting the box through the prefilter. The surface of the prefilter became coated with a layer of dust approximately 1/8-inch thick and the pressure drop rose to as high as eight inches water column (W.C.) At this time the prefilter was valved out of service and the box was ventilated through an adjacent filter. The surface of the medium was vacuumed off using a 3/8-inch plastic hose connected to a vacuum receiver.

After vacuuming, the prefilter was returned to service. Table VII presents data observed over a two-week test period.

Table VII. Performance of Prefilter with Waterweb Medium

Elapsed Time (Days)	Pressure Drop Across Prefilter (Inches WG)	Comment
0	1.2	
1	3.5	
2	5.0	
3	5.5	Before vacuuming filter face.
3	1.0	After vacuuming filter face.
4	3.0	
8	8.5	Before vacuuming filter face.
8	1.0	After vacuuming filter face.
9	3.0	
10	7.6	
15	8.5	

Observations were continued over a two-month period during which time the medium was vacuumed seven times. The medium was then removed from service and washed with water; no sign of degradation was observed.

An improved holder for the medium was designed and constructed. See Figure 7. Holders of this design are being evaluated in production service. Figure 8 illustrates how the prefilter holder also doubles as a hold-down for the HEPA filter which it precedes. The "watchcase" feature allows the prefilter to be removed without disturbing the HEPA filter.

ACS Demister Medium

Another type of demister medium being tested as a prefilter is Mistermesh® (Mistermesh is a trademark of ACS Industries, Woonsocket, R.I.). Mistermesh medium is fabricated from multifilament glass with parallel knit polypropylene. This material is not normally used as a filter for dry particulate.

Stainless steel frames, shown in Figure 9, were constructed to accommodate different thicknesses of the demister medium. The medium is friction fitted into the frame and held in place by a slip frame. When the unit is assembled it is approximately six inches thick and is used in place of a HEPA filter at the glovebox exhaust.

One prefilter, employing a pad of Mistermesh 8" x 8" x 3", was installed at the exhaust of a glovebox used for plutonium recovery.

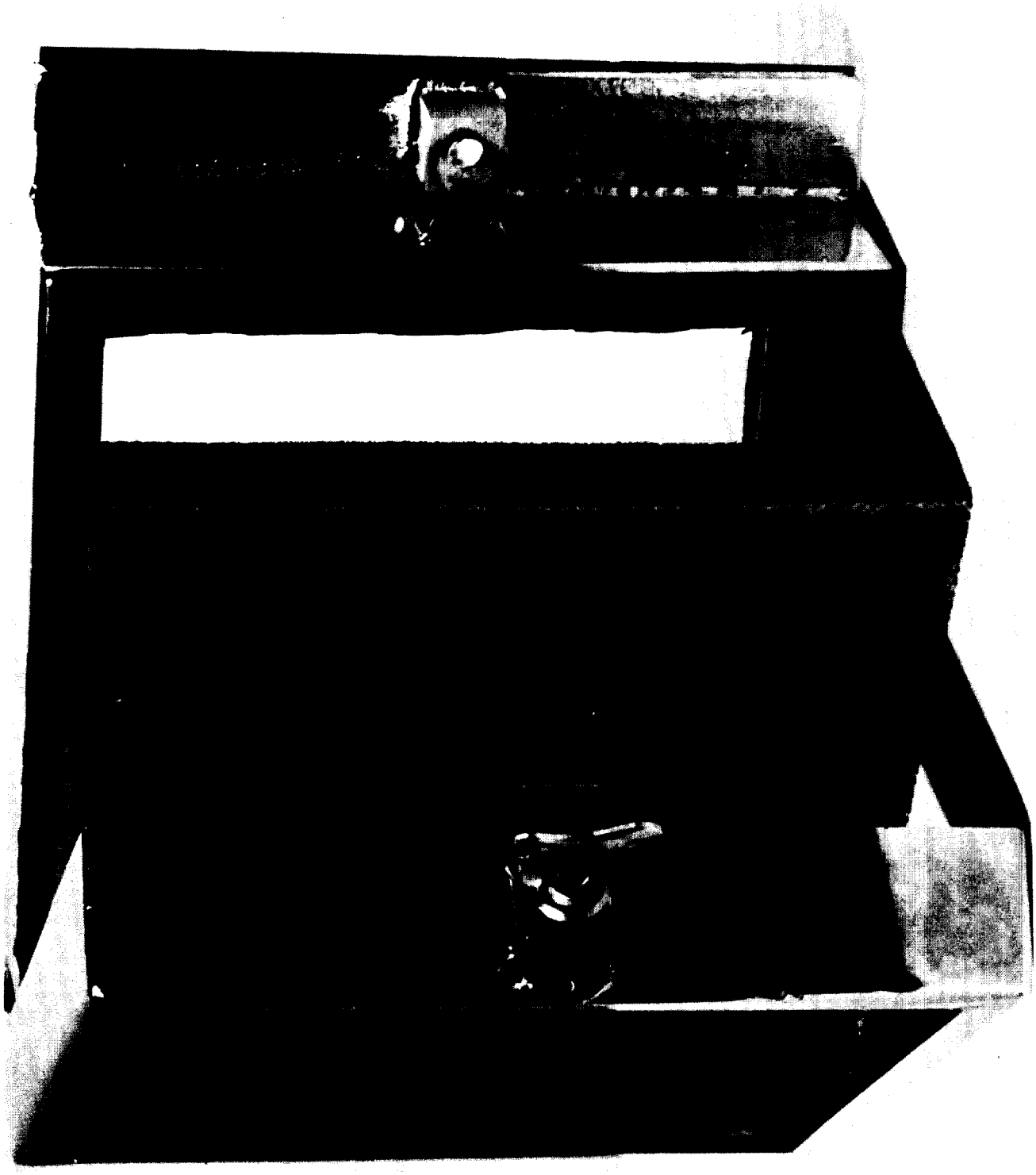

Figure 7. Prefilter Holder